From *In Vitro* Screens to Telomeric Phenotypes: Identification and Initial Characterisation of Two Novel Telomere-Associated Proteins in *Saccharomyces cerevisiae*

Dissertation

Zur Erlangung des Grades

Doktor der Naturwissenschaften

am Fachbereich Biologie

der Johannes Gutenberg-Universität Mainz

Varvara Verkhova

geb. am 2. Januar 1993 in Vladimir, Russland

Mainz, 2025

Dekan: Prof. Dr. Eckhard Thines

1. Berichterstatter:

2. Berichterstatter:

Tag der mündlichen Prüfung:

(blank)

Table of Contents

Summary

A telomere (literally, “end piece” from Greek *télos* “end” and *méros* “part”) is a specialised nucleoprotein structure located at each end of a linear eukaryotic chromosome. Its presence is essential for genome stability and the integrity of DNA termini, ensuring their intactness by preventing gratuitous fusion and recombination events from occurring. In addition, telomeres, together with the enzyme telomerase, facilitate the replication and maintenance of chromosomal ends, thereby preventing premature onset of senescence and the progressive loss of genetic material.

In most organisms, telomeric DNA consists of short, repetitive sequences. The nominally canonical TTAGGG repeat is believed to be ancient and broadly conserved among eukaryotes. It is all the more remarkable, then, that telomeric repeat sequences in *Saccharomycotina* yeasts are exceptionally diverse – typically TG-degenerated, generally not G/C-rich, and varying in both the overall length and tandem repeat sequence patterns among species.

One of the most widely used model organisms, the budding yeast *Saccharomyces cerevisiae*, is evolutionarily young on the yeast phylogenetic tree. Interestingly, species from more basal clades tend to retain greater similarity to the canonical TTAGGG repeat, whereas more derived species show increasing divergence. Consequently, telomere-binding and telomere-associated proteins (TBPs) in yeasts are not necessarily conserved and may vary across clades, occasionally even swapping their functional roles.

In this thesis, species-specific telomeric repeat sequences were used in *in vitro* pull-down assays to investigate the co-evolution of TBPs within the *Ascomycota* group of yeasts, with the aim of identifying novel telomere binders. As a result, two TBPs – transcription factors and paralogs, Tda9 and Rsf2 – were identified as telomere-binding proteins in several yeast species *in vitro*, and also confirmed to bind telomeric DNA *in vivo* in *S. cerevisiae*. Subsequent experiments focused on *S. cerevisiae*, revealing that deletion of these proteins impacts several telomeric features. These include changes in telomere length and telomeric silencing, impaired formation of Type II survivors during replicative senescence and telomere lengthening upon overexpression of one of the two proteins.

Overall, this study aims to contribute to the broader understanding of telomere integrity in yeast and, more generally, to expand our knowledge of telomere biology, composition and function. In doing so, it offers an incremental yet meaningful perspective that could, in time, support advances in therapeutic strategies related to cancer and healthy ageing.

Zusammenfassung

Ein Telomer (wörtlich "Endstück" aus dem Griechischen *télos* "Ende" und *méros* "Teil") ist eine spezialisierte Nukleoproteinstruktur, die sich an jedem Ende eines linearen eukaryotischen Chromosoms befindet. Seine Anwesenheit ist essentiell für die Genomstabilität und die Integrität der DNA-Termini und gewährleistet deren Unversehrtheit, indem unnötige Fusions- und Rekombinationsereignisse verhindert werden. Darüber hinaus erleichtern Telomere zusammen mit dem Enzym Telomerase die Replikation und Aufrechterhaltung von Chromosomenenden, wodurch ein vorzeitiges Einsetzen der Seneszenz und der fortschreitende Verlust von genetischem Material verhindert werden.

In den meisten Organismen besteht Telomer-DNA aus kurzen, sich wiederholenden Sequenzen. Es wird angenommen, dass die nominell kanonische TTAGGG-Wiederholung uralt und unter Eukaryoten weitgehend konserviert ist. Umso bemerkenswerter ist es daher, dass Telomer-Wiederholungssequenzen in Hefen der Gruppe *Saccharomycotina* außergewöhnlich vielfältig sind – typischerweise TG-degeneriert, im Allgemeinen nicht G/C-reich und sowohl in der Gesamtlänge als auch in den Tandem-Wiederholungssequenzmustern zwischen den Arten unterschiedlich.

Ein weit verbreiteter Modellorganismus, die knospende Hefe *Saccharomyces cerevisiae*, ist evolutionär jung auf dem phylogenetischen Baum der Hefe. Interessanterweise neigen Arten aus basaleren Kladen dazu, eine größere Ähnlichkeit mit der kanonischen TTAGGG Wiederholung beizubehalten, während abgeleitete Arten eine zunehmende Divergenz aufweisen. Folglich sind Telomerbindende und Telomerassoziierte Proteine (TBPs) in Hefen nicht unbedingt konserviert und können zwischen den Kladen variieren, gelegentlich sogar ihre funktionellen Rollen vertauschen.

In dieser Dissertation wurden speziesspezifische Telomerwiederholungssequenzen für *in vitro* Pull-Down-Assays verwendet, um die Koevolution von TBPs innerhalb der *Ascomycota*-Hefegruppe zu untersuchen, mit dem Ziel neue Telomerbinder zu identifizieren. Als Ergebnis wurden zwei TBPs die Transkriptionsfaktoren und Paraloge, Tda9 und Rsf2 – als telomerbindende Proteine in mehreren Hefespezies in vitro identifiziert und auch bestätigt, Telomere *in vivo* in *S. cerevisiae* zu binden. Nachfolgende Experimente konzentrierten sich auf *S. cerevisiae* und zeigten, dass die Deletion dieser Proteine mehrere Telomermerkmale beeinflußt. Dazu gehören Veränderungen der Telomerlänge und der Telomerstummschaltung, eine beeinträchtigte Bildung von Typ-II-Überlebenden während der replikativen Seneszenz und eine Telomerverlängerung bei Überexpression eines der beiden Proteine.

Insgesamt zielt diese Dissertation darauf ab, zum breiteren Verständnis der Telomerintegrität in Hefe beizutragen und unser Wissen über Zusammensetzung und Funktion von Telomeren zu erweitern. Hierbei wird eine aussagekräftige Perspektive, die mit der Zeit Fortschritte bei Therapiestrategien im Zusammenhang mit Krebs und gesundem Altern unterstützen könnte, angeboten.

List of Abbreviations

5-FOA	5-Fluroorotic Acid
aa	Amino Acid(s)
ACDH	Acetaldehyde Dehydrogenase
AID	Auxin Inducible Degron
ALT	Alternative Lengthening of Telomere
APB	ALT-associated Promyelocytic Leukaemia Body
ARS	Autonomously Replicating Sequence(s)
BIR	Break Induced Replication
bp	Base Pair(s)
ChIP	Chromatin Immunoprecipitation
CST	CDC1-STN1-TEN1 complex
Cys	Cysteine
CPT	Camptothecin
DBD	DNA-Binding Domain
DDR	DNA Damage Response
DML	Dimethyl Labelling
DNA Pol	DNA Polymerase
ds	Double Strand
DSB	Double Strand Break
dsDNA	Double Strand DNA
DTT	Dithiothreitol
E. coli	*Escherichia coli*
EMSA	Electrophoretic Mobility Shift Assay
eV	Empty Vector
FP	Fluorescence Polarisation
G4	G-quadruplex
h	Hour(s)
HAT	Histone Acetyltransferase
HDR	Homology Directed Repair
HIR	Histone Regulation Complex
HIS	Histidine
HPLC	High Performance Liquid Chromatography
HU	Hydroxyurea
HYG	Hygromycin
IAA	Indol-3-Acetic Acid/ 2-iodoacetamide
IgG	Immunoglobulin G
ITS	Interstitial Telomeric Sequences
KAN	Kanamycin
kDa	Kilo Dalton
KO	Knockout
LEU	Leucine
LIM	Lin-11, Isl-1, Mec-3
Lys (K)	Lysine
me	Methyl/Methylation
min	Minute(s)
MET	Methionine
mDNA	Mitochondrial DNA
MDM2	Mouse Double Minute 2
MRX	MRE11-RAD50-XRS2 complex
MMS	Methyl Methanesulfonate
MS	Mass Spectrometry
MYND	Myeloid, Nervy, DEAF-1
nt	Nucleotides
NuRD	Nucleosome Remodelling and Deacetylase
NHEJ	Non-Homologous End Joining
oE	Overexpression
ORF	Open Reading Frame
PAGE	Polyacrylamide Gel Electrophoresis
PAP	Peroxidase Anti-Peroxidase
PCR	Polymerase Chain Reaction
PD	Population Doubling
PHD	Plant Homology Domain
POT1	Protection Of Telomeres 1
Pol	Polymerase
PTM	Post-Translational Modification
qPCR	Quantitative PCR
Raf	Raffinose
RAP1	Repressor Activator Protein 1

rcf	Relative Centrifugal Force
rDNA	Ribosomal DNA
RING	Really Interesting New Gene
RPA	Replication Protein A
RSF2	Respiration Factor 2
RSC	Remodel the Structure of Chromatin complex
RT	Room Temperature
RT-qPCR	Real Time Quantitative PCR
ss	Single Strand/ Singke-stranded
ssDNA	Single Strand DNA
SAS	Survivor Associated Senescence
SB	Southern Blot
S. cerevisiae	*Saccharomyces cerevisiae*
S. pombe	*Schizosaccharomyces pombe*
SD	Standard Deviation
SDS	Sodium Dodecyl Sulphate
SC	Synthetic Complete
TAS	Telomere-Associated Sequence(s)
TBP	Telomere-Binding (associate) Protein
T-circles	Telomeric Circles
TF	Transcription Factor
T-loop	Telomeric Loop
TIF	Telomere Induced Foci
TIN2	TRF1-Interacting nuclear protein 2
TPE	Telomere Position Effect
TPE-OLD	Telomere Position Effect Over Long Distances
TPP1	TINF2-interacting protein 1
TRF1	Telomeric Repeat binding Factor 1
TRF2	Telomeric Repeat binding Factor 2
URA	Uracil
UAS	Upstream Activation Sequence
WT	Wild Type
WB	Western Blot
ZnF	Zink Finger
ZBTB10	Zinc Finger and BTB Domain-containing Protein 10

Acknowledgements

(blank)

Introduction

The specialised nucleoprotein complexes found at the ends of linear eukaryotic chromosomes – structures we now refer to as telomeres – first drew scientific attention in the late 1920s and 1930s. Through their studies on chromosomes damaged by X-radiation and their observations of so-called "chromosome healing" events that prevented recombinational fusions, two pioneering scientists, Hermann Muller and Barbara McClintock, concluded that chromosome ends possess distinct properties. They proposed that these termini are structurally and functionally different from the rest of the genome, bearing end protective functions and form (**Zakian, 2013; originally in Muller, 1928; McClintock, 1941**).

Following the discovery of DNA as the carrier of genetic inheritance – and the elucidation of its structure during the 1940s and 1950s by elegant scientific works of many talented scientists – the field progressed rapidly. Building upon these foundations, studies led by James Watson, Francis Crick and Elizabeth Blackburn during the 1970s and 1980s identified two major challenges arising from the linear nature of eukaryotic chromosomes. These were the so-called "end-replication problem" and the idea of leading and lagging strands. As well as the end protection concept and prevention of chromosomal termini from being confused with the double DNA breaks – an event that would lead to deleterious end fusions.

In 1985, Elizabeth Blackburn and her graduate student Carolyn Greider published a seminal paper describing the discovery of the enzyme responsible for telomere elongation. Initially referred to as "telomere terminal transferase", the enzyme was later named telomerase (**Greider & Blackburn, 1985**). This discovery catalysed rapid advances in telomere biology, with subsequent research coming on the composition of Shelterin and Shelterin-like complexes across various organisms, and revealing key roles for telomeres and telomerase in processes such as cancer development, ageing and cellular senescence.

As this study centres on the identification and functional role of the two transcription factors found across several yeast species – specifically focusing on their involvement in telomere biology of the budding yeast *Saccharomyces cerevisiae* – the following introductory sections will be attentive to yeast telomeres, while drawing on other model organisms where relevant.

"End-Replication Problem" and Its Resolution

Given that DNA replication can only proceed in the 5′ to 3′ direction due to the nature of DNA polymerase, one of the strands – the leading strand – is synthesised continuously in that direction. Meanwhile, the other strand – the lagging strand – is synthesised in a discontinuous manner, still in the 5′ to 3′ direction but away from the replication fork, in short segments known as Okazaki fragments (**Figure 1**). In both cases, a short RNA primer, approximately 8-12 nucleotides in length in eukaryotes, is required to initiate DNA synthesis and is removed once replication is complete.

That, as was noticed by J. Watson and Alexey Olovnikov in the 1970s, brings an inevitable problem in replication of the chromosomal ends if this semi-conservative and discontinuous model is applied (**Watson, 1972; Olovnikov, 1973**). Thus, while the leading strand produces a blunt end that is initially unproblematic, removal of the terminal RNA primer from the lagging strand leaves an unreplicated gap at the 5′ end of the newly

synthesised strand. This results in progressive shortening of chromosome ends with each round of replication (**Figure 1**).

This hypothesis aligned well with Leonard Hayflick's earlier observation, made in 1961, of the finite proliferative capacity of eukaryotic cells – a phenomenon later termed as cellular senescence. Thus, the impossibility to copy the very ends of a linear chromosome might be explained by a concept of "***margin***otomy [causing] the appearance, in the daughters of dividing cells, of more and more shortened end-genes, the so-called ***telo***genes, with every new mitosis" (**citation Olovnikov, 1973**). Preceding, L. Hayflick proposed that this degeneration of chromosomal termini might be caused by intrinsic, rather than external, factors (**Hayflick & Moorhead, 1961**).

It is now accepted that both the lagging and leading strands contribute to the problem of telomere shortening. While earlier models attributed the issue primarily to the lagging strand, subsequent research revealed that the blunt end resulting from leading strand synthesis must also be processed to form a 3′ single-stranded overhang – commonly referred to as the G-tail – essential for telomere stability (**Soudet *et al.*, 2014**). This conversion requires 5′-end resection of the complementary C-strand after leading strand synthesis is complete (**Figure 1**). This Tel1-dependent processing generates a ~40nt G-tail and necessitates further fill-in synthesis. Following primer removal from this resected strand, the result mirrors that of lagging strand synthesis – a 3′-overhang, but again shorter than the original template (**Soudet *et al.*, 2014**).

Therefore, every time a eukaryotic cell divides, in theory, its telomeres should lose in length the size of the RNA primer (8-12 nt), or an average of 10 nt at both, leading and lagging strands. However, in practice, the observed loss is somewhat smaller – estimated at approximately 2.5-5 nt per division (**Soudet *et al.*, 2014**) or 3-5 nt per population doubling in telomerase-deficient cells (**Singer & Gottschling, 1994; Marcand *et al.*, 1999**). Interestingly, the resection and processing of the blunt end, particularly from the leading strand, appear to be primary contributors to telomeric-repeat loss. In humans, it has also been shown that the 5′-end resection occurs at the lagging strand end post-replication (**Wu *et al.*, 2012**).

Altogether, telomere erosion is driven by the inherent limitations of DNA replication, 3′-end processing, 5′-end resection, and the incomplete nature of DNA fill-in synthesis (**Figure 1**).

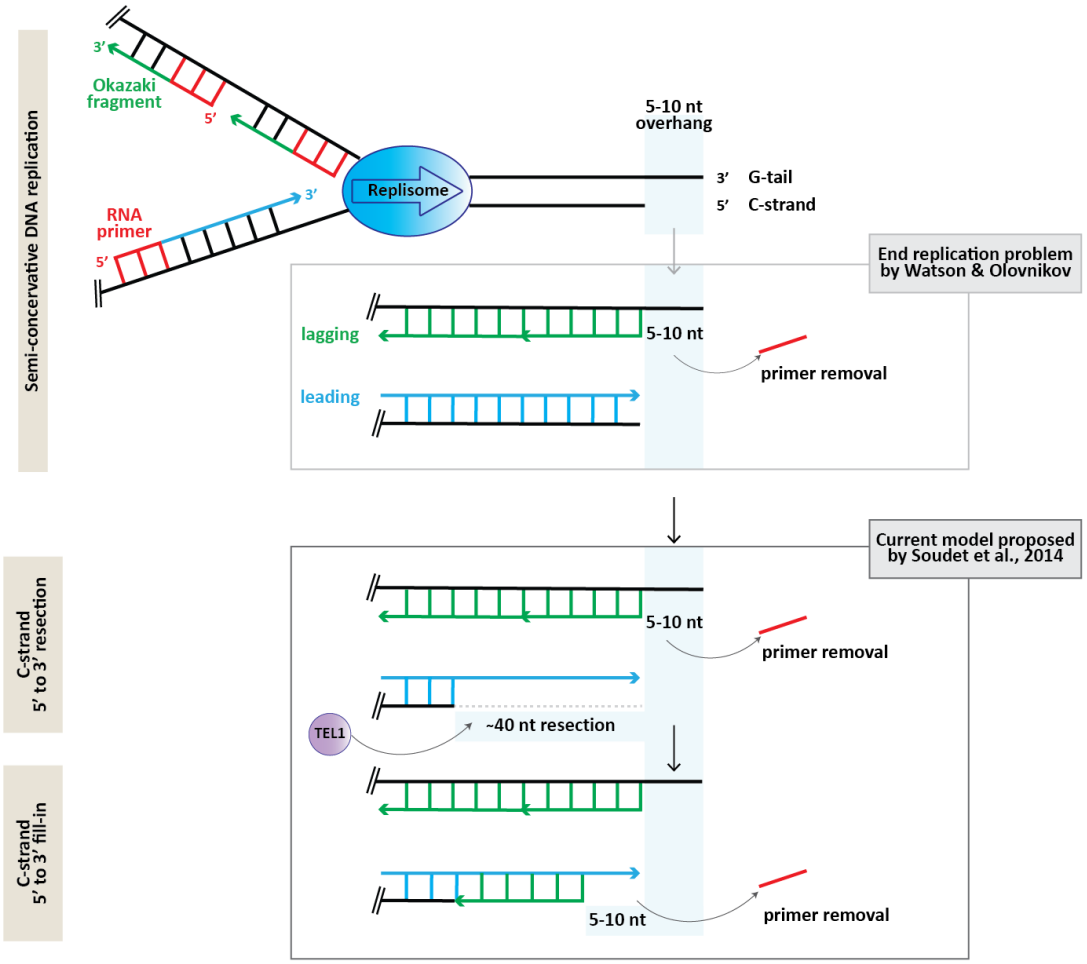

Figure 1. Telomeres and the End Replication Problem at a Glance.
According to Watson & Olovnikov's model, removal of the last primer used for the lagging strand synthesis by the semi-conservative DNA replication leaves a gap that cannot be filled-in as there is no template DNA left to which an additional primer can anneal to; the synthesis of the leading strand produces a blunt end and, therefore, does not cause shortening of that end.
In accordance with the last findings as proposed by **Soudet *et al.*, 2014**, the extent of telomere shortening is defined by both, lagging and leading strands, as the latest is resected extensively with the following gap fill-in which leaves the end shorter by additional 5-10 nt. In this model, the rate of shortening is 2.4-5 bp per population doubling (PD) as stated by the authors.

To both, address the end-replication problem and ensure proper telomere length maintenance, eukaryotes have evolved to employ three principal mechanisms:

i. utilisation of a specialised reverse transcriptase, telomerase (including its re-activation in cancer);

ii. an alternative telomere lengthening pathway (ALT) which relies on homologous recombination (i.e., telomerase-independent mechanism);

iii. non-canonical telomere extension mechanisms involving retrotransposons or complex satellite DNA, as seen in organisms such as fruit flies and midges (**Kordyukova *et al.*, 2018; originally in Levis *et al.*, 1993; Nielsen & Edström, 1993**).

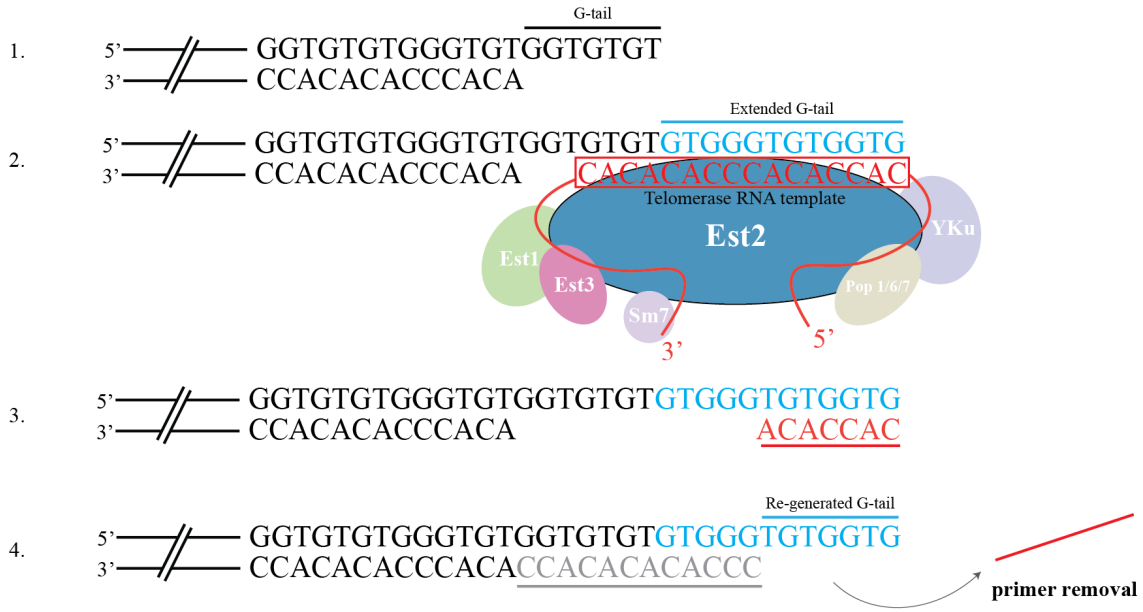

Figure 2. Single Elongation Act of Telomerase-Dependent Telomere Lengthening. **1.** Short telomere in need of its 3'-end to be replenished; **2.** Telomerase is recruited and elongates the 3'-overhang by reverse transcription from the telomerase RNA template (i.e., Tlc1); **3.** An RNA primer can now anneal to the extended end, and conventional DNA replication by DNA-polymerase-primase complex (not shown) results in the C-strand fill-in (grey underlined region under number 4); **4.** Removal of the RNA primer leaves the replenished 3' G-tail with no net loss in telomeric DNA. Figure adapted from **Vega *et al.*, 2003** with modifications.

In most eukaryotes under normal circumstances, telomerase is the primary solution to telomere shortening. Its unique role was first described by Greider and Blackburn in the 1980s. Working with the ciliate *Tetrahymena*, they identified telomerase as a reverse transcriptase composed of two moieties – an RNA template and protein subunits forming its catalytic core. In *S. cerevisiae*, this complex includes (**Figure 2**):

- **Tlc1**, the RNA template with the 3′-CACACACCCACACCAC-5′ sequence that serves as a template for the extension of the 3' G-tail strand (**Singer & Gottschling, 1994**);
- **Est2**, the catalytic reverse transcriptase subunit that performs the reverse transcription from Tlc1;
- **Est1 and Est3**, associated factors involved in recruitment and processivity of the enzyme (**Lendvay *et al.*, 1996; Vega *et al.*, 2003; Chan *et al.*, 2008**).

Unlike in human somatic cells, telomerase is constitutively active throughout the cell cycle in yeast, albeit at low abundance – around 30 copies of Tlc1 for 64 telomere ends in a haploid cell during S-phase (**Mozdy & Cech, 2006**). Telomerase can also bind telomeres outside of their active replication period in late S/G2 phase, the action promoted by YKu site within Tlc1 that permits enzyme's binding via interaction with Sir2-4 proteins. However, this binding is non-productive and does not allow for the elongation to start until proper recruitment signals are triggered. In G1 phase, telomere capping predominantly relies on Rap1 rather than the CST complex (**Taggart *et al.*, 2002; Ge *et al.*, 2020**).

Recruitment and activation of telomerase are tightly spatiotemporally regulated processes. At the time of telomere replication in late S-phase, the ssDNA-binding protein Cdc13 binds to the 3′ G-overhang and recruits Est1, which subsequently recruits Est3, forming an active telomerase complex. Following elongation and to avoid the excessive telomere lengthening, the CST complex displaces telomerase, recaps the telomere ensuring its protection, and recruits the DNA polymerase-primase complex for the C-strand fill-in re-synthesis (**Ge *et al.*, 2020**).

Of particular note, telomerase can only act on telomeres with a 3′-overhang, which are produced by the lagging strand synthesis. For the leading strand end, the MRX complex (Mre11-Rad50-Xrs2), together with Tel1, facilitates resection of the blunt end to generate the necessary 3′ overhang (**Takata *et al.*, 2005**).

Replicative Senescence and ALT as One of the Telomere Maintenance Mechanisms

Apart from the non-canonical telomere lengthening observed in a limited number of species (see chapter *"End-replication Problem and its Resolution"*), eukaryotic cells are generally left with only two strategies to counteract telomere shortening: the reactivation or maintenance of telomerase activity, and the engagement into ALT-pathway. Under normal physiological conditions, the majority of eukaryotes – barring a few notable exceptions – progressively downregulate telomerase after a defined number of cell divisions. In multicellular and biologically complex organisms such as mammals, telomerase is highly expressed in germ cells, expressed at moderate levels in undifferentiated stem and progenitor cells, and is nearly entirely silenced in most somatic tissues (**reviewed in Chakravarti *et al.*, 2021**).

As a result, telomeres shorten progressively with each round of cell division throughout a cell's lifespan. Once telomeres reach a critically short length such that further replication would compromise genomic integrity, the cell enters a state known as cellular senescence. This phenomenon, first described by L. Hayflick in the 1960s, is defined by an essentially irreversible arrest of the cell cycle and cessation of cell proliferation. While senescence can be triggered by various intrinsic and extrinsic stress signals – such as oncogene activation or persistent DNA damage – the most prominent and well-studied cause is telomere attrition and the resulting dysfunction.

Notably, senescence is not exclusively pathological; it can also be part of normal developmental programmes, such as during embryogenesis. Thus, both senescence and ageing are fundamentally natural processes, likely shaped through evolution to prevent malignant transformation, promote tissue regeneration and maintain systemic homeostasis. In this context, cellular senescence serves as a safeguard mechanism for the organism as a whole, triggered when individual cells accumulate excessive damage due to successive rounds of replication, spontaneous mutations, DNA damage and other manifesting alterations in chromatin (**reviewed in Lopez-Otin *et al.*, 2013 & 2023; Chakravarti *et al.*, 2021**).

Once telomeres can no longer adequately perform their protective function, they begin to resemble one-ended double-stranded DNA breaks (DSBs), thereby becoming substrates for recognition by the DNA damage response (DDR) machinery. These uncapped telomeres continuously signal a state of irreparable DNA damage, prompting the cell to cease its division (**Teixeira & Gilson, 2005; Doksani & de Lange, 2014**). The

canonical resolution to this signal are cellular senescence and eventual stop of division. However, some cells are capable of evading this fate, proceeding instead toward malignant transformation. Most cancer cells accomplish this by reactivating telomerase. Nevertheless, a subset – approximately 10-15% of human cancers – adopts a telomerase-independent mechanism based on homologous recombination, known as ALT (**Cesare & Reddel, 2010; Dilley & Greenberg, 2015**).

The ALT mechanism was initially observed in *Saccharomyces cerevisiae* mutants deficient in functional telomerase. While the majority of these cells entered senescence and ceased proliferation, a small subpopulation survived and continued dividing – these were termed “survivors” (**Lundblad & Szostak, 1989; Lundblad & Blackburn, 1993**). It was demonstrated that these survivor cells were able to maintain telomere length through the amplification and acquisition of subtelomeric sequences in a Rad52-dependent manner, thus employing a HR-based pathway. Consequently, in the absence of telomerase, chromosomal ends could be sustained via this alternative, backup mechanism – hence, the term Alternative Lengthening of Telomeres.

Subsequent studies confirmed that ALT also operates in human cells, demonstrating similar dependency on homologous recombination. These findings established mechanistic parallels between yeast and human systems and underscored the utility of yeast as a valuable model for studying the ALT-pathway (**Dunham *et al.*, 2000; reviewed in Neumann & Reddel, 2002**).

Survivors of Replicative Senescence in Yeast

Subsequent studies have identified two distinct classes of telomerase-negative *S. cerevisiae* survivors, designated as Type I and Type II, based on the specific telomeric components involved in telomere maintenance. Each type exhibits unique molecular features and growth characteristics (**Teng & Zakian, 1999; Chen *et al.*, 2001; reviewed in Wellinger & Zakian, 2012**): Type I survivor stabilises length of its chromosome ends via tandem Y’ elements amplification, their terminal repeats stay, however, short. Type I cells also grow at an inconsistent and slow rate. In contrast, Type II survivors maintain length of their telomeres by elongating telomeric repeats themselves with little to no alteration in the subtelomeric regions (**Figure 3, B**). Type II cells also grow at the speed of a wild type culture with an active telomerase despite experiencing cycles of telomere shortening and lengthening. Furthermore, in liquid culture, Type II survivors tend to outcompete Type I survivors, whereas on solid agar media, Type I cells may temporarily prevail.

For some time, it was hypothesised that Type I survivors represent an intermediate or transitional form preceding the emergence of Type II survivors. This "predecessor hypothesis" was supported by observed differences in growth dynamics and was further corroborated by evidence demonstrating the involvement of distinct protein factors in each pathway. Notably, the *RAD52* gene is essential for the formation of both survivor types; its deletion results in complete loss of survivor formation (**Lundblad & Blackburn, 1993; Teng *et al.*, 2000**). Deletion of *RAD51*, *RAD54* or *RAD57* impairs the generation of Type I survivors, while deletion of components of the MRX complex (Mre11, Rad50, Xrs2) or *RAD59* abolishes the formation of Type II survivors, allowing only Type I to emerge. Moreover, double mutants such as *rad50rad51* and *rad51rad59* are non-viable in the absence of telomerase, underscoring the indispensable role of these factors – alongside Rad52 – in establishing the ALT-pathway (**Le *et al.*, 1999; Teng *et al.*, 2000; Chen *et al.*, 2001**).

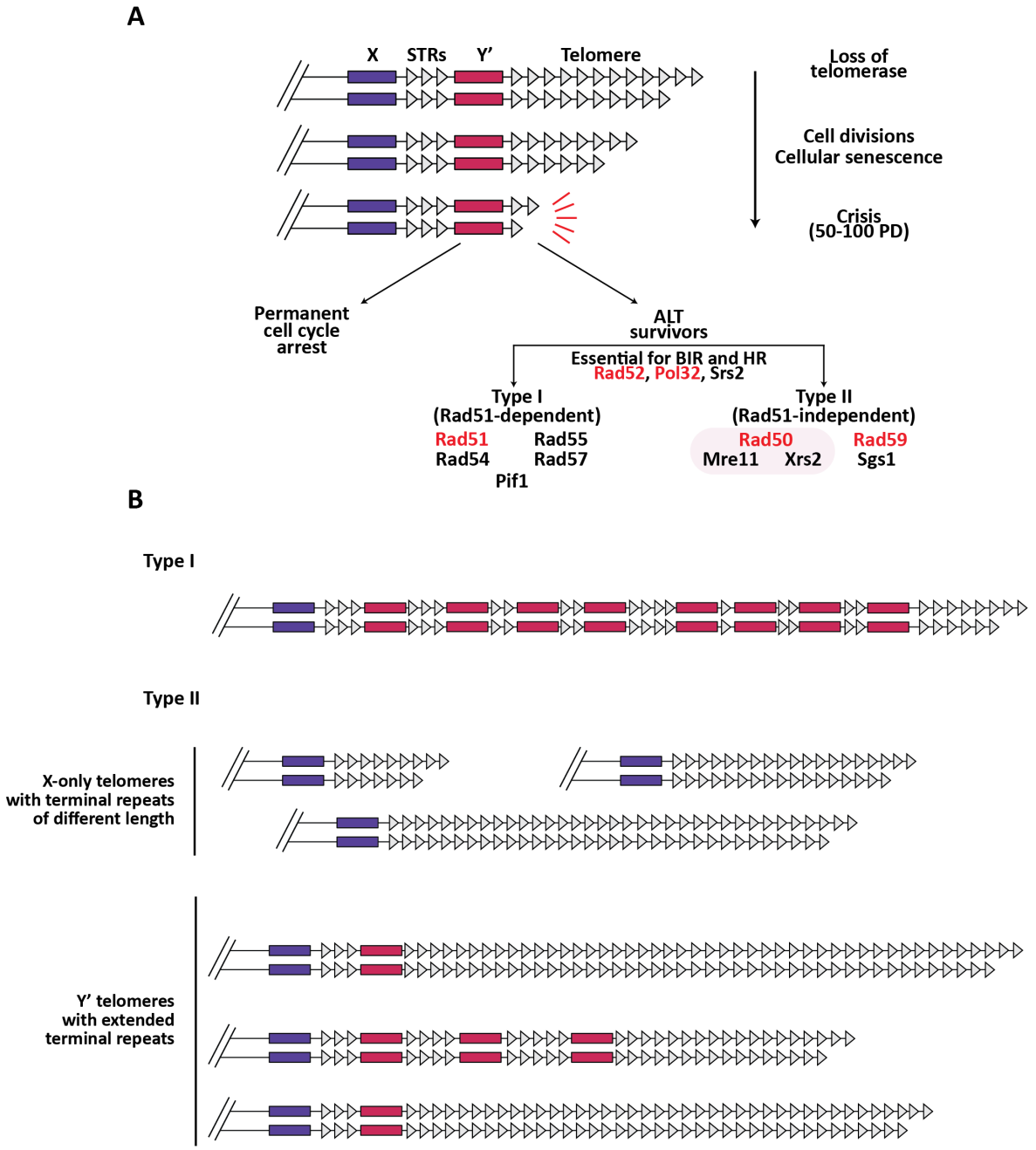

Figure 3. Survivors of Replicative Senescence in Yeast.

A. Proposed two-pathway model of ALT survivor formation. After the loss of telomerase, cells undergo about 50 to 100 population doublings (PD) before majority of them stop dividing entirely. However, a small fraction of cells starts to harness ALT to cope with telomeres erosion. **B.** A schematic of telomers in Type I and Type II survivors. **Abbreviations:** X – X element; Y' – Y' element, STRs – Subtelomeric Repeat Sequences (also known as ITS for Interstitial Telomeres Sequence); BIR – Break Induced Repair; in red – essential proteins; in black – important proteins; pink oval – MRX complex.

Figure is adapted from **Wellinger & Zakian (2012)** with modifications.

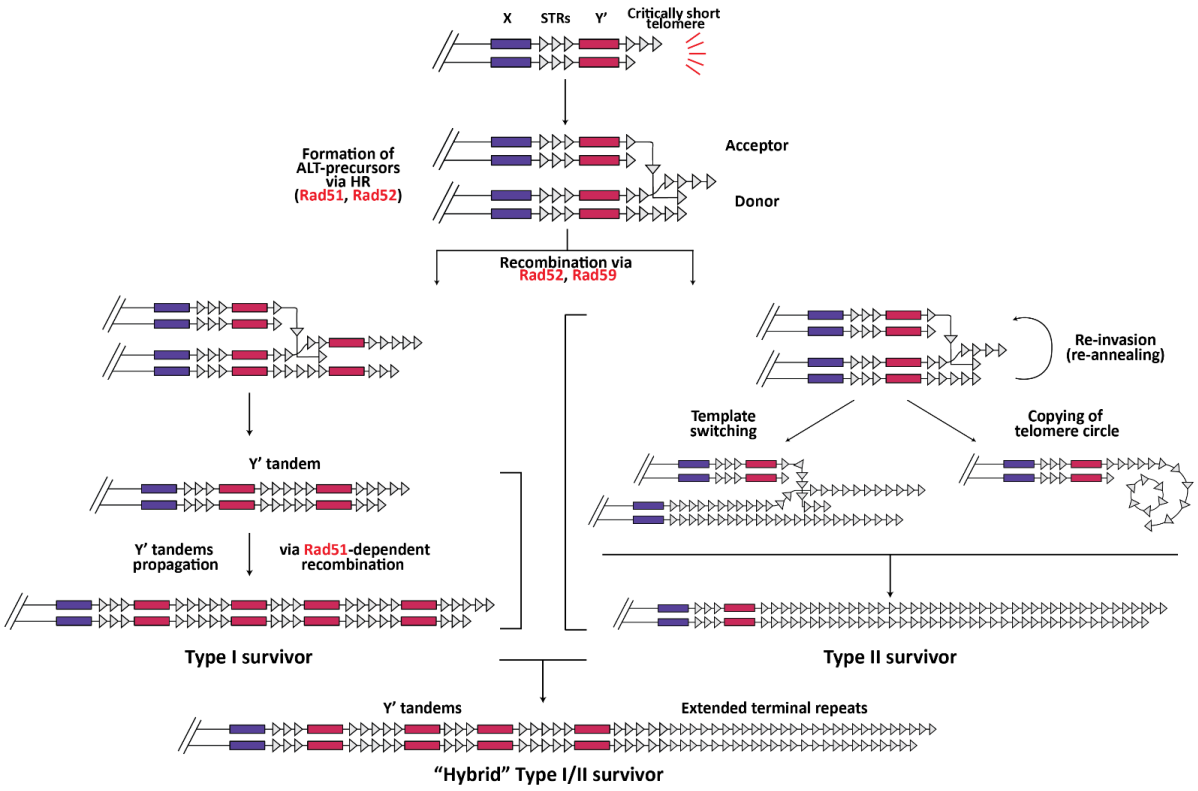

Figure 4. A Unified Model of Two-Pathway Survivor Formation (Kockler *et al.*, 2021).
After telomeres erosion to the state of critically short ones, those cells that overcome permanent cell cycle arrest start to form ALT-precursors via Rad51- and Rad52-dependent homology repair. Both, Rad52 and Rad59, mediate recombination between homology regions of STRs flanking Y' element to form Y' tandems via Rad51-dependent recombination as in Type I survivors. Or Rad52- and Rad59-mediated recombination occurs at the terminal ends as in Type II survivors, which further can be elongated to ultra-long telomeric ends via re-invasion, template switch or by copying telomere circle. In both scenarios, with the help of Rad52 and Rad59, a "hybrid" of two pathways survivor can form. In that case it has both, ultra-long telomeric repeat sequence and a tandem of Y' elements.
Figure is adapted from **Kockler *et al.*, 2021** with modifications.

Collectively, these findings gave rise to the two-pathway model of ALT in yeast. According to this model, ALT operates through a specialised form of HR-based DNA repair known as Break-Induced Replication (BIR). BIR is a type of dsDNA break repair mechanism that involves strand invasion of a homologous template by a single DNA end. And Lydeard *et al.* (2007) provided experimental evidence demonstrating that both ALT types depend on BIR for telomere elongation (**Figure 3, A**). **Figure 3, B** further depicts the distinct telomeric architectures of the two survivor types.

Further refinement of this model was proposed by Kockler *et al.* (2021), who investigated the early steps in ALT initiation starting from critically short telomeres. Interestingly, their study supports a unified model in which the formation of a shared ALT-precursor is followed by divergence into either the Type I or Type II pathway (**Figure 4**). In this model, initial strand invasion requires Rad51 and Rad52 to mediate homologous recombination, establishing the ALT-precursor. Subsequent pathway specification is Rad59-dependent: in the Type I pathway, the short telomere invades an internal sequence upstream of a Y′ element within the donor telomere, leading to tandem Y′ amplification in the recipient telomere. In the Type II pathway, strand invasion targets the terminal

telomeric repeats, facilitating iterative re-invasion events and template switching. This mechanism may also account for the formation of extrachromosomal telomeric C-circles, which are hypothesised to contribute to telomere extension in Type II survivors. Notably, Kockler *et al.* (2021) also indicated the existence of the hybrid-of-both-pathways survivor that combines features of Type I and Type II mechanisms, i.e., a Type I telomere that subsequently undergoes Type II-like terminal elongation (**Figure 4**).

"End-Protection Problem" and Composition of Telomeres in *S. cerevisiae*

According to the definition, a telomere is a specialised nucleoprotein complex found at the end of a linear chromosome. It consists of two major components: the DNA, which is composed of simple, non-protein-coding repetitive sequences, and the proteins associated with this DNA. While the specific telomeric DNA sequences and the composition of the associated proteins vary across organisms, the general structure and function of telomeres are evolutionarily conserved. The following section focuses on the composition of telomeres in budding yeast.

In *S. cerevisiae*, telomeric DNA comprises heterogeneous repeats of the 5'-TG_{1-3}-3' sequence and is approximately 300 ± 75 bp in length (**Figure 5**) (**Wellinger & Zakian, 2012**). Forstemann & Lingner (2001) demonstrated that this heterogeneity arises due to telomerase occasionally failing to align its RNA template correctly with the 3' overhang nucleotides, resulting in abortive reverse transcription. Notably, this phenomenon is not unique to *S. cerevisiae*, but is a general trend across various yeast lineages from different phyla. The chapter *"Co-evolution of Telomere-Associated Proteins and Telomeric DNA in Yeast"* explores the potential evolutionary origins of such sequence heterogeneity.

The presence of a G-tail at the 3' end is essential for telomerase processivity and is a typical feature of a functional telomere. In *S. cerevisiae*, the G-tail is typically 12-15 nucleotides long during most of the cell cycle but extends to ≥30-100 nucleotides during a brief window in late S/G2 phase (**Wellinger *et al.*, 1993; Larrivee *et al.*, 2004**). Importantly, long G-tails are observed even in telomerase-deficient strains (**Wellinger *et al.*, 1999; Dionne & Wellinger, 1998**), indicating that they primarily result from resection of the C-strand rather than direct telomerase action (see **Figure 1**).

Due to its TG-rich composition, the telomeric sequence is guanine-rich on one strand, enabling the formation of G-quadruplexes (G4s) at the telomere ends. These structures play several roles, including (**Moye *et al.*, 2015; reviewed in Bryan, 2020; Carvalho *et al.*, 2020**):

(i) suppressing DNA damage response (DDR) activation during C-strand resection;

(ii) regulating telomerase access to telomeres; and

(iii) promoting telomere involvement in replication bouquet formation during meiosis.

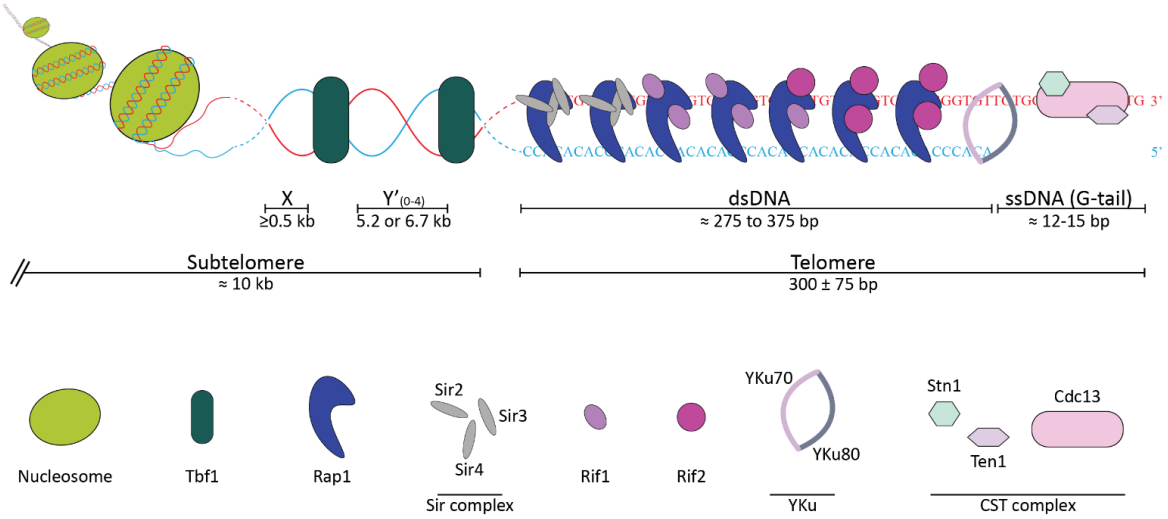

Figure 5. Telomere Structure in *S. cerevisiae*, DNA and Important Telomere Binders. Red strand, G-rich with 3'-overhang (i.e., G-tail); blue strand, C-rich with 5'-end. STRs (subtelomeric repeat sequences) are found between X and Y' elements, as well as between Y' and the telomeric sequence (not indicated on the scheme). Within both, X and Y', Tbf1-binding sites are present. TG-repeats can be found between X and Y', and between two Y' elements, they are also referred to as internal TG-sequences, or ITS (not indicated on the scheme). Rap1 is the major dsDNA binder that recruits Sir2/3/4-complex and Rif1/Rif2 proteins. Cdc13 binds ssDNA 3'-overhang and recruits Stn1-Ten1, together all three form CST complex. YKu complex (YKu70 and YKu80) can bind telomeres at the border between ds and ssDNA, subtelomeric and telomeric repeats and via protein-protein interaction with Sir4 (the last two situations are not depicted on the scheme). The elements depicted are not to scale and serve as a conceptual illustration of the main text. Figure is inspired by **Wellinger & Zakian, 2012**.

Given that G4s stabilise R-loops genome-wide, it has been proposed that similar stabilisation occurs at telomeres through interaction with TERRA, a long nonprotein-coding RNA transcribed from telomeric regions (**Maestroni *et al.*, 2017**). Replication of telomeres is particularly challenging due to G4s, DNA-RNA hybrids, topological constraints (e.g., nuclear envelope anchoring and condensed chromatin), and t-loop-like structures, often resulting in replication fork stalling or a complete collapse of replication machinery (**Bonell *et al.*, 2021; Maestroni *et al.*, 2017**).

Like most eukaryotes, *S. cerevisiae* telomeres are flanked by subtelomeric repetitive elements known as Telomere-Associated Sequences (TAS). These sequences serve various functions including: facilitating heterochromatin formation, generating diverse telomeric transcripts, participating in bypassing replicative senescence, and regulating transcription of telomere-proximal genes. In *S. cerevisiae*, TAS regions can span up to 10 kb and includes two main types of elements: X and Y' (**Wellinger & Zakian, 2012; Kwapisz & Morillon, 2020**).

The X elements are present at all chromosome ends exhibiting sequence and size heterogeneity, while the Y' elements occur on only about half of the chromosome ends and exist in tandem arrays of 1-4 copies (**Wellinger & Zakian 2012, Kupiec 2014; Kwapisz & Morillon, 2020**). Y' elements occur in two major forms: Y' long (6.7 kb) and Y' short (5.2 kb) with a number of insertions and deletions. When both elements are present, Y' is consistently located closer to the terminus. Short internal tracts of telomeric sequences often appear at X-Y' and Y'-Y' junctions (i.e., internal TG-tracts), promoting recombination and contributing to overall genome instability (**Figure 6, B**).

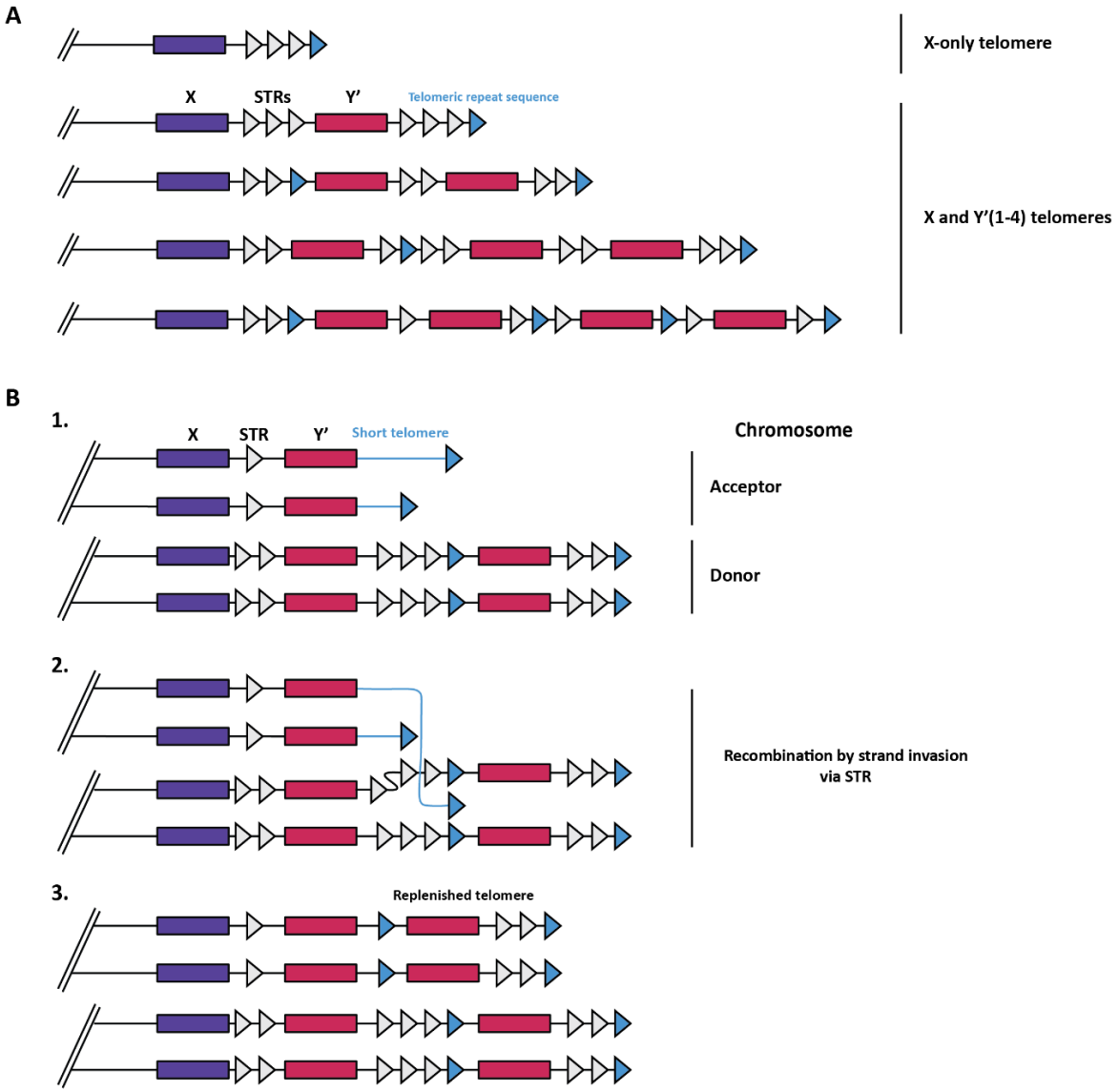

Figure 6. X and Y' Elements at Telomeres in *S. cerevisiae*.
A. Two types of telomeres: X-only and Y'-containing elements. Grey triangles represent subtelomeric repeat sequences (STRs), found between X and Y' elements, as well as between Y' and the telomeric sequence repeat. Blue triangles indicate both, internal TG-sequences/repeats (ITSs) that can be found between X and Y', and between two Y' elements, as well as between telomeric repeat sequence at the terminus and X/Y' element.
B. Recombination between two chromosome's Y' elements **(1)** at which one, donor chromosome, "shares" one of its Y' element with the acceptor chromosome **(2)**, here, in need of telomere replenishment. This mechanism is also observed in Type I survivors of replicative senescence (chapter *"Survivors of Replicative Senescence in Yeast"*).

In telomerase-deficient cells, Y' elements can extend short telomeres via recombination-based self-amplification (**Lundblad & Blackburn, 1993**). Additionally, Y' elements can replace themselves in a transposon-like manner in survivors of replicative senescence (**Maxwell *et al.*, 2004**). Furthermore, both X and Y' elements contain autonomously replicating sequences (ARS) and multiple transcription factor binding sites. Interestingly, chromosomes lacking either or both TAS elements can still proceed through

meiosis and remain stable for at least 4-10 cell divisions before losing stability exhibiting bypass of the Rad9-dependent arrest (**Sandell & Zakian, 1993**).

The second component of the telomere is its associated proteins, which include those binding to single-stranded (ssDNA) and double-stranded (dsDNA) regions. These proteins are critical for telomere end protection, replication, maintenance, as well as chromatin organisation at the regions proximal to telomeres. In *S. cerevisiae*, major telomere-associated proteins include the CST complex – composed of Cdc13, Stn1 and Ten1 – binding the 3' overhang, and Rap1, a dsDNA-binding protein that recruits Rif1, Rif2 and the Sir2/3/4 complex. Other proteins such as the YKu70/80 heterodimer complex and Tbf1 are also associated with telomeric and subtelomeric regions (**Figure 5**) (**Wellinger & Zakian, 2012**).

Subtelomeric regions are organised as heterochromatin and contain nucleosomes, subject to epigenetic regulation. This leads to the telomere position effect (TPE), wherein genes near telomeres are transcriptionally silenced (**Gottschling *et al.*, 1990; Guarente, 1999**). This silencing is mediated by the SIR complex, which is recruited via interactions with Rap1 and YKu70/80 (**Boulton & Jackson, 1998; Kozak *et al.*, 2010**).

Cdc13 is a critical protein that binds the 3' ssDNA overhang, covering approximately 11 out of the typical 12-15 nucleotides, thereby allowing only a single CST complex per telomere (**Hughes *et al.*, 2000; Wellinger & Zakian, 2012**). Once bound, Cdc13 recruits Stn1 and Ten1 to form the CST complex, which protects the telomere from nucleolytic degradation and regulates C-strand resection during replication (**Figure 1)** (**Grandin *et al.*, 2001**). Cdc13 also recruits the Est1 subunit of telomerase in late S-phase to promote telomere elongation (**Bianchi *et al.*, 2004**). Interestingly, while Stn1 and Ten1 have weak DNA-binding capacity on their own, their overexpression can partially compensate for Cdc13 loss (**Petreaca *et al.*, 2006 & 2007**).

Rap1 (Repressor Activator Protein 1) is a versatile transcription factor that regulates numerous genes. Although only a minority of Rap1 localises to telomeres (about 10%), it plays essential roles in telomere maintenance (**Wellinger & Zakian, 2012**). Rap1 binds telomeric dsDNA via its two Myb domains, each recognising the repeat motif 5'-GGTGT-3' with high affinity (i.e., canonical half-site affinity at 0.5 nM), enabling it to accommodate sequence heterogeneity between the two binding motifs (**Konig *et al.*, 1996; Kupiec, 2014**). It is believed that acquisition of the second Myb-domain made it possible for Rap1 to become main dsDNA telomere binder replacing its predecessor (**Konig *et al.,* 1996; Kupiec, 2014; Steinberg-Neifach *et al.,* 2015**) (more on this in the chapter *"Co-evolution of Telomere-associated Proteins and Telomeric DNA in Yeast"*). Rap1 binds approximately every 18 ± 4 bp, resulting in 15-20 proteins per telomere of ~300 bp (**Gilson *et al.*, 1993; Wright & Zakian, 1995; Konig *et al.,* 1996; Wellinger & Zakian, 2012**).

Rap1 also recruits Rif1 and Rif2, with Rif1 primarily associating with more internal telomeric regions and Rif2 localising near the terminus (**Figure 5**) (**Wellinger & Zakian, 2012**). This distribution underpins the Rap1-counting model of telomere length regulation: the more Rap1 binding sites, the greater the inhibitory signal against telomerase-mediated extension (**Marcand *et al.*, 1997; Levy & Blackburn, 2004; Teixeira *et al.*, 2004**). Specifically, Teixeira *et al.* (2004) showed that telomerase extends short telomeres (≤120 nt) more efficiently in the absence of Rap1-Rif1-Rif2, while extension of longer telomeres (>120 nt) is repressed due to greater binding of these inhibitors. Thus, Rap1-Rif1-Rif2 assembly ensures negative regulation of

telomere length – the longer the telomere is, the stronger the inhibition of telomerase due to their presence at a given telomere (**Levy & Blackburn, 2004; Teixeira *et al.,* 2004**).

Despite evidence that Rap1 recruits Rif1 and Rif2 through its C-terminal domain (**Hardy *et al.*, 1992; Wotton & Shore, 1997; Shi *et al.*, 2013**), Rosas Bringas *et al.* (2022) demonstrated Rap1-independent Rif2 recruitment via the MRX complex in tlc1-tm strain with mutant telomeric repeats. Both Rif2 and YKu complexes were shown to inhibit MRX-mediated telomere resection, with Rap1 and Rif2 playing a stronger role in this protective function compared to YKu. These findings support the hypothesis that yeast telomere capping mechanisms are redundant, likely evolving as an adaptive response to rapid changes in telomeric sequences and binding proteins.

Beyond telomere length regulation, Rap1 is known to contribute to telomere maintenance and to take part in many telomere-associated processes (**Kyrion *et al.,* 1993; Negrini *et al.,* 2007; Wellinger & Zakian, 2012; Shi *et al.,* 2013; Amelina *et al.,* 2015**). Thus, it prevents end fusions by blocking non-homologous end joining (NHEJ) and homologous recombination (HR), and ensures that telomeres are not misrecognised as DSBs. Rap1 also promotes TPE, nuclear periphery positioning of telomeres, and clustering during meiosis – key for faithful chromosome segregation. Furthermore, Rap1's roles extend beyond telomeres: upon redistribution from telomeres, it can drastically change cell's transcription profile and pace of senescence, and additionally to modulate its responses to stress such as DNA damage and sugar source starvation (**Platt *et al.*, 2013; Azad & Tomar, 2016**).

Due to Rap1's essential genome-wide roles, its deletion is unfeasible. However, its effects were studied through overexpression or targeted depletion. In Conrad *et al.* (1990), by overexpressing Rap1 from a high-copy plasmid (100-200 copies per cell) authors observed a significant increase in length heterogeneity in a bulk of Y' telomeres, and in some bearing only X element. Interestingly, such length heterogeneity appeared rapidly and almost with no lag. In addition, those cells that lost the plasmid showed no heterogeneity but their telomeres stayed shorter than those of the untransformed control. Cell's death rate was also increased owing chromosome loss and genome instability upon Rap1 excess levels.

Conversely, depletion of Rap1 at telomeres by using strain with mutant telomeric repeats or protein's truncated versions leads to different effects on telomeres including increase in telomere length and loss of TPE (**Rosas Bringas *et al.,* 2022; Kyrion *et al.,* 1993**). However, the role of Rap1 in telomere capping is not entirely essential and can be preserved, at least partially, by another telomere binder – for example, more "ancient" Tbf1 (**Kyrion *et al.*, 1993; Alexander & Zakian, 2003; Brevet *et al.*, 2003**). This redundancy adds to the idea that TBPs' binding to telomeres, especially those that are transcription factors, is just one of several functions performed by these versatile proteins (also, in the chapter *"ZnF Proteins & Genome Integrity"*).

Co-Evolution of Telomere-Associated Proteins and Telomeric DNA in Yeast

The length and sequence of telomeric repeats in yeasts of the Ascomycota phylum vary greatly among species of different clades (i.e., *Taphrinomycotina*, *Pezizomycotina*, and *Saccharomycotina*). The same is true for species of different families within the same clade (e.g., *Debaromycetaceae* and *Metschnikowiaceae*). Even quite closely related

species within one group, such as *Candida spp.*, exhibit differences and a relatively high frequency of nucleotide substitutions (**Figure 7**) (**Gunisova *et al.*, 2009**).

Such diversity might be explained by several scenarios of co-evolution between a telomere-binding protein (TBP) and its cognate target sequence. However, three interrelated concepts underpin all such scenarios (**Steinberg-Neifach *et al.*, 2015; Cervenak *et al.*, 2017 & 2021**):

i. the emergence of homologs from an ancestral recognition protein, followed by their functional specification and modification;

ii. the combinatorial recognition of the target DNA by a protein drawn from a pool of potential binders (typically, transcription factors);

iii. the adoption of alternative conformations and relaxation of recognition within the binding surface(s) of a TBP.

On the one hand, the emergence of non-canonical (i.e., non-TTAGGG) telomeric repeats might be explained by alterations in the template domain of yeast telomerase RNA (TER) at some point in evolution. This may have occurred due to a drastic environmental change or the gradual accumulation of point mutations that escaped evolutionary selection (**Teixeira & Gilson, 2005; Cervenak *et al.*, 2017 & 2021**). The presence of a new DNA sequence could have resulted in reduced binding affinity of the then-main TBP, while simultaneously enabling interactions with proteins previously not associated with telomeres and facilitating the emergence of novel TBPs.

This may be the case for Rap1, as the gene or its orthologs can be identified in many species of basal clades, where it serves as a transcriptional activator/repressor. However, in species of higher – and thus evolutionarily younger – clades, Rap1 assumes the role of a direct, rather than indirect (via protein-protein interactions as in, e.g., *S. pombe*), telomeric DNA-binding protein. Therefore, becoming the primary telomeric dsDNA-binding companion (**Figures 7 & 8**).

The Teixeira & Gilson (2005) review in *Springer* supports the hypothesis that Rap1's retention at telomeres was mainly enabled by the acquisition of a second Myb-domain at a certain evolutionary point. The ancestral proximity of Rap1 to telomeric DNA in basal clade species, combined with its two DNA-binding domains, made it possible for the protein to become the main dsDNA TBP in certain *Saccharomycotina* lineages.

Furthermore, as noted by Steinberg-Neifach & Lue (2015), the presence of two Myb-domains allows for flexible spacing between the binding sites, enabling Rap1 to tolerate variations in base pairs at the target DNA. Moreover, Rap1 is known for its flexibility – if not near-promiscuity – in DNA-binding sequence preferences, targeting at least 5% of all genes. This makes it an ideal candidate in the event of a TER-sequence-change "emergency" (**Platt *et al.*, 2013**).

It can also undergo various post-translational modifications and adopt alternative conformations, allowing it to relocate throughout the genome, radically altering the cell's gene expression profile during senescence, and recruit different co-factors depending on the specific sequence it binds (**König *et al.*, 1996; Pina *et al.*, 2003; Platt *et al.*, 2013; Steinberg-Neifach & Lue, 2015**). Interestingly, despite its essential role in many species, Rap1 was lost entirely in some lineages – failing to acquire any significant function, let alone a telomeric one (e.g., *Lipomycetaceae*, *Yarrowia* clade; **Figure 7 & 8**).

In addition, “evolutionally new” TBP such as Taz1 in *Taphrinomycotina* (**Figure 7**), in a similar to Rap1 fashion, displays a pattern of flexibility in binding to the target DNA sequences (**Sepsiova *et al.,* 2016**).

Overall, a general trend can be observed wherein a telomere’s historically predominant dsDNA-binding protein – typically one recognising the canonical TTAGGG, or similar, repeat found in more basal clades – gradually relinquishes its role as the main TBP. Thus, for instance, Tbf1 and Teb1 now serve as subtelomeric binding factors and/or transcription regulators instead (**Steinberg-Neifach & Lue, 2015; Cervenak *et al.*, 2017 & 2021**). This tendency underlines the functional plasticity and role-swapping potential of DNA-binding proteins.

On the other hand, the major ssDNA-binding protein Cdc13, which operates as part of the CST complex in *S. cerevisiae*, displays a high degree of structural plasticity and evolutionary resilience within the *Saccharomycotina* clade. Data on its organisational and functional properties suggest that the Cdc13A and Cdc13B versions were most likely fused in a common ancestor of *Saccharomycotina* yeasts (**Lue & Chan, 2013; Steinberg-Neifach & Lue, 2015**). This could explain why all *Saccharomyces* and *Kluyveromyces* species carry a single, relatively bulky, homologous version of the merged Cdc13 that structurally resembles the one found in *S. cerevisiae*. In contrast, most *Candida* species still possess two separate homologs – or, as in *C. parapsilosis*, a heterodimer of Cdc13A and Cdc13B that can bind complex telomeric sequences with greater than either homodimer alone affinity (**Steinberg-Neifach & Lue, 2015; Cervenak *et al.*, 2017**).

In the scenario where homologs emerged and one underwent functional specialisation to become a novel TBP, co-evolution of that TBP with its telomeric DNA target can be explored in species where a protein other than Rap1 serves as the main dsDNA binder (**Figure 7 & 8**). For example, *S. pombe* includes three dsDNA-binding proteins that function as TBPs in different species – Rap1, Tay1/Teb1 and Taz1 – yet only one of them, Taz1, fulfils the main telomeric role in this organism. Teb1, and its homolog Tay1 in *Y. lipolytica*, is among the oldest dsDNA TBPs with high affinity for TTAGGG repeats. However, the telomeres of *S. pombe* are heterogeneous, TG-rich tracts almost entirely lacking canonical repeats. Consequently, Teb1 is unlikely to associate with telomeres *in vivo* in *S. pombe* (**Cervenak *et al.*, 2017**). Meanwhile, Rap1 remains part of the shelterin complex in this species, although not as a direct telomeric dsDNA binder but as an interactor of Taz1. Cervenak *et al.* (2017) also propose that the transition from the canonical TTAGGG repeat to heterogeneous ones prompted the emergence of Taz1 and led to the loss of Teb1’s telomeric role, although retaining its functions in the internal parts of the genome.

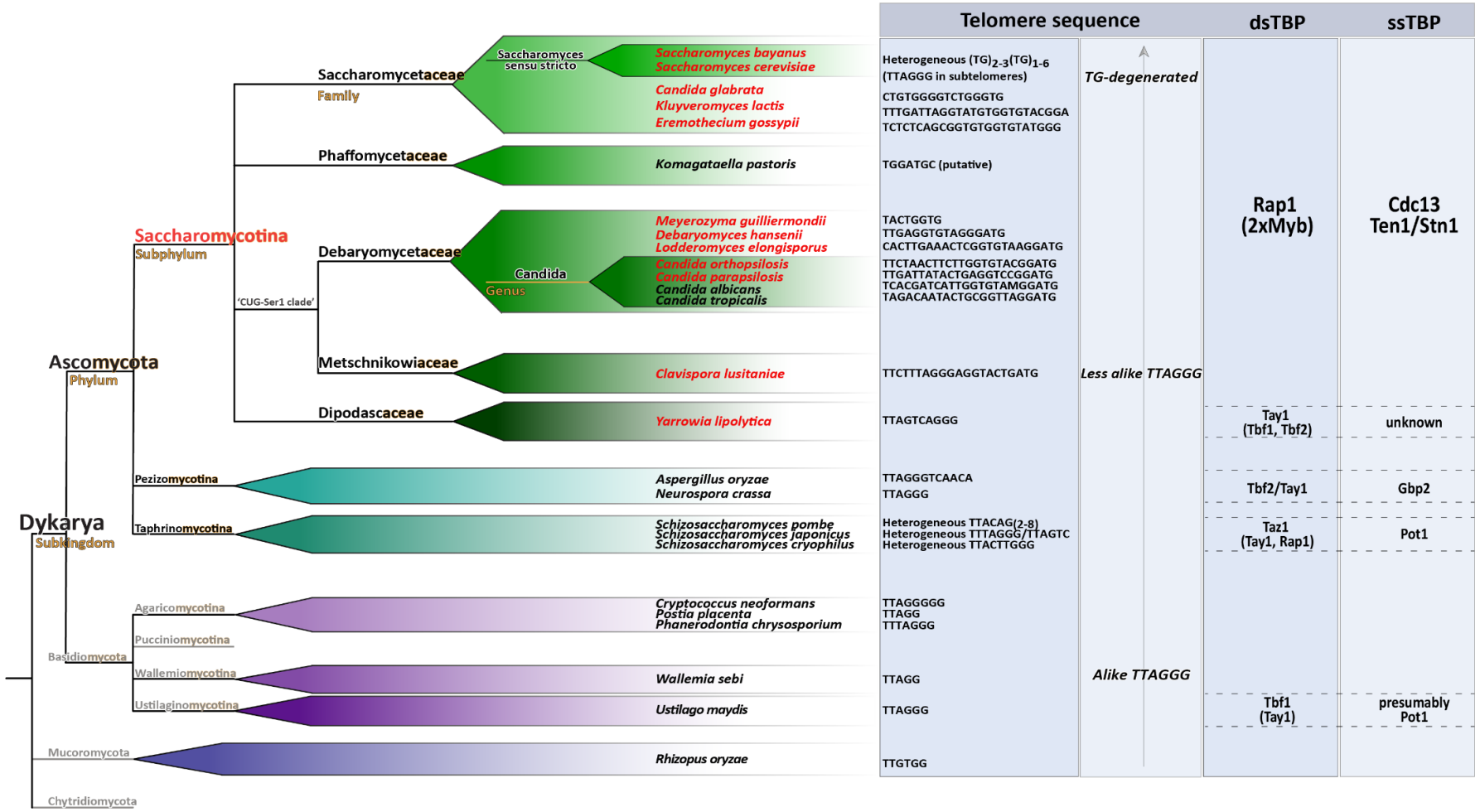

Figure 7. Overview of the Phylogenetic Tree of Yeast Species Relevant to This Study.
Telomere sequences are from **Myrray *et al.*, 1986; Champay *et al.*, 1984; McEachern & Blackburn, 1994; Lepingle *et al.*, 2000; Dietrich *et al.*, 2004; Teixeira & Gilson, 2005; Gunisova *et al.*, 2009; Cervenak *et al.*, 2017 & 2021**. Species marked in red were used in Telomere pull-downs (chapter *"Identifying Novel Telomere-Associated Proteins in Ascomycota Yeast Species"*). The tree topology is adapted from **Dujon *et al.*, 2010; Li *et al.*, 2021**. NCBI Tree Viewer was used to assemble the tree.
Abbreviations: dsTBP – double-stranded Telomere Binding Protein; ssTBP – single-stranded Telomere Binding Protein.

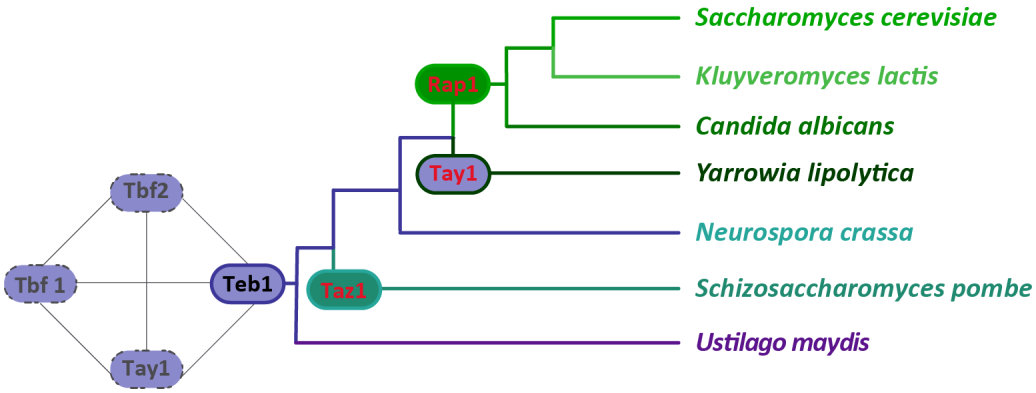

Figure 8. Proposed Model of Telomeric Protein Exchange and Evolution in Response to Telomeric DNA Sequence Divergence in Yeast.
Purple branches represent species with canonical or moderately modified telomeric repeat that use either Tbf1 or Teb1 as the main dsTBP. In this case – and most likely – Teb1 is the ancestral telomere-binding protein. In *Y. lipolytica*, Tay1 (dark green branch) which is a homolog of Teb1, is the only dsTBP in that species discovered to date; its binding telomeric repeat is proposed to be an insertion variant of the canonical TTAGGG (**Kramara *et al.*, 2010**). Taz1 (green branch) is a known main TBP in *Schizosaccharomyces* species. Rap1 (light green branch) is evolutionally novel main telomere-binder that is found in species of higher clades – such as *Candida*, *Kluyveromyces* and *Saccharomyces*.
Figure is adapted from **Cervenak *et al.*, 2017** with modifications.

There is also a hypothetical scenario that a *Saccharomycotina* ancestor might have been invaded by an intracellular pathogen targeting and cleaving either the TER or telomeric DNA sequences. This event may have promoted changes in these sequences, driving selection for modified variants (**Lue *et al.*, 2010**). In response, TBPs would have had to adapt to preserve their telomeric functions – via the mechanisms outlined above – in order to survive this evolutionary contest.

To encapsulate, current understanding suggests that an initial trigger – possibly environmental or pathogenic – provoked a drastic change in the telomeric sequence of an ancestral yeast, originally bearing either the canonical TTAGGG or a highly similar repeat. This likely occurred around the diversification of the *Dikarya* subkingdom into *Ascomycota* and *Basidiomycota* (**Figure 7**). The event led to the replacement of the then-main dsDNA TBP, which retained high binding affinity for the TTAGGG repeat, by a protein with less orthodox binding preferences. This successor may have emerged following whole genome duplication and/or through acquisition/duplication of DNA-binding domain(s) – evolutionary milestones that facilitated an appreciable diversification of TBPs. As a result, four major telomeric (and/or subtelomeric) players have been identified across the yeast phylogenetic tree to date: Tbf1, Tay1, Taz1 and Rap1, alongside a broad spectrum of telomeric repeats – ranging from significantly to minimally divergent from the canonical TTAGGG – found in these species (**Figure 7 & 8**).

Zinc Finger Proteins & Genome Integrity

A zinc finger domain (ZnF) is a small structural protein motif characterised by the presence of one or more Zn^{2+} ions coordinated by cysteine (Cys) and histidine (His) amino acids in a number of combinations. Through interaction with these amino acids, Zn^{2+} stabilises their positions within the protein, thereby serving as a prerequisite for the protein's overall stabilisation, folding and conformation. Depending on the specific distribution pattern of Cys and His residues, a variety of ZnF domains are distinguished. In humans, proteins containing ZnF domains represent one of the largest classes of DNA-binding proteins, comprising more than 50 distinct domains encoded by approximately 3-5% of all human genes (**Klug, 2010; Vilas *et al.*, 2018**).

The first ZnF-domain-containing protein, TFIIIA (Transcription Factor IIIA), was reported in the 1980s. It was isolated from oocytes of the African clawed frog (*Xenopus laevis*) and shown to contain 7-11 zinc atoms arranged in nine similar domains of approximately 30 amino acids, with invariant Cys-His pairs – commonly observed ligands for Zn^{2+} ions (**Miller *et al.*, 1985; Diakun *et al.*, 1986**). Since then, various Cys-His compositions have been described. However, the most abundant and widely studied class of ZnFs is the "classical/canonical" or "typical" C2H2-type (also abbreviated as Cys2His2-type), characterised by the Cys-x-Cys-x-His-x-His motif, where "x" denotes a variable amino acid. This domain includes two β-sheets and one α-helix, forming a "pinch grip"-like structure which, together with the Zn^{2+} ion, can "grasp" DNA – hence the term "finger" (**Zhang *et al.*, 2011**). This ability for site-specific DNA recognition made ZnFs valuable tools in genome editing prior to discovery of the eminent CRISPR-Cas9.

Interestingly, beyond the well-known C2H2-type, several other ZnF groups are recognised based on their ability to mediate interactions with other proteins, in addition to or instead of DNA-binding. These include LIM (Lin-11, Isl-1, Mec-3), RING (Really Interesting New Gene), PHD (Plant Homology Domain), and MYND (myeloid, Nervy, DEAF-1) domains – all of which are Zn^{2+}-binding motifs coordinating two zinc ions (**Figure 9**) (**as classified in Matthews *et al.*, 2009**).

Typically, ZnF proteins contain multiple functional domains, enabling them to participate in diverse signalling and chromatin-related pathways while fulfilling a variety of roles. Their capacity to bind substrates including DNA, RNA, proteins and lipids (**Figure 11**), combined with considerable structural and functional diversity, makes ZnFs pivotal for normal cellular function and, all in all, organismal well-being. While many ZnF proteins – particularly from the C2H2 group – are known primarily as transcription factors, a substantial number also contribute to genome stability and integrity without functioning in transcription.

For instance, ZnFs from the RING group are commonly associated with ubiquitination and are frequently found in E3 ubiquitin protein ligases. A key example is MDM2 (Mouse Double Minute 2), a ZnF protein that does not function as a transcription factor but acts as a negative regulator of the tumour suppressor p53, a protein often mutated in human cancers. MDM2 modulates p53 transcription, stability and localisation. It promotes p53 ubiquitination, targeting it for proteasomal degradation, and inhibits its interaction with target genes. Furthermore, MDM2 can bind directly to the N-terminus of p53, causing its translocation from the nucleus to the cytoplasm, thereby preventing gene activation. MDM2 expression is amplified in approximately 7% of human cancers, including liposarcomas, osteosarcomas, soft tissue tumours and oesophageal carcinomas (**reviewed in Oliner *et al.*, 2016; Cassandri *et al.*, 2017**).

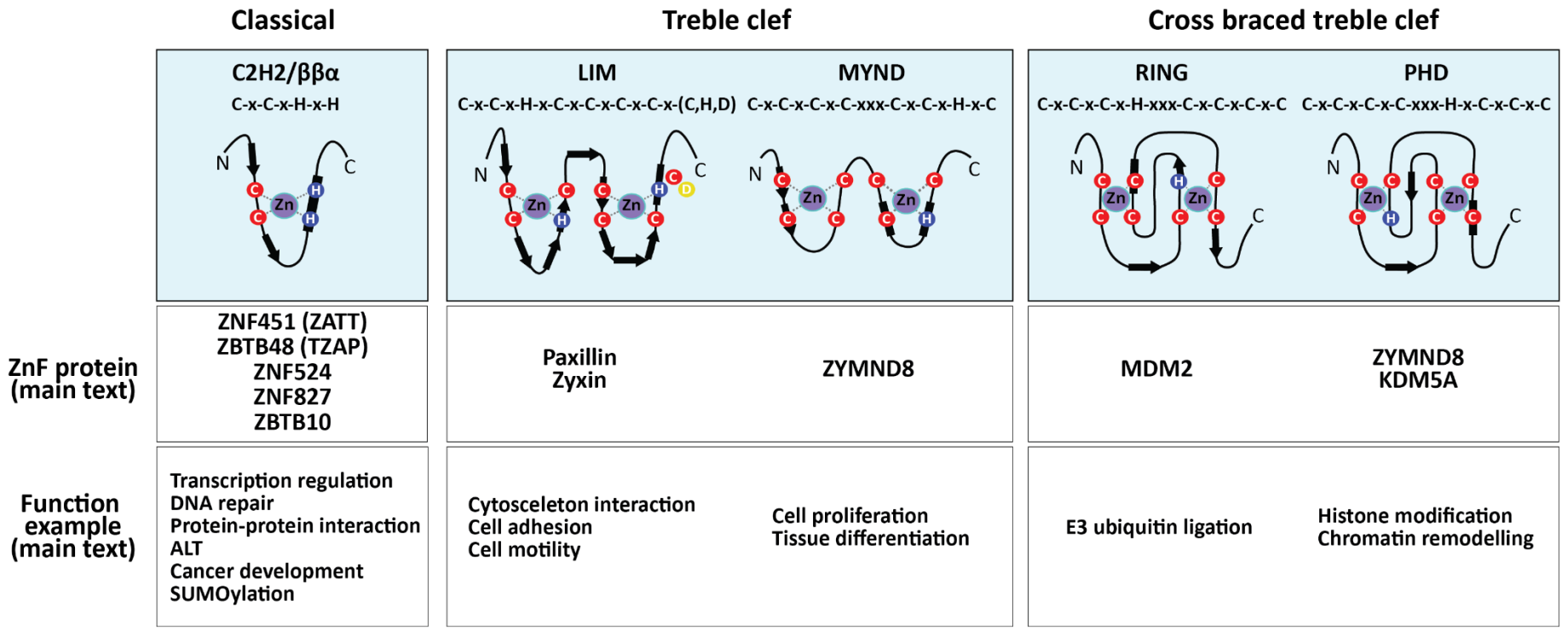

Figure 9. Types of ZnF Protein Domains.
Topology of five ZnF domains, protein examples and their functions (from the main text).
Abbreviations: C – Cysteine, H – Histidine, D – Aspartate; ALT – Alternative Lengthening of Telomeres.

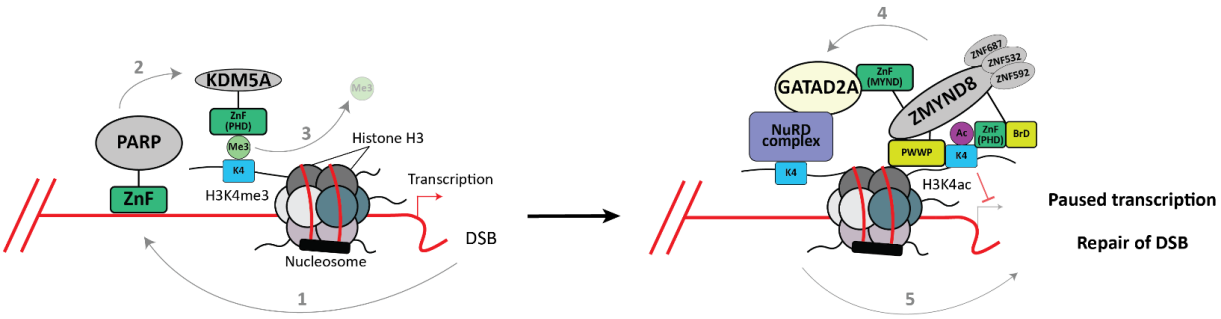

Figure 10. ZMYND8-Mediated DNA Damage Response (DDR) Pathway.
PARP recognises DNA damage signal and binds upstream of the DSB via its ZnF domains (**1**); Binding of PARP promotes recruitment of KDM5A (**2**) which recognises and promotes demethylation of lysine 4 (K4) at histone H3 via its PHD ZnF domain (**3**); ZMYND8 can now bind to acetylated chromatin (H3K4ac) via its PWWP, PHD ZnF and bromodomain (BrD) and, at the same time, interact with GATAD2A subunit of NuRD complex (**4**) that recognises demethylated chromatin and promotes repression of active transcription until DSB is repaired (**5**).

Notably, PHD domain-containing ZnFs are typically implicated in histone post-translational modifications (PTMs) and in DNA structure-dependent processes such as DNA repair, chromatin regulation and remodelling. The PHD motif (C-x-C-x-C-x-C-xxx-H-x-C-x-C-x-C) bears structural similarity to the RING motif (C-x-C-x-C-x-H-xxx-C-x-C-x-C-x-C), and both were initially thought to serve as ubiquitin ligases (**Aravind *et al.*, 2003; reviewed in Matthews *et al.*, 2009; Singh & van Attikum, 2021**).

A good example of ZnF proteins with multiple functional domains, including PHD, are those involved in the KDM5A-PARP and ZMYND8-NuRD complex-mediated DDR and DSB repair pathways (**Figure 10**).

ZMYND8 is a chromatin-associated protein containing four functional domains, including two ZnFs – PHD and MYND. It also features a bromodomain, which recognises acetylated lysine residues on histone tails, and a PWWP domain, another chromatin methylation reader that binds both DNA and histone methylated lysin (**Li *et al.*, 2016; Savitsky *et al.*, 2016**).

KDM5A is a histone demethylase targeting the H3K4me3 epigenetic mark and contains three PHD ZnFs (**Kataria & Tyagi, 2023**). PARP recognises ssDNA and dsDNA breaks through its two DNA-binding ZnFs (**Kanev *et al.*, 2024).**

The NuRD complex (Nucleosome Remodelling and Deacetylase) is a major ATP-dependent chromatin remodelling complex involved in DDR, histone modification, nucleosome positioning, cell cycle progression, embryonic development, oncogenesis, and more (**reviewed in Basta & Rauchman, 2015**).

Functionally, the ZMYND8-NuRD association mediates transcriptional repression and activation of DNA repair machinery at DSB sites via homologous recombination. Initially, PARP detects the break via its ZnFs (**Figure 10**), which recruits KDM5A to demethylate H3K4me3 in the vicinity, allowing ZMYND8-NuRD to localise to the break and pause nearby

transcription until repair is completed. ZMYND8 also recruits additional ZnF proteins – ZNF532, ZNF592 and ZNF687 – although their exact roles remain elusive (**Gong *et al.*, 2015 & 2017; Torres *et al.*, 2015; Savitsky *et al.*, 2016; Spruijt *et al.*, 2016**).

Proteins of the LIM group exhibit diverse topologies and functions, including gene expression regulation, cell adhesion and motility, cytoskeletal interactions and signal transduction (**Figure 9**) (**reviewed in Matthews *et al.*, 2009**). This ZnF motif mediates protein-protein interactions, allowing LIM-containing proteins to act as molecular scaffolds or bridges (**Gamsjaeger *et al.*, 2007**). For example, paxillin and zyxin both contain LIM domains and serve as adaptor proteins, recruiting cytoskeletal regulators and collectively promoting actin recovery at sites of stress fibre strain (**Smith *et al.*, 2013**).

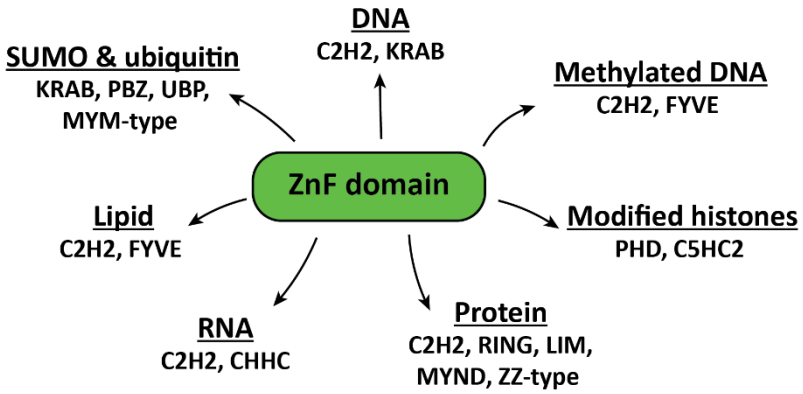

Figure 11. ZnF Proteins Bind Diverse Substrates Depending on ZnF Domain Type.
Underscored are substrates with the examples of ZnF domains permitting the interaction. See main text for details.

Many ZnF proteins contribute to genome integrity, with classical C2H2-type ZnFs being especially widespread and capable of recognising altered DNA structures. For instance, aprataxin is an enzyme involved in resolving abortive DNA ligation intermediates, such as cytotoxic 5′-adenylated (5′AMP) DNA termini produced by oxidative stress – particularly in neurons, which exhibit high oxidative metabolism. Aprataxin's ZnF domain confers high-affinity binding to AMP-DNA, enabling hydrolase activity and damage resolution. Mutations or truncations in this ZnF result in DNA damage accumulation and are linked to the neurodegenerative disorder ataxia oculomotor apraxia (**Seidle *et al.*, 2005; Ahel *et al.*, 2006; Rass *et al.*, 2007; Tumbale *et al.*, 2011**).

Another C2H2 ZnF-containing protein involved in genome maintenance is ZATT (ZNF451), a SUMO E3 ligase (Small Ubiquitin-related protein Modifier) with several C2H2-type ZnFs. ZATT interacts with TDP2 and TOP2. The latter is a topoisomerase that creates DSBs helping to resolve DNA supercoiling and topological stress during transcription and replication (**Cappadocia *et al.*, 2015**). However, TOP2 can become stalled in protein-DNA cleavage complexes (TOP2cc) as transient intermediates, posing a threat to genome stability.

ZATT facilitates the SUMOylation of TOP2 when it is bound by tyrosyl-DNA phosphodiesterase TDP2, and also stimulates TDP2's activity to resolve TOP2cc protein-DNA crosslinks (**Cappadocia *et al.*, 2015; Schellenberg *et al.*, 2017; Tammaro *et al.*, 2013**). These features make ZATT a potential target in chemotherapies that employ etoposides – topoisomerase inhibitors that increase TOP2cc levels (**reviewed in Pommier, 2013; Tammaro *et al.*, 2013).**

Importantly, beyond contribution to DDR and genome stability, a considerable number of ZnF proteins have been implicated in telomere biology (**Figure 12**). One of the first ZnFs reported as to be involved in telomere length regulation was ZSCAN4 (ZnF and SCAN domain-containing protein 4), which is essential in embryonic stem cells for telomere extension during early developmental stages. ZSCAN4 promotes genome-wide DNA demethylation, enabling telomerase-mediated telomere elongation. Depletion of ZSCAN4 or mutation of the fourth ZnF-domain in its C-terminus results in the loss of demethylation function leading to telomeres shortening and elevated levels of recombination during early stages of embryogenesis (**Dan *et al.*, 2017**).

A number of ZnFs were also reported to take part in ALT (**Figure 12**). For instance, ZNF827 (C2H2-type) can recruit forementioned nucleosome-remodelling NuRD complex to telomeres that utilise ALT. Thus, ZNF827 recruitment to telomeres occurs via two nuclear hormone receptors – TR4 and COUP-TF2 – which can bind variant telomeric repeat, T**C**AGGG, frequently found in ALT cells. NuRD-ZNF827 interaction facilitates the recruitment of DNA repair proteins promoting telomere-telomere HR and elongation of chromosome termini via ALT (**Conomos *et al.*, 2014**).

ZBTB48 (TZAP), with eleven C2H2 ZnFs, binds canonical TTAGGG repeat on overly elongated telomeres – those with low Shelterin protein levels. Such telomeres can cause genome instability, and by binding them TZAP ensures the mechanism known as "telomere trimming", which places an upper limit on telomere length making TZAP a negative regulator of telomere length. Further length homeostasis is achieved via competition between TRF1-TRF2 and TZAP (**Pickett *et al.*, 2009; Jahn *et al.*, 2017; Li *et al.*, 2017; Rivera *et al.*, 2017**).

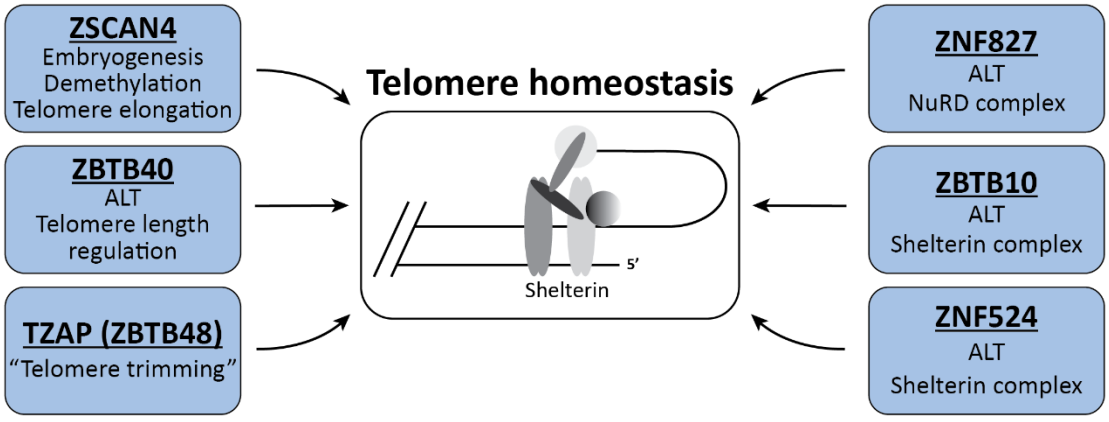

Figure 12. ZnF Proteins and Telomere Maintenance.
Examples of ZnF proteins that promote telomere homeostasis via different mechanisms (see main text). **Abbreviations:** ALT – Alternative Lengthening of Telomeres.

Similarly to ZBTB48 as BTB- and ZnF-containing protein, ZBTB10 associates with telomeres in ALT-positive cells by binding TT**G**GGG variant repeat. ZBTB10 interacts with TRF2/RAP1, though it does not appear to affect telomere length or to compete with Shelterin components (**Bluhm *et al.*, 2019; Wang *et al.*, 2023**).

ZNF524 also binds telomeres directly in both ALT- and telomerase-positive cells, with predominant activity in the former. Interestingly, it moderately influences TRF2-RAP1 localisation at telomeres, however, without affecting expression of either or via direct interaction. The exact mechanism, in this case, remains to be further explored (**Braun & Xu *et al.*, 2023**).

Recently, ZBTB40 (ZNF923) was identified as a negative regulator of telomere length. Its loss in ALT cells results in telomere elongation and accumulation of telomere dysfunction-induced foci (TIFs). ZBTB40 may also regulate telomeric recombination, as suggested by increased ALT-associated promyelocytic leukaemia bodies (APBs) upon knockout (**Zhou *et al.*, 2023**).

To conclude, as with other ZnF proteins found at telomeres – in addition to the eminent Shelterin complex members – an intricate network of those that are less abundant at chromosomal termini, yet important, is emerging. Especially under abnormal conditions such as ALT. Given the capacity of ZnFs to bind varied substrates and participate in diverse pathways – even within the same domain class – the question of how this functional network of interactions is regulated to ensure balanced DNA damage response, telomere dynamics and genome integrity remains to be fully elucidated.

Rationale

Telomeres, as safeguards of chromosomal termini, are fundamental components of chromosomal architecture that ensure genome stability and integrity. Their primary functions include protecting DNA ends from degradation and end-to-end fusions, as well as preventing inappropriate activation of DNA repair pathways. These essential roles rely heavily on proteins that associate with and bind to telomeric DNA.

Zinc finger domain-containing proteins (ZnFs) are known to participate in a broad array of molecular pathways and processes, including alternative lengthening of telomeres (ALT), cancer development and progression, the DNA damage response (DDR), and telomere maintenance. Moreover, numerous studies have highlighted their widespread and significant contributions to genome integrity, even when their individual roles may be context-specific or only facilitative.

The identification and characterisation of such proteins are crucial for advancing our understanding of telomere biology and genomic regulatory mechanisms. These insights, in turn, may have implications that extend beyond fundamental science, particularly in relation to human diseases and cancer research. In other words, elucidating ZnF protein functions holds potential for translational applications in cancer, ageing, and other conditions linked to genomic instability.

Yeast, and notably the budding yeast *Saccharomyces cerevisiae*, has proven to be an invaluable model organism, widely utilised to explore a variety of biological questions, including those related to telomere biology. A substantial body of work has been conducted – at least in part – in yeast, investigating replicative senescence, telomere maintenance and stability, DDR, ALT and survivor formation, telomeric transcription, and other related processes (**e.g., Yu *et al.*, 2014; Liu *et al.*, 2019; Jurikova *et al.*, 2020; Yao *et al.*, 2021; Misino *et al.*, 2018 & 2022**).

In this thesis, two novel telomere-associated ZnF proteins were identified using quantitative interactomics – an approach that has proven to be a powerful tool for discovering new factors in a variety of biological contexts (**Kappei *et al.*, 2017**).

In addition to identifying these proteins across several *Ascomycota* yeast species, their initial characterisation in relation to telomere biology was carried out in *S. cerevisiae*. The transcription factors and paralogs identified – Tda9 and Rsf2, both ZnF-domain-containing proteins – were shown to associate with telomeres and to influence multiple aspects of telomere maintenance, integrity, and architecture in yeast. Notably, neither of these proteins had previously been implicated in connection with telomeres.

This work, thus, provides valuable insights into two ZnF-domain proteins that were previously uncharacterised in the context of telomere biology. Although their precise roles at yeast telomeres remain to be fully elucidated, the evidence for their telomeric association is compelling and establishes a solid foundation for future investigation.

Results and Discussion

Identifying Novel Telomere-Associated Proteins in *Ascomycota* Yeast Species

As shown in the chapter *"Co-evolution of Telomere-Associated Proteins and Telomeric DNA in Yeast"*, telomeric sequences within Ascomycota yeasts – particularly those belonging to the *Saccharomycotina* subphylum – are exceptionally diverse and typically TG-degenerated (see **Figure 7**). Consequently, telomere-associated and telomere-binding proteins are not necessarily conserved across species and may differ substantially between clades. To explore this further, we employed a quantitative proteomics approach, following methodologies similar to those described in Kappei *et al.* (2017) and Nischwitz, Schoonenberg *et al.* (2023).

In brief, biotinylated DNA oligonucleotides corresponding to the published or proposed at the time telomeric sequences (DNA bait) for each of the 12 yeast species examined in this study, along with a random sequence control (DNA control), were used to perform telomeric pull-down assays using whole-cell protein extracts (**Figure 13, A**). The pulled-down proteins were subsequently analysed via dimethyl labelling (DML) mass spectrometry (MS). By comparing control and telomere-bait outputs, we were able to identify proteins that associate *in vitro* with telomere-mimicking sequences in these yeast species.

Given the evolutionary conservation of gene orthologs and their established roles in telomere-related processes, we expected to detect Rap1 in many, if not all, of the species studied. Indeed, Rap1 was among the most enriched proteins in 9 out of 12 species, with particularly strong enrichment in *Saccharomycotina* species (**Figure 13, B**). It is worth noting that due to the generally poor annotation of the databases used for MS data interpretation in non-model yeasts, we relied on Gene Orthology (GO) analysis – using the *S. cerevisiae* genome as a reference – to identify Rap1 and other orthologous proteins. However, the consistent and substantial enrichment of Rap1 across 75% of the species served to validate both our approach and the robustness of the resulting data.

Thus, Rap1 was found to associate *in vitro* with telomeric sequences in 9 species (**Figure 13, B**). Despite multiple rounds of protocol optimisation, I was unable to detect Taz1 – the primary double-stranded telomeric DNA binder – in *S. pombe*.

Similarly, the expected major telomere-binding protein Tay1 in *Y. lipolytica* was among non-enriched proteins. This, however, is likely attributable to an incorrect telomeric repeat sequence being used as bait; the sequence available and proposed at the time (GGACGATTG; **Teixeira & Gilson, 2005)** was later revised (TTAGTCAGGG; **Cervenak *et al.*, 2021**).

Interestingly, in three species – *C. parapsilosis*, *C. glabrata* and *M. guilliermondii* – a zinc finger-containing protein, Spt10 (YJL127C), was identified as an enriched ortholog (**Figure 13, C**). In *S. cerevisiae*, Spt10 functions as a histone H3 acetylase and transcriptional activator of histone genes, particularly involved in S phase-specific H3K56 acetylation at histone promoters – a modification required for recruitment of the SWI/SNF chromatin remodelling complex. Spt10 also plays roles in DNA repair and in silencing near telomeres, at the silent mating-type loci and within ribosomal DNA (rDNA) repeats. In *spt10* deletion mutant, telomeric silencing is impaired, and mutations in the protein influence both Sir protein

recruitment and histone modifications at telomeric regions. Interestingly, however, neither Spt10 nor its known interactor Spt21 has been shown to associate directly with chromatin at telomeres (**Chang & Winston, 2011**).

Another orthologous protein, Npl3 (YDR432W), previously identified via a similar pull-down approach in *S. cerevisiae*, was also detected in this study in two species: *S. pombe* and *D. hansenii* (**Figure 13, C**). Npl3 has been shown to bind TERRA and stabilise R-loops at short telomeres, thereby promoting HDR with the effect on prevention of the premature development of replicative senescence onset (**Perez-Martinez *et al*., 2020**).

Overall, in all analysed species, GO enrichment analysis of cellular components revealed a predominance of nuclear-localised proteins (**Figure 14**). Importantly, the use of whole-cell extracts (rather than isolated nuclear fractions) in the pull-downs strengthens the case for the specificity and efficacy of the experimental approach.

GO analysis of molecular function among these nuclear proteins indicated notable enrichment in clusters associated with zinc/metal ion binding, telomeric DNA binding and sequence-specific DNA binding (**Figure 14**).

Taken together, many of the orthologous proteins identified in the pull-downs are transcription factors, with a substantial fraction of these containing zinc finger domains (**Figure 13, C and Figure 14**).

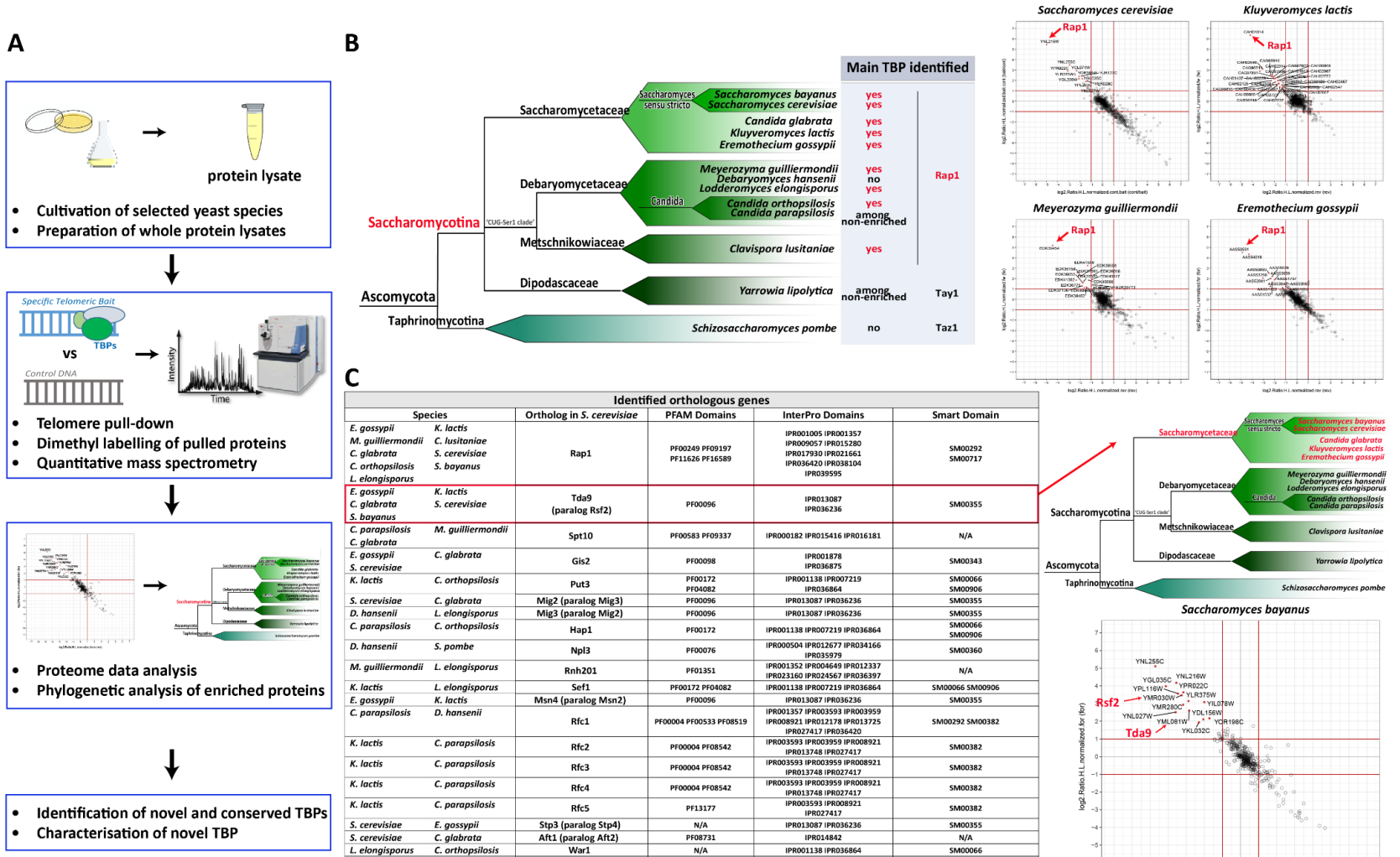

C

Identified orthologous genes					
Species		Ortholog in *S. cerevisiae*	PFAM Domains	InterPro Domains	Smart Domain
E. gossypii *M. guilliermondii* *C. glabrata* *C. orthopsilosis* *L. elongisporus*	*K. lactis* *C. lusitaniae* *S. cerevisiae* *S. bayanus*	Rap1	PF00249 PF09197 PF11626 PF16589	IPR001005 IPR001357 IPR009057 IPR015280 IPR017930 IPR021661 IPR036420 IPR038104 IPR039595	SM00292 SM00717
E. gossypii *C. glabrata* *S. bayanus*	*K. lactis* *S. cerevisiae*	Tda9 (paralog Rsf2)	PF00096	IPR013087 IPR036236	SM00355
C. parapsilosis *C. glabrata*	*M. guilliermondii*	Spt10	PF00583 PF09337	IPR000182 IPR015416 IPR016181	N/A
E. gossypii *S. cerevisiae*	*C. glabrata*	Gis2	PF00098	IPR001878 IPR036875	SM00343
K. lactis	*C. orthopsilosis*	Put3	PF00172 PF04082	IPR001138 IPR007219 IPR036864	SM00066 SM00906
S. cerevisiae	*C. glabrata*	Mig2 (paralog Mig3)	PF00096	IPR013087 IPR036236	SM00355
D. hansenii	*L. elongisporus*	Mig3 (paralog Mig2)	PF00096	IPR013087 IPR036236	SM00355
C. parapsilosis	*C. orthopsilosis*	Hap1	PF00172	IPR001138 IPR007219 IPR036864	SM00066 SM00906
D. hansenii	*S. pombe*	Npl3	PF00076	IPR000504 IPR012677 IPR034166 IPR035979	SM00360
M. guilliermondii	*L. elongisporus*	Rnh201	PF01351	IPR001352 IPR004649 IPR012337 IPR023160 IPR024567 IPR036397	N/A
K. lactis	*L. elongisporus*	Sef1	PF00172 PF04082	IPR001138 IPR007219 IPR036864	SM00066 SM00906
E. gossypii	*K. lactis*	Msn4 (paralog Msn2)	PF00096	IPR013087 IPR036236	SM00355
C. parapsilosis	*D. hansenii*	Rfc1	PF00004 PF00533 PF08519	IPR001357 IPR003593 IPR003959 IPR008921 IPR012178 IPR013725 IPR027417 IPR036420	SM00292 SM00382
K. lactis	*C. parapsilosis*	Rfc2	PF00004 PF08542	IPR003593 IPR003959 IPR008921 IPR013748 IPR027417	SM00382
K. lactis	*C. parapsilosis*	Rfc3	PF00004 PF08542	IPR003593 IPR003959 IPR008921 IPR013748 IPR027417	SM00382
K. lactis	*C. parapsilosis*	Rfc4	PF00004 PF08542	IPR003593 IPR003959 IPR008921 IPR013748 IPR027417	SM00382
K. lactis	*C. parapsilosis*	Rfc5	PF13177	IPR003593 IPR008921 IPR027417	SM00382
S. cerevisiae	*E. gossypii*	Stp3 (paralog Stp4)	N/A	IPR013087 IPR036236	SM00355
S. cerevisiae	*C. glabrata*	Aft1 (paralog Aft2)	PF08731	IPR014842	N/A
L. elongisporus	*C. orthopsilosis*	War1	N/A	IPR001138 IPR036864	SM00066
D. hansenii	*Y. lipolytica*	Mga2 (paralog Spt23)	PF01833 PF12796	IPR002110 IPR002909 IPR013783 IPR014756 IPR020683 IPR036770	SM00248 SM00429

Figure 13. Results of Telomere Pull-Downs in Ascomycota Yeast Species.

A. Schematic of phylogenetic approach and project outline. **B.** Rap1, as validating the approach control, identified in 75% species used in this study. **C.** Results of gene orthology analysis identified two novel telomere binders, Tda9 and its paralog Rsf2, in *Saccharomycetaceae* spp. **Abbreviations:** TBP – Telomere Binding Protein.

Data from table under **C** produced by [redacted].

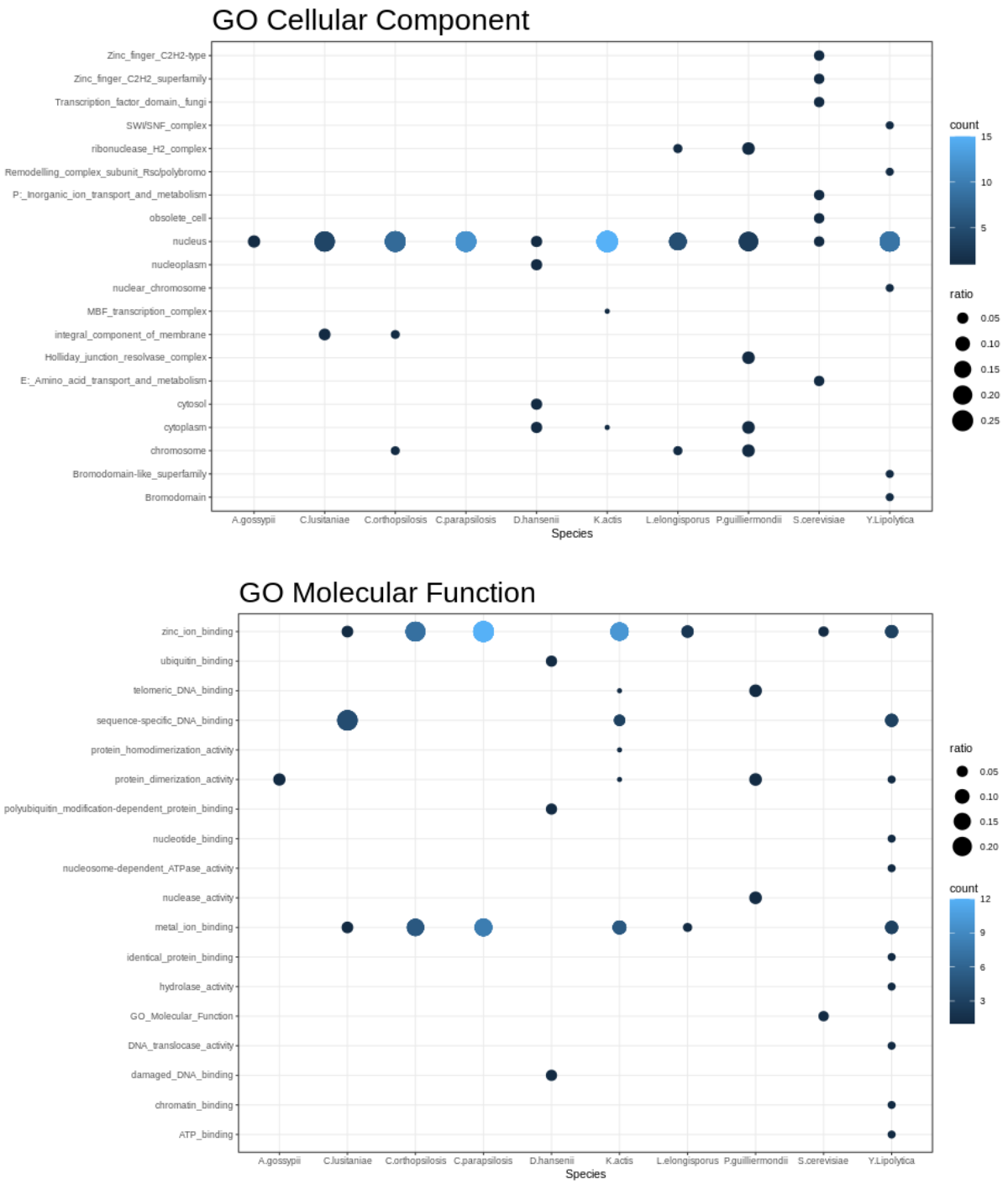

Figure 14. GO Enrichment Analysis of Cellular Components & Molecular Functions. Majority of analysed enriched proteins pulled across different species localise to nucleus (**Go Cellular Component**) with a significant fraction of those being from clusters of Zn^{2+}-binding (**GO Molecular Function**). The size of the dots indicates enrichment ratios, and colour intensity indicates protein counts associated with each term.
Data [redacted].

Paralogs TDA9 and RSF2 Bind Yeast Telomeric Sequences *in vitro*

In the pull-downs, the second most enriched orthologous protein after Rap1 was Tda9 (Topoisomerase I Damage Affected, YML081W). In *S. cerevisiae*, this protein has a paralog, Rsf2 (Respiration Factor 2, YJR127C), which arose from the whole-genome duplication event (**Figure 13, C**). Depending on the biological replicate and MS run, either one or both proteins were observed among enriched ones in *S. cerevisiae* and *S. bayanus*. Additionally, GO term analysis identified Tda9 as an enriched orthologous gene in three further yeast strains. In total, Tda9/Rsf2 were detected in *E. gossypii*, *K. lactis*, *C. glabrata*, *S. cerevisiae* and *S. bayanus* (**Figure 13, C**).

Tda9 was among ten previously uncharacterised proteins in terms of their association with Top1. It was identified and named based on results from a high-throughput screen involving overexpression of the *top1-T722A* allele. In this screen, Tda9 was classified as one of the proteins affected by Topoisomerase I-induced DNA damage, as its null mutant exhibited sensitivity to *top1-T722A* overexpression, leading to cell death (**Reid *et al.*, 2011**). Topoisomerases are enzymes that resolve DNA topological stress by introducing single-stranded breaks during DNA replication, transcription, and repair, and they are key targets in anti-cancer chemotherapy (**Afzal *et al.*, 2015**). The *top1-T722A* mutant allele mimics treatment with camptothecin (CPT), a drug that stabilises Topoisomerase I-DNA complexes and prevents DNA religation, ultimately causing DNA breaks. CPT is known for its potent anti-tumour activity (**Reid *et al.*, 2011; Slichenmyer *et al.*, 1993; Liu *et al.*, 2000**).

Tda9 has also been reported to function as a transcription factor involved in the regulation of acetic acid production (**Walkey *et al.*, 2012**). Specifically, it modulates mRNA levels of *ALD6* (encoding mitochondrial ACDH) and, to a lesser extent, *ALD4* (cytosolic ACDH), both enzymes involved in acetate synthesis via the pyruvate dehydrogenase bypass. The study reported that Tda9 stimulates *ALD6* transcription via a predicted GAGGGG binding site located 590 bp upstream of the start codon.

Rsf2, on the other hand, has been characterised as a transcription factor that regulates nuclear and mitochondrial gene expression, including genes such as *GUT1* and *GUT2*, and others involved in respiratory metabolism (e.g., *MRP13*, *COX4*, *LEU3*, *ALD6*) and glycerol utilisation (**Lu *et al.*, 2005**). Despite possessing two classical ZnF domains, the same study by Lu *et al.* (2005) could not identify Rsf2's upstream activating sequences (UASs) for target genes, thus, suggesting it may not bind DNA directly. Lu *et al.* (2005) proposed that Rsf2 could act higher up in the transcriptional regulatory network by modulating the expression of other transcription factors.

Nevertheless, both pGUT2 and pALD6 upstream regions were used in this study to design primers for "putative" ChIP positive controls (chapter *"TDA9 and RSF2 Associate to Telomeres in vivo"*, **Figure 16, D and Figure 17, A**).

Tda9 and Rsf2 are relatively large proteins – Tda9 consists of 1251 amino acids (141.5 kDa), and Rsf2 of 1380 amino acids (155 kDa). Both proteins contain two classical C2H2-type ZnF domains near the N-terminus and a fungal transcription factor regulatory middle homology domain (fungal_TF_MHR, cd12148), commonly found in transcription factors with ZnFs (**Figure 15, A**). Neither gene is essential, as yeast mutants with single or double deletions are viable (**yeastgenome.org**). Although Tda9 and Rsf2 lack direct human

orthologs, BLAST analysis against the human genome identified 13 matching sequences collectively showing ~52% similarity to PRDM9.

PRDM9 is a ZnF-domain histone methyltransferase that can trimethylate H3K4 and H3K36, promoting nucleosome reorganisation and establishing nucleosome-free regions that serve as focal points for DSB formation – essential for enabling HR as DNA exchange between chromosomes at meiotic recombination hotspots. PRDM9 also forms complexes with other proteins to recruit recombination machinery to DSB sites (**reviewed in Paigen & Petkov, 2018**).

To date, neither Tda9 nor Rsf2 has been reported to associate with telomeres. However, STRING analysis of their predicted interactors suggests their potential involvement in DNA replication stress response and histone-related functions (**Figure 15, D**).

For example, Pham *et al.* (2007) proposed that Tda9 likely recruits histone acetyltransferase (HAT) to activate gene expression. In that study, reduced H3K18 acetylation was observed in *tda9* deletion mutant at the promoter of uncharacterised protein *YDR525W* (Api2). In a subsequent study by Dai *et al.* (2009), a Kolmogorov-Smirnov statistical test on TF-acetylation association cohorts confirmed that Tda9-H3K18 was among ~47% of pairs showing significant gene expression changes upon TF deletion ($P < 0.01$).

As for Rsf2, predicted interactors such as Cat8 and Tsl1 are reported to exhibit increased expression and nuclear localisation under DNA replication stress (**string-db.org; yeastgenome.org**). Notably, Cat8 was also typically enriched in our telomere pull-downs in *S. cerevisiae*, *S. bayanus*, *K. lactis* and *C. parapsilosis*, which may suggest a protein-protein interaction.

Overall, the available data on Tda9 and Rsf2 interactors are scarce. Most are poorly characterised transcription factors with undefined biological roles, although many appear to be involved in diverse metabolic processes (**Figure 15, D**).

The PWM-predicted DNA-binding motif for both proteins' ZnF domains consists of repeated guanines, with secondary nucleotide preferences for thymine or adenine (**Figure 15, B (1)**). This sequence aligns well with the TG-degenerated telomeric repeats characteristic of *Ascomycota* species. Notably, Badis *et al.* (2008) confirmed Tda9's DNA-binding activity using Electrophoretic Mobility Shift Assay (EMSA) with a sequence closely matching the PWM prediction, employing its Pfam-defined DBD along with 50 flanking residues (**Figure 15, B (2)**). While Rsf2 was not experimentally tested, Badis *et al.* (2008) genome-wide DNA-binding motif predictions for *S. cerevisiae* transcription factors suggested an identical consensus site.

Figure 15, C illustrates potential binding sites for Rap1 and Tda9/Rsf2, based on their sequence preferences. The actual DNA bait oligo used in the pull-downs is depicted. However, the figure does not account for the number of Rap1 molecules typically bound at a telomere, nor the distance between the two bound proteins, as depicted bait sequence is non-concatemerised such as in the pull-downs.

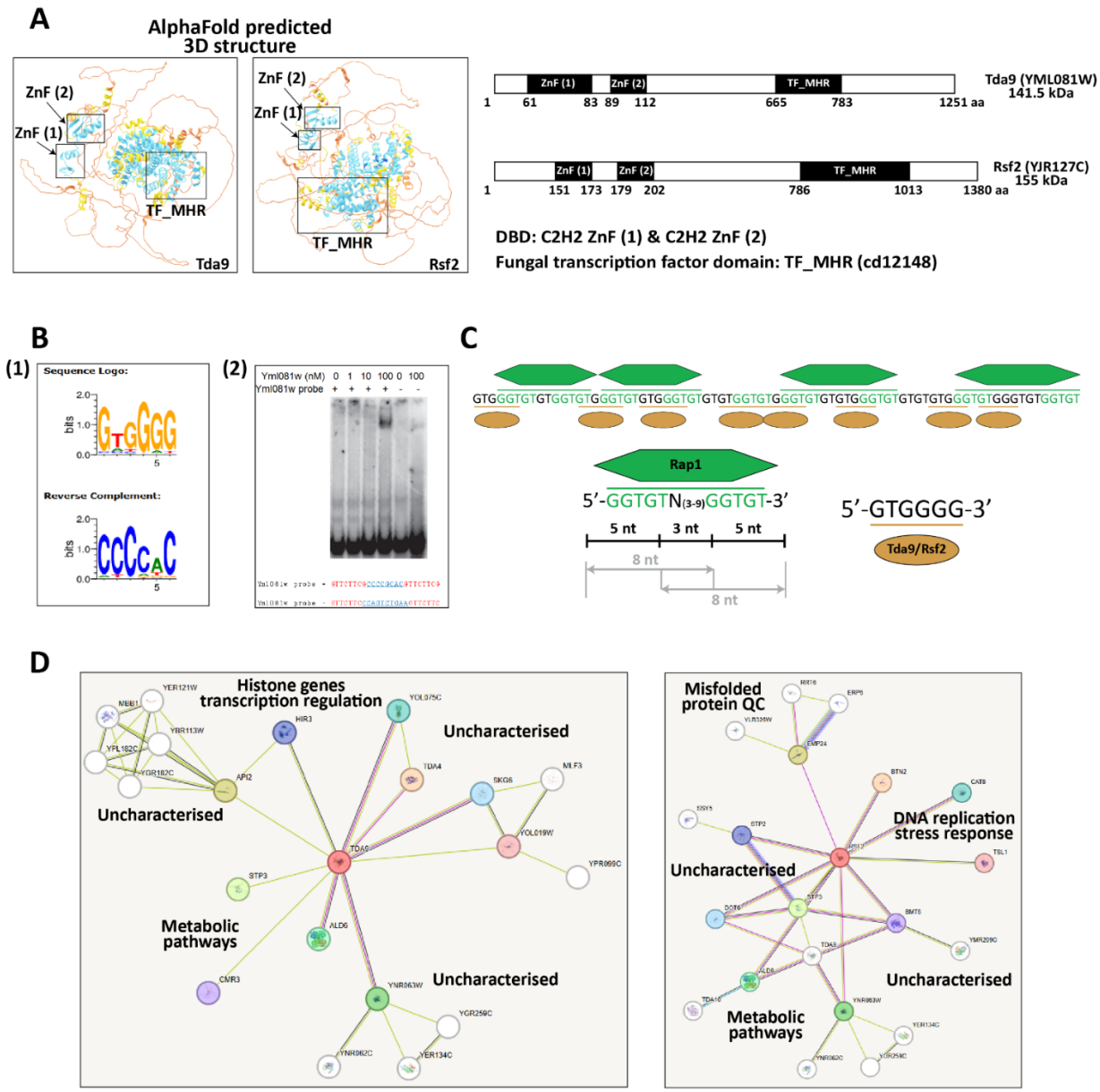

Figure 15. Paralogs TDA9 and RSF2.
A. AlphaFold (alphafold.ebi.ac.uk) predicted 3D structures of Tda9 and Rsf2. Domain positions as defined by UniProt (uniprot.org). **B. (1)** Predicted by PWM (zf.princeton.edu; Persikov & Singh, 2014) DNA binding domain of Tda9 and Rsf2; Random Forest Regression based on affinity-preserved B1H dataset method. **(2)** EMSA (Electrophoretic Mobility Shift Assay) for Tda9, figure reproduced from supplementary material NIHMS99944_01 of **Badis *et al.* (2008)**. **C.** Potential binding sites of Tda9/Rsf2 and Rap1 within DNA bait oligo used in the pull-downs. **D.** STRING (string-db.org) analysis of Tda9 and Rsf2 interactors. **Abbreviations**: DBD – DNA binding domain; QC – Quality Control.

While Rap1's high-affinity binding site is defined as the 5′-GGTGT-3′ half-site (for one MYB domain, **Figure 15, C**), *S. cerevisiae* Rap1 (*Sc*Rap1) demonstrates significant flexibility in recognising a range of target sequences (**Steinberg-Neifach *et al.*, 2015**). This flexibility includes tolerance of a variable spacing between half-sites – typically three nucleotides (8 bp centre-to-centre). However, there is also evidence that *Sc*Rap1 can tolerate the centre-to-centre distance of up to 14 nt – potentially, by looping out the rest of the DNA (**Wahlin & Cohn, 2000; Pina *et al.*, 2003; reviewed in Steinberg-Neifach *et al.*, 2015**).

Due to protein's large sizes, the full-length samples of Tda9 and Rsf2 could not be purified by Protein Production Core Facility. Instead, both ZnF domains (with 6 and 2 flanking residues on either side) were successfully purified.

However, despite several rounds of optimisation in the fluorescence polarisation (FP) assay, including buffer supplementation with varying Zn^{2+} concentrations, I could not demonstrate binding to either telomeric ssDNA, dsDNA or TERRA-mimicking oligos.

Notably, the proteins bound efficiently to a heparin column – whose surface mimics nucleic acids – during purification steps. This observation, together with the aforementioned EMSA results (**Figure 15, B (2)**; **Badis *et al.*, 2008**), suggests that at least Tda9 should bind DNA directly. It is possible that using ZnF domains with longer flanking regions, as was done in Badis *et al*. (2008), might have improved protein stability and conformation, potentially resulting in a successful FP-assay outcome.

Nevertheless, due to project time constraints, we opted to proceed with *in vivo* binding assessment via ChIP, the results of which are discussed in the following chapter.

TDA9 and RSF2 Associate to Telomeres *in vivo*

To perform ChIP, Tda9 and Rsf2 were tagged with a TAP (Tandem Affinity Purification) tag under the control of their endogenous promoters (**Figure 16, A**). To verify that the tagged proteins retained functionality, two experiments were conducted:

i. a senesce assay in *tlc1* background strains (**Figure 16, C**), and
ii. measurement of colony diameters from the haploid meiotic progeny derived from sporulated *TDA9/TDA9*-TAP and *RSF2/RSF2*-TAP diploids (**Figure 16, B**).

The *TDA9-TAP tlc1* and *RSF2-TAP tlc1* strains exhibited senescence and recovery kinetics comparable to the *tlc1* control strain (**Figure 16, C**). Additionally, colony size measurements showed that TAP-tagged strains formed colonies of similar diameter to the ones of their untagged wild-type counterpart (**Figure 16, B**). Taken together, these results indicate that the TAP tag does not impair the functional activity of Tda9 or Rsf2.

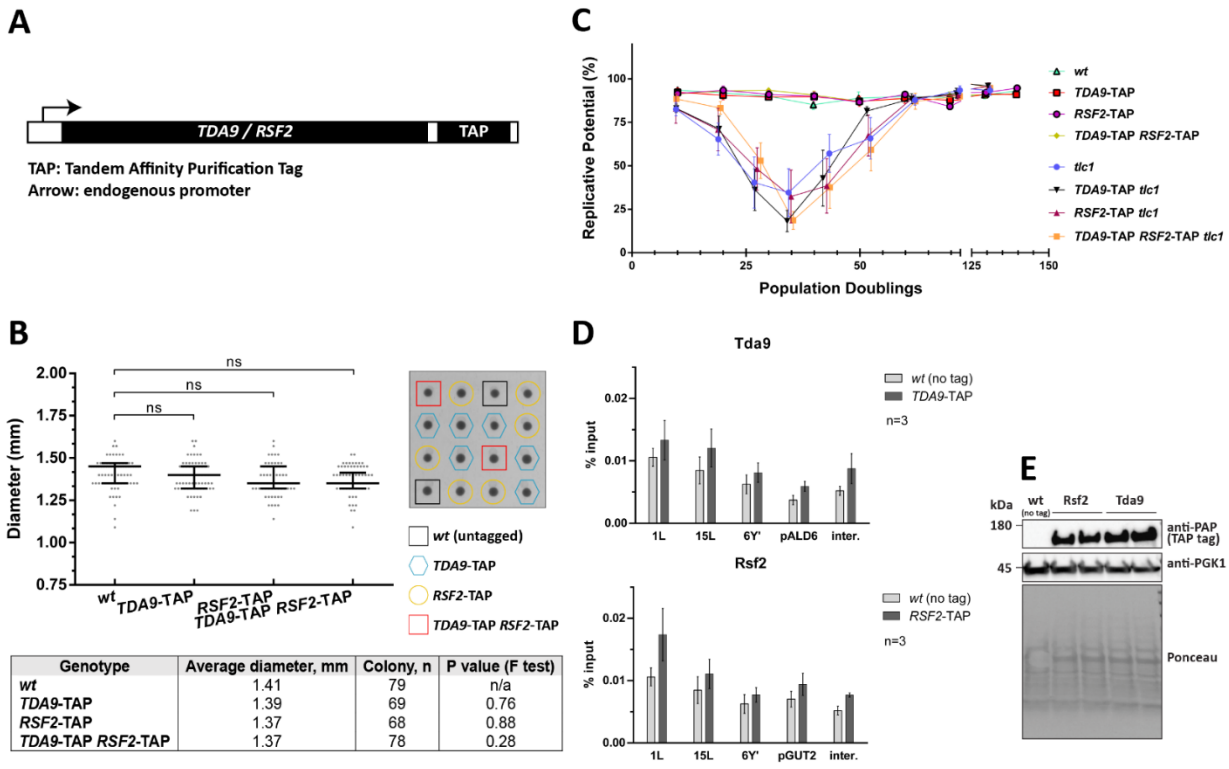

Genotype	Average diameter, mm	Colony, n	P value (F test)
wt	1.41	79	n/a
TDA9-TAP	1.39	69	0.76
RSF2-TAP	1.37	68	0.88
TDA9-TAP *RSF2*-TAP	1.37	78	0.28

Figure 16. TDA9-TAP and RSF2-TAP Functionality Test and ChIP with TAP-tag.
A. Schematic of TAP tagging. **B.** Functionality test. Measurement of colony size diameters of the haploid meiotic progenies derived from sporulation of diploids with tagged/untagged genotype at 48h after the dissection (representative photo of dissected tetrads at 48h, each column of colonies arose from a single tetrad). Median with interquartile range, unpaired t-test (not shown) and F-test (table, last column) did not identify the difference between sample groups. **C.** Senescence curve with strains where Tda9 and/or Rsf2 are/is TAP-tagged in telomerase positive and telomerase negative (*tlc1*) backgrounds. Daily OD_{600} were used to calculate a relative growth potential (Replicative potential, %) of each strain as the relative to the measured on the first day OD_{600} (considered as 100% viability), and plotted over the time course as $\log_2(OD_{600}/0.01)$ and population doublings. **D.** ChIP-qPCR analysis of TAP-tagged Tda9 and Rsf2 association to 6Y', 1L, 15L telomeres (i.e., association to "native" telomeres; for levels of association to telomeres in survivors refer to **Figure 21, A**). pALD6/pGUT2 promoter regions (positive controls) and "inter." – intergenic non-telomeric locus (negative control). The level of enrichment at indicated telomeres presented as mean % input ± SEM (n=3, paired t-test of *wt* vs tagged sample identified $p > 0.05$ in all groups). **E.** Western blot with strains where Tda9 or Rsf2 is TAP-tagged. These strains were used for the ChIP under **D**. Anti-PAP (anti-peroxidase) antibody; Pgk1 is a loading control.

ChIP-qPCR analysis revealed modest enrichment of Tda9-TAP and Rsf2-TAP at telomeres compared to the untagged wild-type control, which was used to estimate background signal (**Figure 16, D**). Despite multiple rounds of optimisation for cross-linking duration, enrichment levels at the three telomeres tested (1L, 15L and 6Y') were comparable to those at the positive controls (pALD6 for Tda9 and pGUT2 for Rsf2) and the negative control (an intergenic, non-telomeric locus, referred to as "inter."). Furthermore, t-test did not reveal statistically significant difference in enrichment levels between the TAP-tagged samples and the wild-type control.

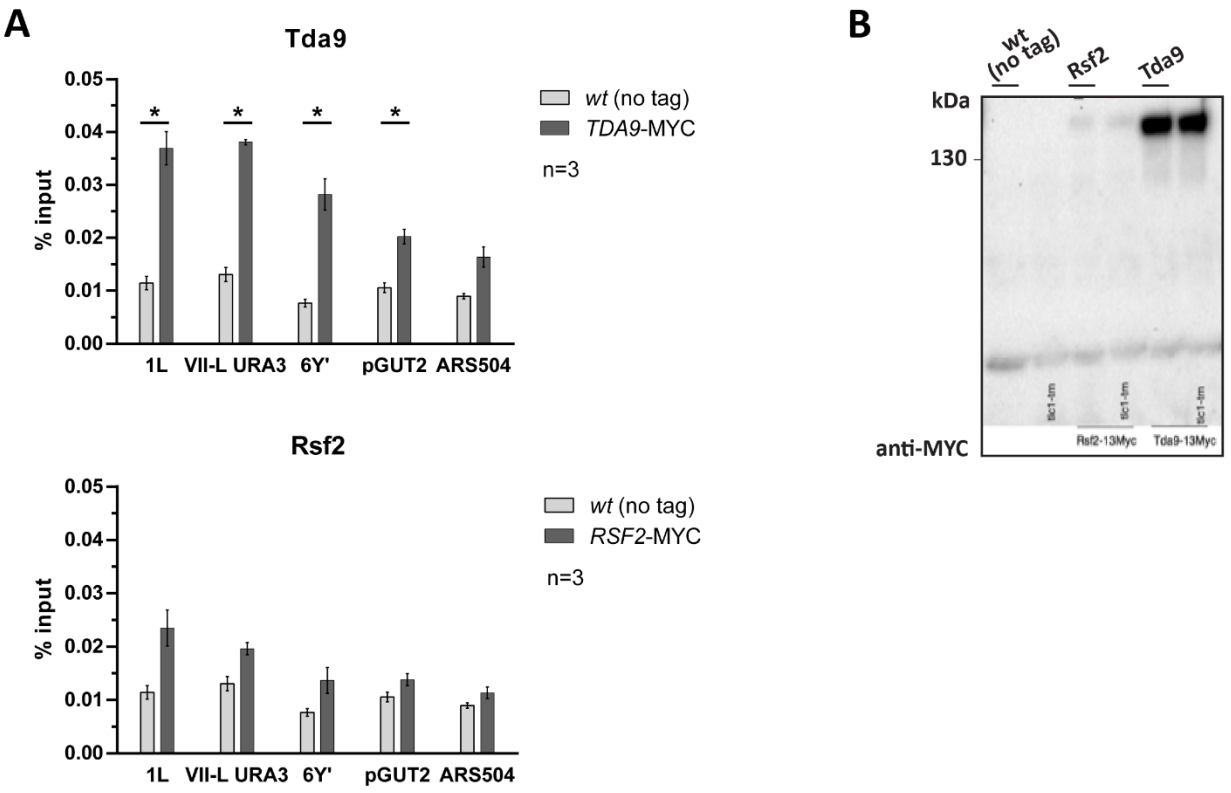

Figure 17. ChIP with TDA9-MYC and RSF2-MYC (Data [redacted]).

A. ChIP-qPCR analysis of MYC-tagged Tda9 and Rsf2 association to 6Y', 1L, VII-L *URA3* telomeres; pGUT2 promoter region (positive control) and ARS504 (negative control). The level of enrichment at indicated telomeres presented as mean % input ± SEM (n=3, paired t-test, * p<0.05). **B.** Western blot with strains where Tda9 or Rsf2 is MYC-tagged. These strains were used for the ChIP under **A**.

To further investigate, [redacted] (collaborator, [redacted] laboratory, the Netherlands) kindly agreed to perform ChIP-qPCR using MYC-tagged versions of Tda9 and Rsf2. In this experiment, enrichment was measured at telomeres 1L, VII-L (*URA3*) and 6Y' (**Figure 17, A**). pGUT2 served as the positive control, and ARS504 – an autonomously replicating, non-transcribed, and non-telomeric region – served as the negative control. Additionally, the VII-L telomere was URA3-labeled in this strain. Aside from these differences, the two ChIP experiments are directly comparable.

In contrast to the TAP-tagged ChIP, the MYC-tagged ChIP-qPCR showed clear enrichment of Tda9 at all tested telomeres, with statistically significant binding ($p < 0.05$) (**Figure 17, A**). Importantly, no significant enrichment was detected at the negative control (ARS504), supporting the specificity of binding.

Rsf2 also showed enrichment at the tested telomeres, with levels comparable to or slightly above the positive control (pGUT2), indicating it may associate with telomeres *in vivo*, though to a lesser extent than Tda9. Notably, Rsf2-MYC produced a weaker signal in Western blot analysis compared to Tda9-MYC, which may explain the lower ChIP enrichment observed (**Figure 17, B**).

Based on these results, it is feasible to conclude that Tda9 binds telomeres in *S. cerevisiae in vivo* with substantial enrichment. Notably, this is consistent with EMSA results published by aforementioned Badis *et al.* (2008) – *in vitro* DNA binding where Tda9 was shown to preferentially bind TG-rich sequences typical of *Saccharomycotina* telomeres (**Figure 15, B (2)** in the chapter *"Paralogs TDA9 and RSF2 Bind Yeast Telomeric Sequences in vitro"*).

In contrast, the evidence for Rsf2's direct telomeric DNA binding remains inconclusive. While Lu *et al.* (2005) suggested that Rsf2 may not directly bind DNA, our findings – combined with its paralogy to Tda9, presence of similar ZnF DNA-binding domains, and modest telomeric enrichment in both ChIP experiments – leave open the possibility that Rsf2 can associate with telomeres, at least, to a certain degree. This, however, might be its redundant characteristic when compared to Tda9. It also might be that these two paralogs can simply do both – act as transcription factors and bind telomeres, but each with its functional preference and capabilities to do either or both.

To further investigate the potential roles of these proteins at telomeres, we next examined the phenotypes of single and double deletion strains. Their effects on telomere length and senescence profiles are presented in the following chapters.

Deletion of TDA9 and RSF2 Leads to Shorter Telomeres

To generate the *tda9rsf2* double knockout strain, haploid single deletion strains from the collection were first crossed. Following sporulation, tetrad dissection, and genotyping, it was observed that the colony sizes of the resulting haploid meiotic progeny varied in diameter. Notably, the *tda9rsf2* double knockout consistently exhibited a ~1.5-fold reduction in colony diameter compared to the wild-type control – an indication of loss of the fitness (**Figure 20, B**). This prompted us to investigate whether the observed phenotype might be associated with telomere length in this strain.

Interestingly, after already 40 PD the Y' telomeres in the *tda9rsf2* were significantly shorter than in the wild type (**Figure 18, A**). This was confirmed by two methods – Southern blot where gDNA was digested with XhoI and Y'-specific telomere PCR, both showing similar results. Thus, the difference between *wt* and *tda9rsf2* telomere length was between 31±4 nt (Southern blot) and 15±5 nt (Telo-Y'-PCR), or on average between the two methods 23±5 nt (tables in **Figure 18, A**). At the same time, the single knockout strains, *tda9* and *rsf2*, had the telomere length comparable to that of the wild type.

The same measurements were performed on cultures propagated for 100 PD (**Figure 18, B**). After an additional 60 PD, the difference in telomere length between the *wt* and the *tda9rsf2* strain became even more pronounced. On average, across both methods, the difference was 66 ± 6 nt (i.e., 61 ± 7 nt as measured by Southern blot and 71 ± 4 nt using the Telo-Y′-PCR method). Collectively, these results suggest that the telomeres in the *tda9rsf2* strain shortened by approximately 43 ± 6 nt over the course of 60 PD. Given that these strains were telomerase-positive, the processivity of the enzyme in the absence of Tda9 and Rsf2 appears to be reduced by approximately 0 to 2 nt per PD compared to the *wt* cells – or, on average, by 1 nt per PD (0.72 ± 0.2 nt).

A similar trend was observed at other telomeres. The lengths of telomeres 1L and 6R were assessed using Telo-PCR at 50 and 160 PD (**Figure 18, C**), and both were found to be shorter in the *tda9rsf2* double knockout strain compared to *wt* cells at the same PDs. However, no further significant shortening was observed at the 6R telomere, which appeared to remain stably shorter. Interestingly, the 1L telomere showed a length comparable to that of the *wt* at 50 PD, but became noticeably shorter by 160 PD as cell divisions progressed. With regard to Y′ telomeres in this experiment, the pattern of telomere shortening was consistent with previous observations (**Figure 18, A & B**), showing progressive shortening in the *tda9rsf2* strain over time. However, the calculations did not reproduce the precise values obtained in the 40 vs 100 PD experiments, and thus failed to definitively confirm telomerase inefficiency in this case (hence, p 0.08 on the Telo-Y'-PCR plot in **Figure 18, C**).

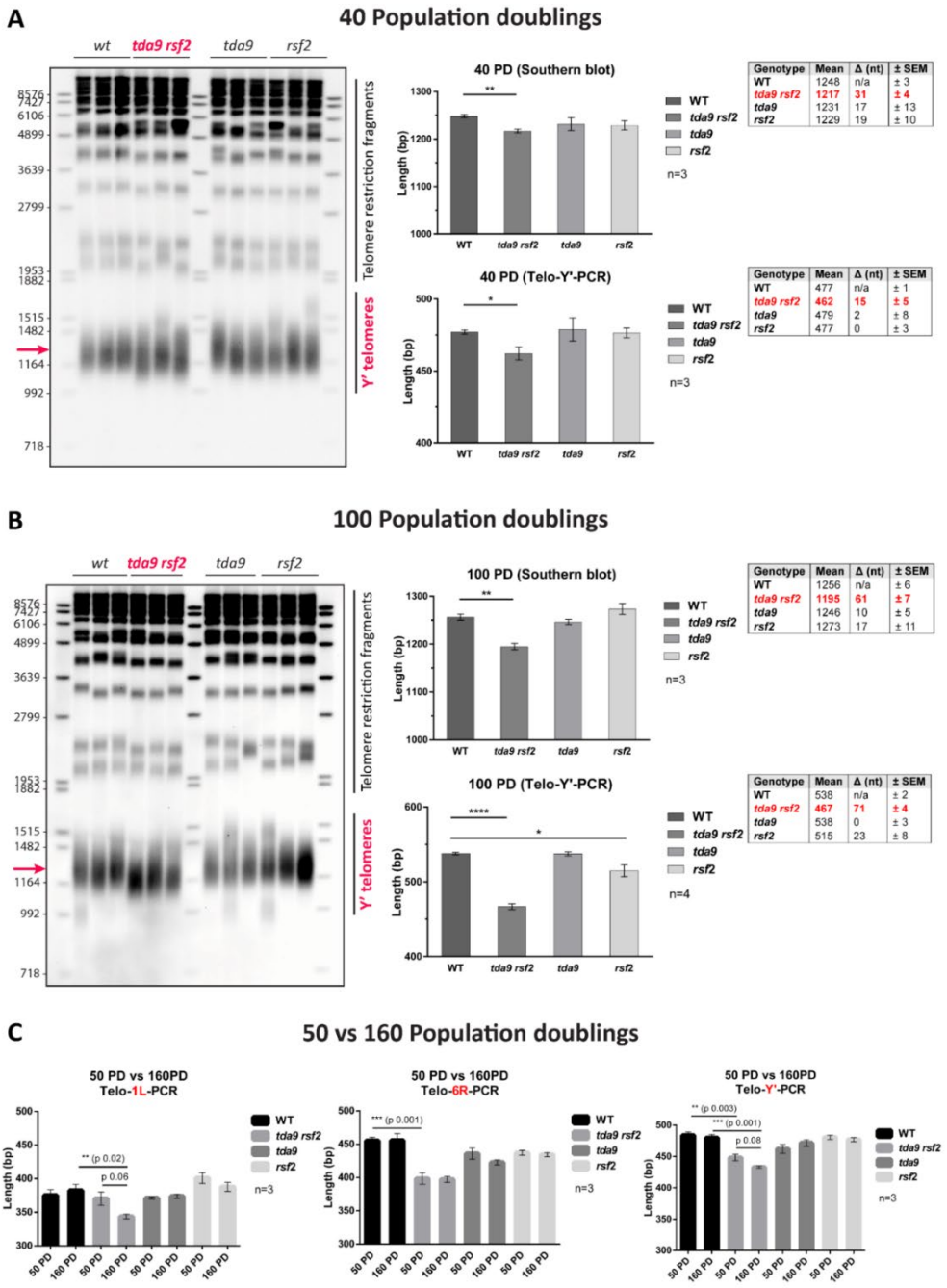

Figure 18. Deletion of TDA9 and RSF2 Alters Telomere Length.
A. Telomere length at 40 population doublings (PD) measured by Southern blot and PCR specific to Y' telomeres (Telo-Y'-PCR) demonstrating Y' telomeres in the *tda9rsf2* are significantly shorter than in *wt* cells. **B.** The same as for **A** but at 100 PD. Data in both **A** and **B** are depicted as Mean ± SEM, n is either 3 or 4 (indicated on the corresponding plot). The p-values obtained from t-test, *p < 0.05, **p < 0.01, ***p < 0.001, ****p < 0.0001. Red arrow in both Southern blots indicates Y' telomeres smear quantified on the plots on the right. Samples used in Southern blot and in Telo-Y'-PCR at the same PD are identical. Tables indicate telomere length quantification and mean difference between the *wt* and indicated genotype. **C.** Length measurements of different telomeres as obtained from PCRs specific to the indicated telomers at 50 and 160 PD. Data are depicted as Mean ± SEM, n=3. Indicated on the plots p-values obtained from t-test.

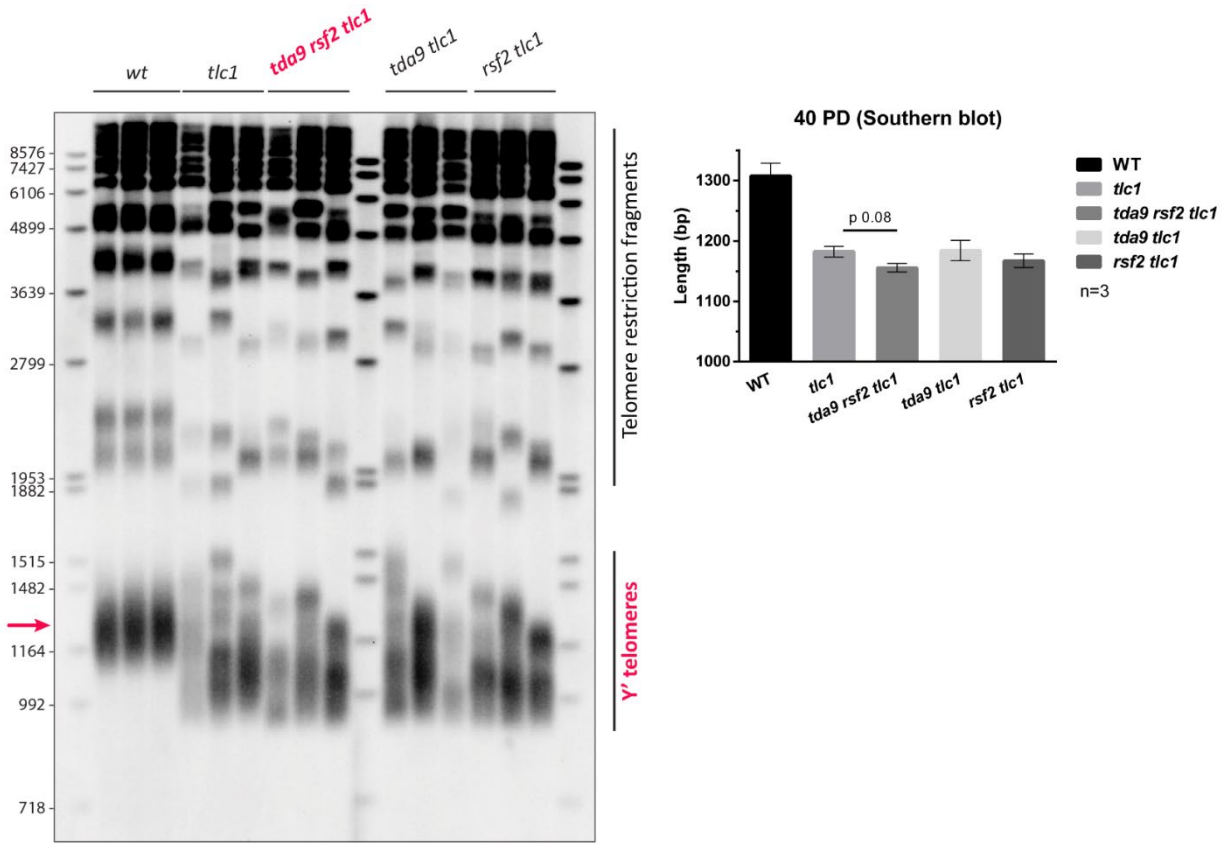

Figure 19. Telomere Length Measurement in Telomerase Negative Background.
Telomere length at 40 PD in telomerase negative background (*tlc1*) measured by Southern blot and its plotted Mean ± SEM quantification on the right (t-test, n=3). Red arrow indicates Y' telomeres smear quantified on the plot on the right. Here, *wt* samples are included for the comparison of telomere length when telomerase is active at the same 40 PD count.

Next, I examined the Y′ telomere length in a telomerase-negative background at 40 PD (**Figure 19**). At this stage, telomeres are significantly shorter than in the wild type due to the loss of telomerase, but have not yet reached a critically short length that would activate ALT and lead to the emergence of survivors. As in previous experiments, telomere length was assessed by Southern blot, with gDNA digested using XhoI, which cuts at Y′ element sites. The average telomere length in the *tda9rsf2tlc1* strain was comparable to that observed in the *tlc1* control. Visually, nonetheless, the bulk smear appeared less intense in the *tda9rsf2tlc1* strain, suggesting slightly less telomere length heterogeneity; however, the shortest telomeres were of similar length to those in the *tlc1* strain. Moreover, t-test did not reveal a statistically significant difference between the two strains (p 0.08) (plotted Mean ± SEM quantification in **Figure 19**). Consistent with findings in the telomerase-positive background, the single knockout strains also showed no difference in telomere length and were indistinguishable from the *tlc1* control.

Cumulatively, the results of these experiments in both, telomerase positive and negative backgrounds, indicate that telomerase in the absence of Tda9 and Rsf2 is not as effective as when both of the proteins are present:

Background	Telomere length
Telomerase **+**	*tda9rsf2* < *wt* (control)
Telomerase **-**	*tda9rsf2* = *tlc1* (control)

As stated above, as cell divisions progress, telomeres in the *tda9rsf2* strain shorten at an average rate of approximately 1 nt per PD compared to the *wt* cells (**Figure 18, A & B**). Despite this gradual shortening, telomeres do not reach the critically short lengths typically observed following complete loss of telomerase activity. Instead, they appear to remain stably shorter than in the *wt*, without triggering cell cycle arrest or other detectable perturbations (**Figure 18, C**). Furthermore, no additional shortening was observed in the double knockout strain in telomerase-negative background (**Figure 19**). Notably, shortened telomeres were only detected in the double knockout strain, while single deletions showed no significant differences in telomere length in either background when compared to controls.

This observation correlates with the finding that meiotic progenies of the *tda9rsf2* strain consistently exhibit significantly smaller colony diameters than those of *wt* or either single deletion strains (**Figure 20, B**) – an indication of reduced cells fitness. A similar trend in reduced colony size was observed in both telomerase-negative (**Figure 20, B**) and *rad51* backgrounds (**Figure 22, A & B**).

Given that deletion of both proteins clearly influences telomere length as a measurable phenotype, we next sought to determine whether this might also impact the profile of replicative senescence and the formation of survivors in the double knockout strain. These results are discussed in the following chapter.

Formation of Type II ALT-Survivors in the Absence of TDA9 and RSF2 is Delayed

To investigate whether deletion of Tda9, Rsf2, or both influences the replicative senescence profile, tetrads from the dissection of a heterozygous diploid strain (*TDA9/tda9 RSF2/rsf2 TLC1/tlc1*) were subjected to senescence assays in both, liquid culture (**Figure 20, A**) and on solid media (**Figure 21, B**). During dissection and genotyping, it was observed that meiotic progenies lacking Tda9 or Tda9 in combination with Tlc1 (i.e., *tda9* and *tda9tlc1* strains, respectively) consistently produced smaller colonies than their respective control genotypes (*wt* and *tlc1*) (**Figure 20, B**).

Notably, the double knockout strains in both telomerase-positive (*tda9rsf2*) and telomerase-negative (*tda9rsf2tlc1*) backgrounds exhibited the smallest colony diameters among all genotypes derived from the dissection. This observation is, again, indicative of reduced cell fitness upon concurrent deletion of Tda9 and Rsf2.

Next, to determine whether deletion of a specific protein influences replicative senescence, ALT activity, and survivor formation, a senescence curve can be employed.

In this assay, cells are passaged every 24 hours at a constant starting OD_{600} in liquid culture, typically over a 12–14-day period. The number of divisions a culture undergoes within 24 hours is referred to as a Population Doubling (PD) and is plotted against the replicative potential of the culture as a percentage (see *"Materials and Methods"* for further details).

When telomerase is deleted, telomeres progressively shorten with each round of replication, lacking the ability to replenish themselves. This ultimately leads to a loss of replicative potential and entry into senescence. At this point, the majority of cells can no longer divide and undergo permanent cell cycle arrest. However, a small proportion of cells can activate ALT mechanisms to compensate for the absence of telomerase and form survivors (reviewed in the chapter *"Replicative Senescence and ALT as One of the Telomere Maintenance Mechanisms"*).

When cells are repeatedly passaged as in senescence curve, wild-type cultures with functional telomerase typically undergo 10 PDs per day. The *tlc1* strain usually reaches minimal replicative potential by day 4 or 5, after which ALT-survivors can restore replicative potential to wild-type levels by day 8–10 ("wild type potential"). Since Type II survivors exhibit a growth advantage over Type I, they are preferentially selected in liquid cultures. Conversely, plate-based passaging yields a mixture of both survivor types. Given that survivor emergence is a stochastic process and the timing of senescence onset can vary between cultures, five spores of the same genotype were used per experiment to ensure the reliability of results and calculations.

Neither the deletion of Tda9 or Rsf2 alone, nor the combined deletion of both proteins, appeared to affect the rate at which cells enter into senescence (points #3–4, senescence curve in **Figure 20, A** and "Senescent cells" in **Figure 21, B**). The timing of entry into replicative senescence was comparable to that of the *tlc1* control, indicating that the absence of these proteins does not accelerate the onset of senescence. When assessed on plates, cells overcame the replicative senescence crisis at a similar to the control rate, with the majority forming survivors by passage 3 and 4 ("Survivors" in **Figure 21, B**).

In contrast, the double knockout *tda9rsf2tlc1* reproducibly showed a significant delay of approximately 2 days in formation of Type II survivors (**Figure 20, A & Table 1**). In addition, when on plates, this delay was not that prominent (compare *tlc1* and *tda9rsf2tlc1* from Passage 3 and 4 in **Figure 21, B**).

To confirm that, indeed, this delay is caused by the formation of Type II survivors specifically, I first employed Southern blot analysis where gDNA was collected on each day of the senescence curve and digested with a mixture of 4 enzymes – AluI, HaeIII, HinfI and MspI (**Teng & Zakian, 1999; Teng *et al.,* 2000; Liu *et al.,* 2023**). When gDNA is digested with this mixture, it is reduced to an average 96 bp. These enzymes have many sites they can cut within Y' elements including those of 358 bp downstream of its 5' end and 42 bp upstream of the 3' of Y' element. In *wt*, digestion with these enzymes yields in hybridising to the telomere probe fragments of ~400 bp from Y'-bearing telomeres, fragments of ~500 bp from tandem Y' elements and fragments of up to 1100 bp from X telomeres (see smears in "*wt*" sample in **Figure 20, A** Southern blot). In Type I survivors, digestion of gDNA with these enzymes yields in short fragment of ~250 bp. In contrast, in Type II survivors it yields in fragment of larger than 1100 bp which look like an extensive smear of up to 12 kbp.

As follows from the Southern blot analysis, *tlc1* begins forming survivors by day 3, which are fully established in the culture by day 4, despite the overall replicative potential remaining low on these days (compare days 3–5 of senescence curve with the corresponding days on Southern blot in **Figure 20, A**).

For the double knockout *tda9rsf2tlc1*, collecting sufficient amount of cells for gDNA extraction on the same days proved very challenging, even after increasing the culture volume tenfold. As a result, the Southern blot signals appear faint. However, I speculate that by day 5, the double knockout initiates survivor formation similarly to *tlc1* on day 3, with survivors fully present in the culture by day 6, as indicated by the distinctive smear (Southern blot on the right in **Figure 20, A**).

Notably, no smear was detectable in *tda9rsf2tlc1* samples on either day 3 or 4 as in the *tlc1* (**Figure 20, A**), even with increased to the maximum exposure (data not shown). Furthermore, in line with the Southern blot and senescence curve data, the two-day delay is also reflected in the reduced number of population doublings observed during this period when both *tlc1* and *tda9rsf2tlc1* are compared (**Table 1**).

Collectively, these results indicate that the double knockout *tda9rsf2tlc1* exhibits impaired formation of Type II survivors in the absence of both proteins. This impairment is not observed in the single deletion strains, which senesce and recover in a manner fully comparable to the *tlc1* control (**Figure 20, A and Figure 21, B**).

Table 1. Overview of Population Doubling Rates in Senescence Curve from Figure 20, A.

Day	*wt* (PD)	*tlc1* (PD)	*tda9rsf2tlc1* (PD)	
3	30	29	28	➢ PD rates are relatively the same. ➢ The double knockout is 1 PD slower.
4	40	36	35	
5	50	42	41	
6	60	**50**	45	➢ *tlc1* restores its replicative potential significantly overnight (day 6), PD is close to 10, or the “wt potential”. ➢ Double knockout shows **two-day delay** in formation of the survivors and cannot reach PD close to “wt potential”.
7	70	59	50	
8	80	69	**57**	
9	90	78	66	➢ *tlc1* reaches PD of 10 by day 10. ➢ Double knockout recovers and reaches PD of 10 by day 11.
10	100	**88**	75	
11	110	98	**85**	

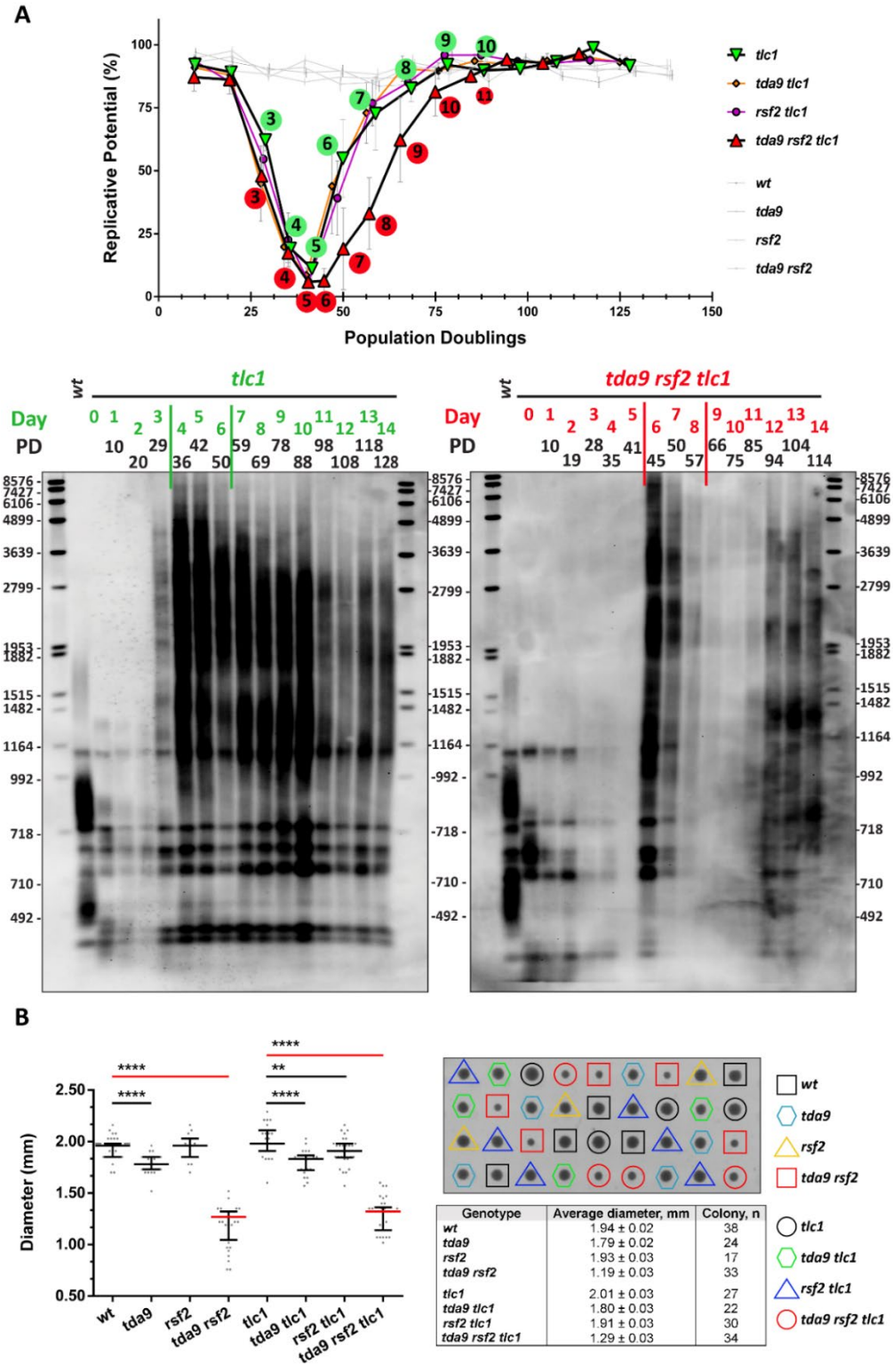

Figure 20. Formation of ALT-Survivors in the Absence of TDA9 and RSF2 is Delayed.
A. Senescence curve as Mean ± SEM with single and double deletion mutants in *tlc1* background. Daily cell viability was measured and plotted. Replicative potential (%) is calculated based on optical

densities (OD_{600}), normalised daily values to the first time point (referred to as 100% or day 0, here not shown and the count starts from day 1). Numbers in red and green circles indicate days in correlation with the Southern blots below the curve. **Southern blots** for control *tlc1* and double knockout *tda9rsf2tlc1*. Samples collected on each day of the senescence curve above, gDNA digested with a mixture of 4 enzymes (AluI, HaeIII, HinfI and MspI), run at 60V on 1.2% agarose gel overnight, and hybridised with telomeric DIG-probe. On the blots, left vertical line indicates the day when ALT Type II survivors are fully present in the culture, right vertical line indicates end of the period before culture starts to actively overcome replicative crisis (i.e., culture shows PD of 9 for a period of 24h). Note how formed by the two lines window is two-day shifted in *tda9rsf2tlc1* compared to the *tlc1* control.
B. Measurement of colony size diameters of the haploid meiotic progenies derived from sporulation of *TDA9/tda9 RSF2/rsf2 TLC1/tlc1* diploid at 48h after the dissection. Plotted Median with interquartile range, t-test. Representative photo of dissected tetrads at 48h, each column of colonies arose from a single tetrad).

Interestingly, the levels of Tda9 and Rsf2 at telomeres in survivors do not appear to be elevated, nor do they show an overall change when compared to their levels at native telomeres ("native telomere" levels, **Figure 16, D**; "survivor telomere" levels, **Figure 21, A**). It is possible, however, that these proteins exhibit increased association with telomeres during early stages of survivor formation, but not once survivors are fully established and the culture has regained replicative potential comparable to that of the wild-type (i.e., the stage at which samples for the ChIP in **Figure 21, A** were collected). This could potentially explain the delay in overcoming the replicative crisis observed in the *tda9rsf2tlc1* knockout strain, assuming that Tda9 and Rsf2 are involved in facilitating the initial recombination events leading to ALT-precursor formation, or in the progression towards fully developed Type II survivors.

To determine whether telomeric association of these proteins fluctuates throughout the senescence curve, samples would have needed to be collected at each timepoint for ChIP analysis. However, due to the difficulty already encountered in obtaining sufficient material for gDNA extraction from the *tda9rsf2tlc1* culture, such an approach was not feasible, as ChIP assay requires significantly more cellular material.

Therefore, we decided instead to demonstrate that the double deletion mutant in the *rad51tlc1* background would likely exhibit a pronounced impairment in overcoming replicative senescence, or potentially be non-viable altogether, given that deletion of Rad51 is known to abolish the formation of Type I survivors (reviewed in the chapter *"Survivors of Replicative Senescence in Yeast"*). The results of this investigation are discussed in the following chapter.

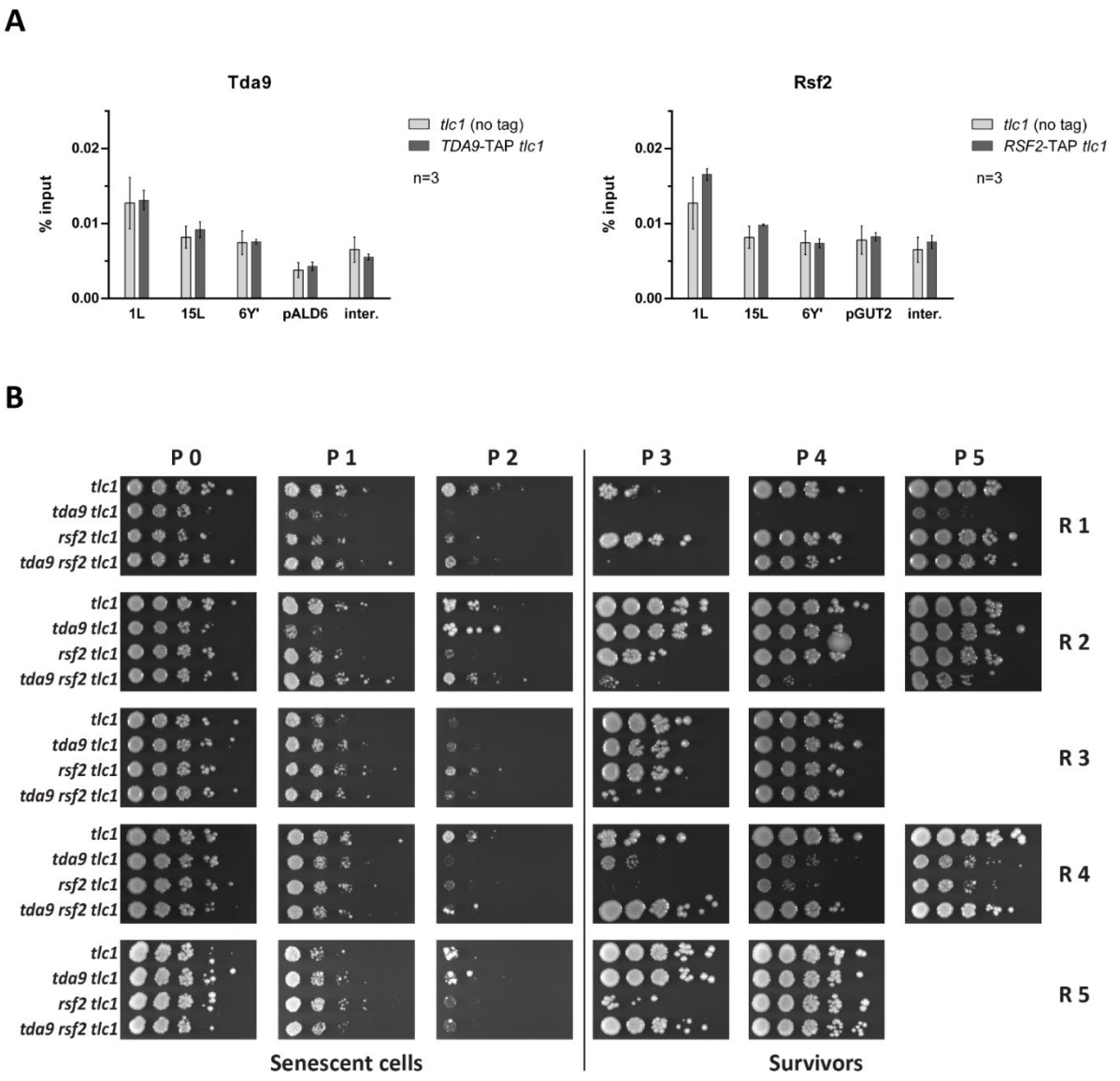

Figure 21. Levels of TDA9 and RSF2 at Telomeres in Survivors & Senescence on Plates.

A. ChIP-qPCR analysis of TAP-tagged Tda9 and Rsf2 association to 6Y', 1L, 15L telomeres in survivors (samples taken on day 12 of the senescence curve in **Figure 20, A**; to compare to "native" telomeres refer to **Figure 16, D**). pALD6/pGUT2 promoter regions (positive controls) and "inter." – intergenic non-telomeric locus (negative control). The level of enrichment at indicated telomeres presented as mean % input ± SEM (n=3, paired t-test of *tlc1* vs tagged sample in the same background identified $p > 0.05$ in all groups). WB was not done as the strains were derived from the cross and dissection of the tagged strains for which TAP-tag expression was checked as on **Figure 16, E,** and later on during the genotyping. **B.** Senescence on plates with 10-fold serial dilutions of the indicated genotypes derived from a single dissection of *TDA9/tda9 RSF2/rsf2 TLC1/tlc1* diploid. P indicates the passage number; R stands for the biological replica. Plates were cultivated for 72h at 30^0C between the two passages. After each passage, cells were streaked onto respective selective media to exclude cross-contamination during the frogging in the previous passage.

Growth and Senescence Profile Impairments in the Deletion Mutants When Formation of Type I Survivors is Abolished (*rad51* Background)

Building on the findings discussed in the previous chapter, we sought to investigate whether the double knockout *tda9rsf2tlc1* would have major growth and senescence impairment if, in addition, Rad51 was deleted. As outlined in the introductory chapter *"Survivors of Replicative Senescence in Yeast"*, deletion of Rad51 prevents the formation of Type I survivors. Therefore, given that the absence of both Tda9 and Rsf2 in the *tda9rsf2tlc1* strain was shown to impair the formation of Type II survivors, simultaneous disruption of Type I survivor formation might render such cells non-viable or cause them to experience considerable difficulty, if not complete failure, in overcoming the replicative senescence crisis.

Indeed, already upon the dissection of *TDA9/tda9 RSF2/rsf2 RAD51/rad51 TLC1/tlc1* diploid, it was noticed that the colony size diameters of the haploid meiotic progenies of the quadruple knockout *tda9rsf2rad51tlc1* genotype are the smallest among the three including *tda9rsf2* and *tda9rsf2tlc1* (**Figure 22, A & C**). Overall, when compared to the respective background control genotype, in all groups concurrent deletion of Tda9 and Rsf2 lead to significantly smaller colony diameters (**Figure 22, A**).

Figure 22, B shows that deletion of either Tda9 or Rsf2 alone does not significantly impact colony size in the *rad51tlc1* background.

Taken together, the analyses across various genetic contexts – including telomerase-positive, telomerase-negative, and Rad51-deficient strains (**Figure 20, B and Figure 22**) – consistently indicate reduced cellular fitness when both Tda9 and Rsf2 are deleted. Additionally, there is a subtle trend toward reduced colony size, and thus decreased fitness, when Tda9 is deleted alone, particularly in telomerase-positive and -negative backgrounds (**Figure 20, B**), a pattern not observed with Rsf2 deletion.

When the quadruple knockout strain *tda9rsf2rad51tlc1* was subjected to replicative senescence in liquid culture, it exhibited the lowest replicative potential among all genotypes as early as day 1, with a reduction to approximately 47% (smaller graphs on the right in **Figure 23, A & B**). Unlike the individual senescence curves where replicative potential is plotted against population doublings per strain, the growth impairment in this strain becomes particularly evident when instead comparing optical densities (OD_{600}) across population doublings (larger graphs on the left in **Figure 23, A & B**).

It is therefore apparent that the double knockout in the *rad51tlc1* background demonstrated the lowest growth capacity from the first passage onwards, maintaining this throughout the 13-day experiment, with OD_{600} values never exceeding 0.2 (red line on the left OD_{600} graph in **Figure 23, A**).

Surprisingly, by approximately 50 population doublings (day 9), the *tda9rsf2tlc1rad51* strain began to recover gradually and was eventually able to overcome the replicative senescence crisis. However, its progression remained notably slower compared to all other genotypes, with consistently lower population doublings recorded across the same timeframe (**Figure 23, C**). To rule out cross-contamination during cell passaging, daily genotyping was carried out for all five biological replicates of each genotype (excluding *wt* and *rad51*).

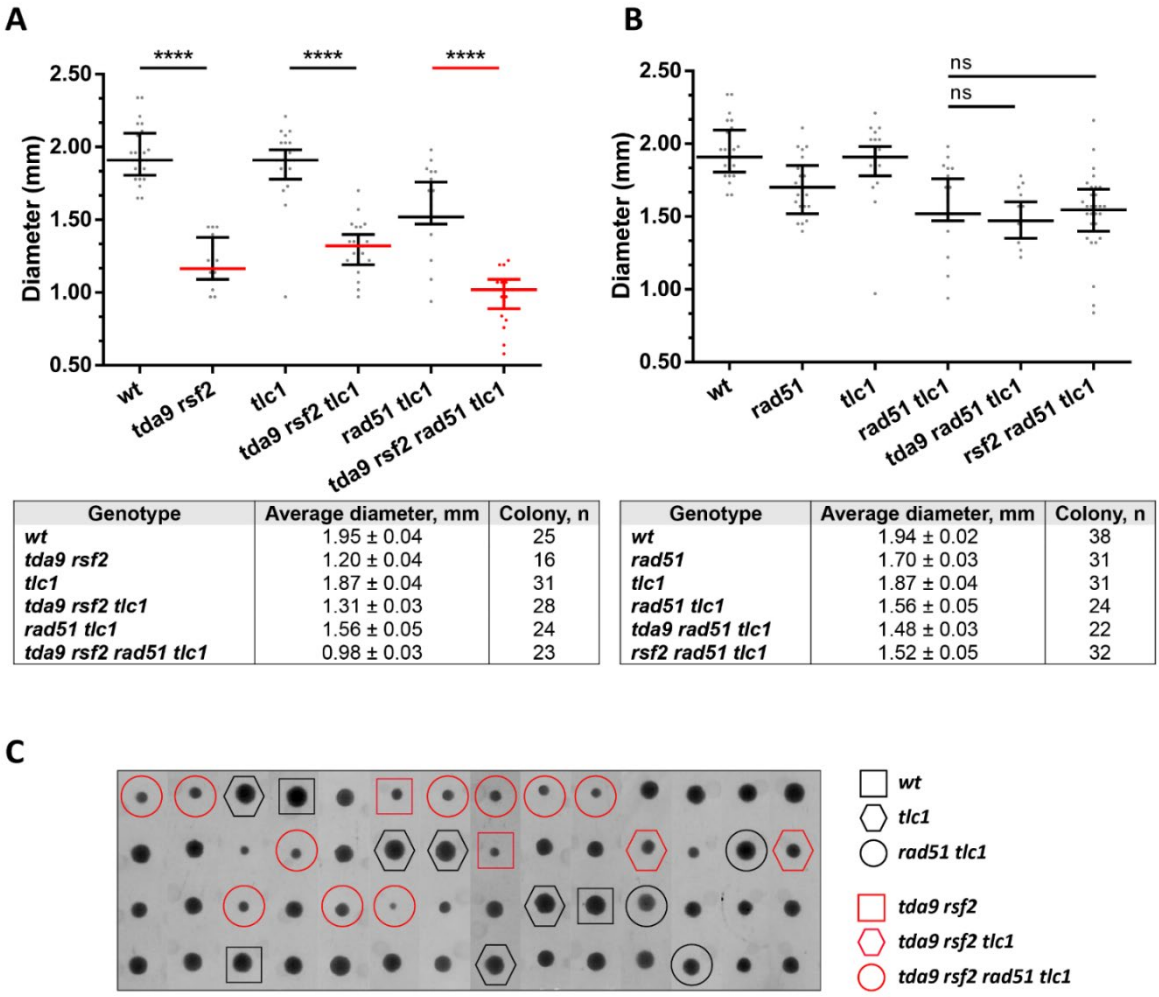

Genotype	Average diameter, mm	Colony, n
wt	1.95 ± 0.04	25
tda9 rsf2	1.20 ± 0.04	16
tlc1	1.87 ± 0.04	31
tda9 rsf2 tlc1	1.31 ± 0.03	28
rad51 tlc1	1.56 ± 0.05	24
tda9 rsf2 rad51 tlc1	0.98 ± 0.03	23

Genotype	Average diameter, mm	Colony, n
wt	1.94 ± 0.02	38
rad51	1.70 ± 0.03	31
tlc1	1.87 ± 0.04	31
rad51 tlc1	1.56 ± 0.05	24
tda9 rad51 tlc1	1.48 ± 0.03	22
rsf2 rad51 tlc1	1.52 ± 0.05	32

Figure 22. Comparison of the Colony Size Diameters Upon Deletion of RAD51.
A & B. Measurement of colony size diameters of the haploid meiotic progenies derived from sporulation of *TDA9/tda9 RSF2/rsf2 RAD51/rad51 TLC1/tlc1* diploid at 48h after the dissection. In both cases, the repetitive genotypes on the two plots (i.e., *wt*, *tlc1*, *rad51tlc1*) are derivatives of the same dissection, and are showed repeatedly for a better comparison to other genotypes. Plotted Median with interquartile range, t-test. **C.** Collage of representative photos of dissected tetrads plotted under **A & B** at 48h. Each column of colonies arose from a single tetrad.

Despite the *tlc1* strain exhibiting a less steep senescence curve in this particular experiment (as opposed to **Figure 20, A**), the *rad51tlc1* strain senesced more rapidly and lagged behind *tlc1*, as expected (**Figure 23, A and B**). The *tda9rsf2tlc1* strain showed an intermediate profile, once again displaying a delay in overcoming the replicative crisis compared to *tlc1* (light-green and black lines in **Figure 23, A**, respectively).

Meanwhile, the single deletion mutants did not exhibit a significantly different senescence profile from the *rad51tlc1* control (grey lines and purple line in **Figure 23, B**, respectively). However, on days 3 and 4, these strains demonstrated both a lower replicative potential and reduced OD_{600} compared to *rad51tlc1*.

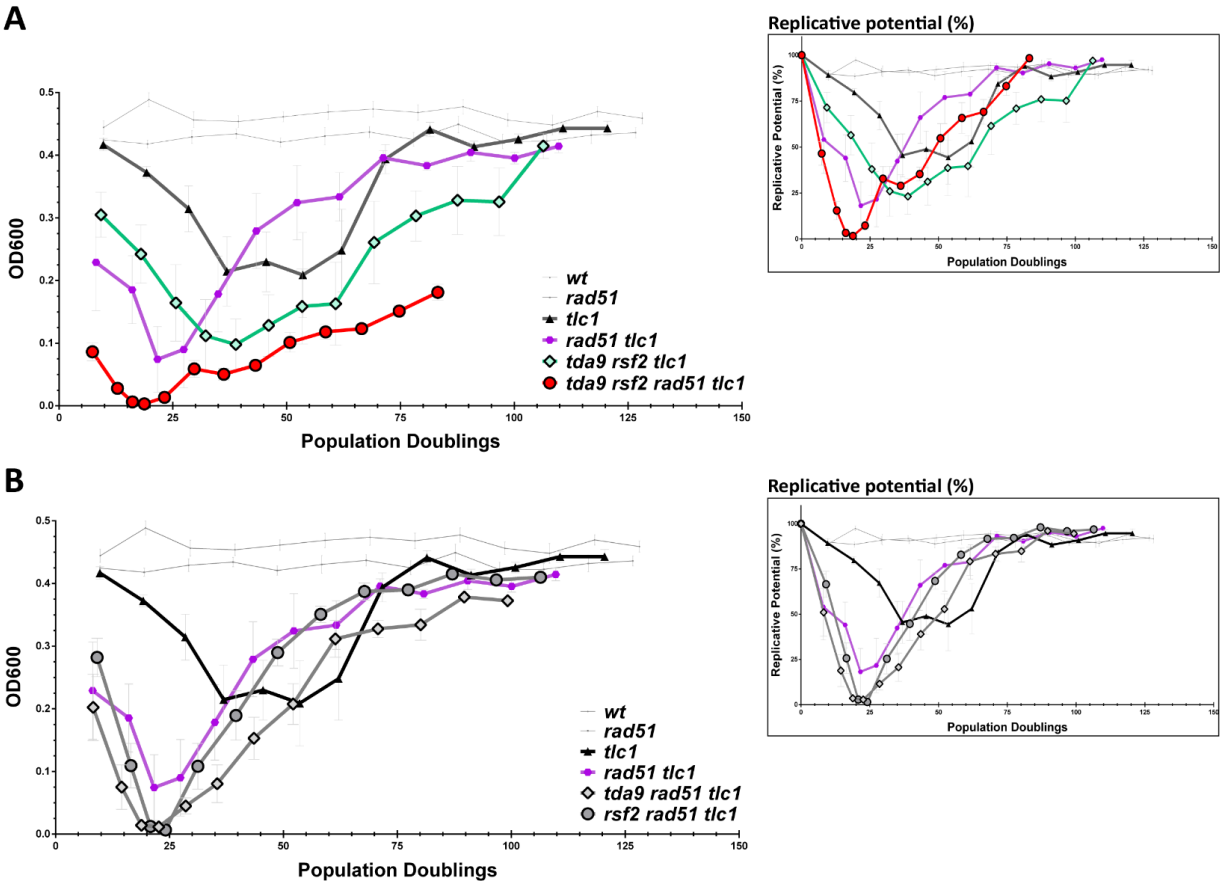

C

	Day of senescence curve												
	d1	d2	d3	d4	d5	d6	d7	d8	d9	d10	d11	d12	d13
Genotype	**Population doubling**												
wt	10	20	30	40	50	60	70	80	90	100	110	120	130
tlc1	**10**	**19**	**29**	**37**	**46**	**54**	**62**	**72**	**82**	**91**	**110**	**111**	**121**
rad51 tlc1	**8**	**16**	**22**	**27**	**35**	**43**	**52**	**62**	**71**	**81**	**90**	**100**	**110**
tda9 rsf2 rad51 tlc1	**7**	**13**	**16**	**19**	**23**	**30**	**36**	**43**	**51**	**59**	**67**	**75**	**83**
tda9 rsf2 tlc1	**9**	**18**	**26**	**32**	**39**	**46**	**53**	**61**	**69**	**78**	**88**	**97**	**106**
tda9 rad51 tlc1	8	15	19	23	29	35	44	52	61	71	80	90	99
rsf2 rad51 tlc1	9	17	21	24	31	40	49	58	68	77	87	97	106

Figure 23. Growth Impairment in the Double Deletion Mutant When Type I Survivor Formation Is Abolished.

A & B. Senescence curves as Mean ± SEM with single and double deletion mutants in *rad51tlc1* background. **Bigger plots** on the left plotted as OD_{600} over population doublings. **Smaller plots** on the right represent replicative potential (%) over population doublings. Replicative potential (%) is calculated based on optical densities (OD_{600}), normalised daily values to the first time point for each strain individually (referred to as 100% or day 0). **C.** Table of PD comparison across the strains derived from senescence curves under **A & B**.

Similarly to aforementioned subtle trend towards reduced colony size – and therefore cellular fitness – in single *tda9* deletion mutants (**Figure 20, B**), the absence of Tda9 also appears to have a slightly greater impact than the absence of Rsf2 on entry into and recovery from senescence when in addition to Tlc1, Rad51 is deleted (i.e., in the *rad51tlc1* background, **Figure 23, B**).

Accordingly, if the two senescence curves are compared – single deletions in the *rad51tlc1* background in **Figure 23, B** and single deletions in *tlc1* background in **Figure 20, A** – the effect of Tda9 deletion relative to Rsf2 single deletion becomes more pronounced. Specifically, the *tda9rad51tlc1* strain shows delayed recovery compared to *rsf2rad51tlc1* (**Figure 23, B**), a trend that mirrors the delayed recovery observed in the *tda9rsf2tlc1* strain (**Figure 20, A**).

That said, to avoid the risk of overinterpretation, ideally, additional biological replicates of senescence curves in the *rad51tlc1* background would be needed to confirm the observations with single deletions.

Taken together, these results demonstrate that deletion of Rad51, which disrupts Type I survivor formation, results in pronounced growth defects in the double knockout mutant already impaired in Type II survivor formation. This is evident from both, the tetrad dissection (**Figure 22**) and the senescence curve (**Figure 23, A**). Such cells enter senescence rapidly but, surprisingly, remain viable and eventually manage to form survivors, thereby, overcoming the replicative senescence crisis (**Figure 23, A**). Overall, the *tda9rsf2tlc1rad51* strain exhibited the smallest tetrad colony diameters across all backgrounds tested (**Figure 22, A**), highlighting its compromised fitness and aligning with the observed senescence profile.

Overexpression of TDA9, but not RSF2, Alters Telomere Length

Since deletion of Tda9 and Rsf2 in telomerase-positive background resulted in shorter telomeres (chapter *"Deletion of TDA9 and RSF2 Leads to Shorter Telomeres"*), we sought to determine whether overexpression of either protein could, conversely, increase telomere length or otherwise influence telomere dynamics.

To investigate this, wild-type cells were transformed with 2-micron multicopy overexpression plasmids containing the respective ORFs under the control of the GAL promoter (i.e., oE for overexpression), or with an empty vector (eV for empty vector control). Each plasmid carried a selectable marker to enable growth on the appropriate amino acid dropout media (see *"Materials and Methods"* for more details).

Tda9 and Rsf2 possess DNA-binding sequence similar to that of Rap1 (**Figure 15, B and C** in chapter *"Paralogs TDA9 and RSF2 Bind Yeast Telomeric Sequences in vitro"*). Considering this, in addition to overexpressing our proteins of interest individually, I also aimed to assess the effects of co-overexpression of Rap1 with Tda9, and Rap1 with Rsf2. For this, wild-type cells were simultaneously transformed with two distinct 2-micron multicopy overexpression plasmids, each with or without the respective ORF under the control of the GAL promoter. To ensure retention of both plasmids, cells were grown on double amino acid dropout media, maintaining selective pressure (see *"Materials and Methods"*).

Overexpression of Rap1, the primary telomere-binding protein, has previously been shown to induce several cellular effects, including growth inhibition and genomic instability. For instance, Freeman *et al.* (1995) demonstrated that the toxicity associated with elevated Rap1 levels is primarily linked to its DNA-binding domain and adjacent regions, with specific mutations in these areas alleviating the toxic effects. The authors proposed that when in abundance, excess amounts of Rap1 interfere with essential transcriptional activation functions, thereby causing pronounced growth inhibition.

Similarly, Conrad *et al.* (1990) reported that Rap1 overexpression induces various telomeric abnormalities, including chromosomal rearrangements, loss of chromosomes, genomic instability and ultimately cell lethality. The overproduction of Rap1 led to increased heterogeneity in the lengths of Y' telomeres, as well as elongation of a subset of other telomeres. This was shown by Southern blotting of gDNA digested with XhoI. Furthermore, the same effect was observed at X-bearing telomeres, with smearing patterns indicating elongation and heterogeneity.

Interestingly, the exaggerated telomeric heterogeneity was lost upon the removal of the overexpression plasmid; however, individual telomeres tested remained approximately 100 bp shorter than those in cells harbouring the empty vector control. In the study, poor growth and cell lethality resulting from Rap1 overexpression were attributed to elevated rates of chromosome loss (**Conrad et al., 1990**).

As expected, cells overexpressing Rap1 exhibited poor growth, as shown by the spotting assay in **Figure 24, A** (upper spotting panels). Similarly, overexpression of Tda9 appeared to be toxic and inhibited cell proliferation. In contrast, overexpression of Rsf2 had no such noticeable effect on cell growth. When Rap1 and Rsf2 were co-overexpressed, the inhibitory effect on growth was comparable to that observed with Rap1 overexpression alone. Co-overexpression of Rap1 and Tda9 resulted in almost no growth compared to cells overexpressing either protein individually (lower spotting panels in **Figure 24, A**).

These results suggest that abundance of Tda9 alone can impair cell growth, and when co-overexpressed with Rap1, it leads to pronounced toxicity and severely compromises cell viability. This effect, however, may result from the combined overexpression of the two transcription factors, leading to substantial disruption of essential transcription activation processes within the cell.

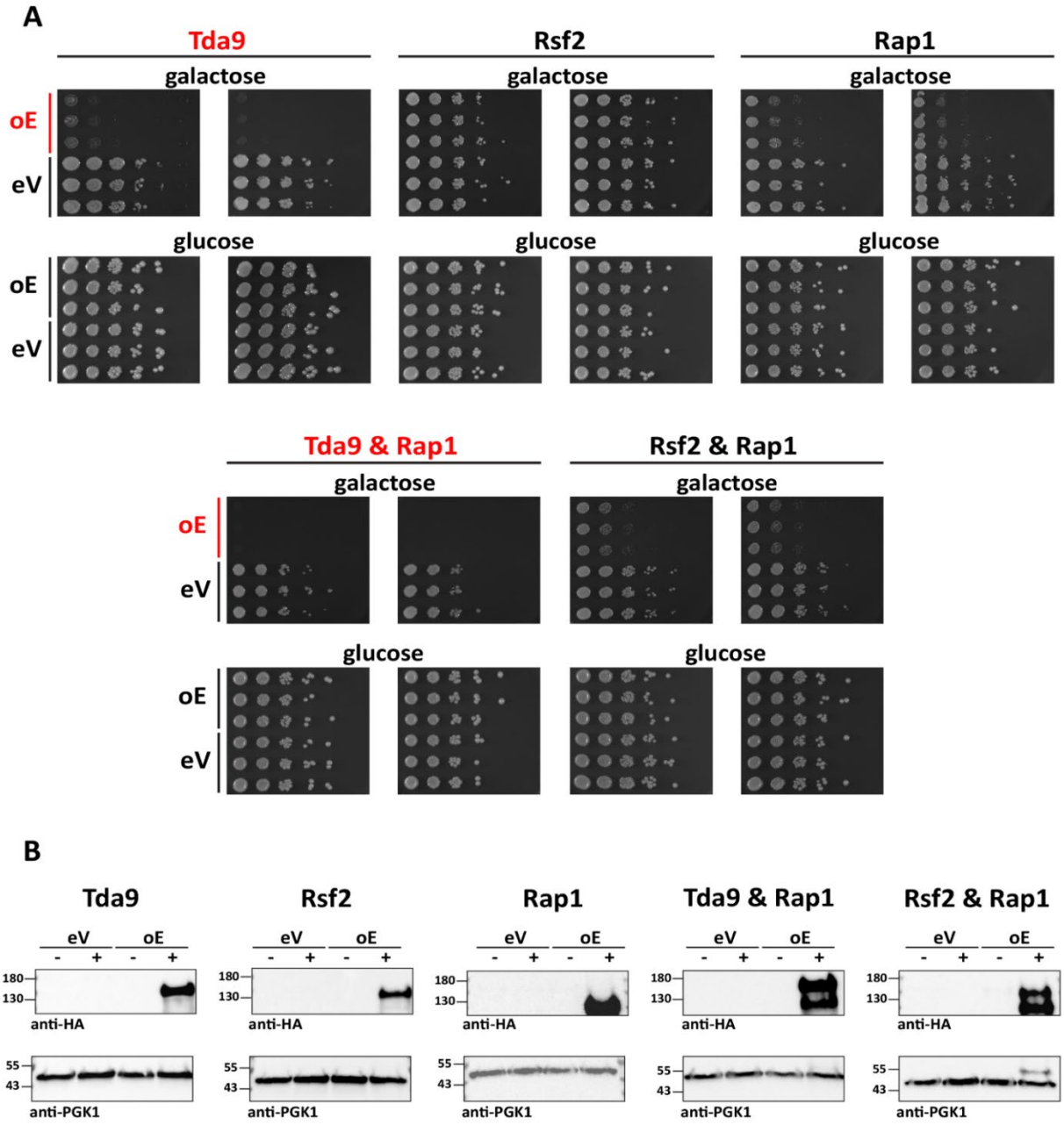

Figure 24. Overexpression of TDA9 Inhibits Cell Growth.
A. Spotted on selective dropout media 10-fold serial dilutions of cells overexpressing Tda9, Rsf2, Rap1 or indicated combinations of those. Galactose containing plates ensure overexpression of the proteins; spotting on glucose plate serves as a control (no overexpression). Cells were grown overnight in selective media containing glucose prior to spotting. Images taken after 72 h (i.e., approximately, 25 PD). Spotting was carried out several times, two representative photos of biological replicas are shown. **B.** Western blot analysis of overexpression upon induction. Cells were grown overnight in selective media containing glucose, day cultures prepared in selective media containing raffinose, induction by adding galactose was permitted for 3.5 h prior to cells collection. **Abbreviations:** oE – overexpression (vector with the corresponding ORF under GAL1 promoter); eV – empty vector control (without cloned ORF). (-) no induction, (+) induction with galactose. Pgk1 serves as a loading control.

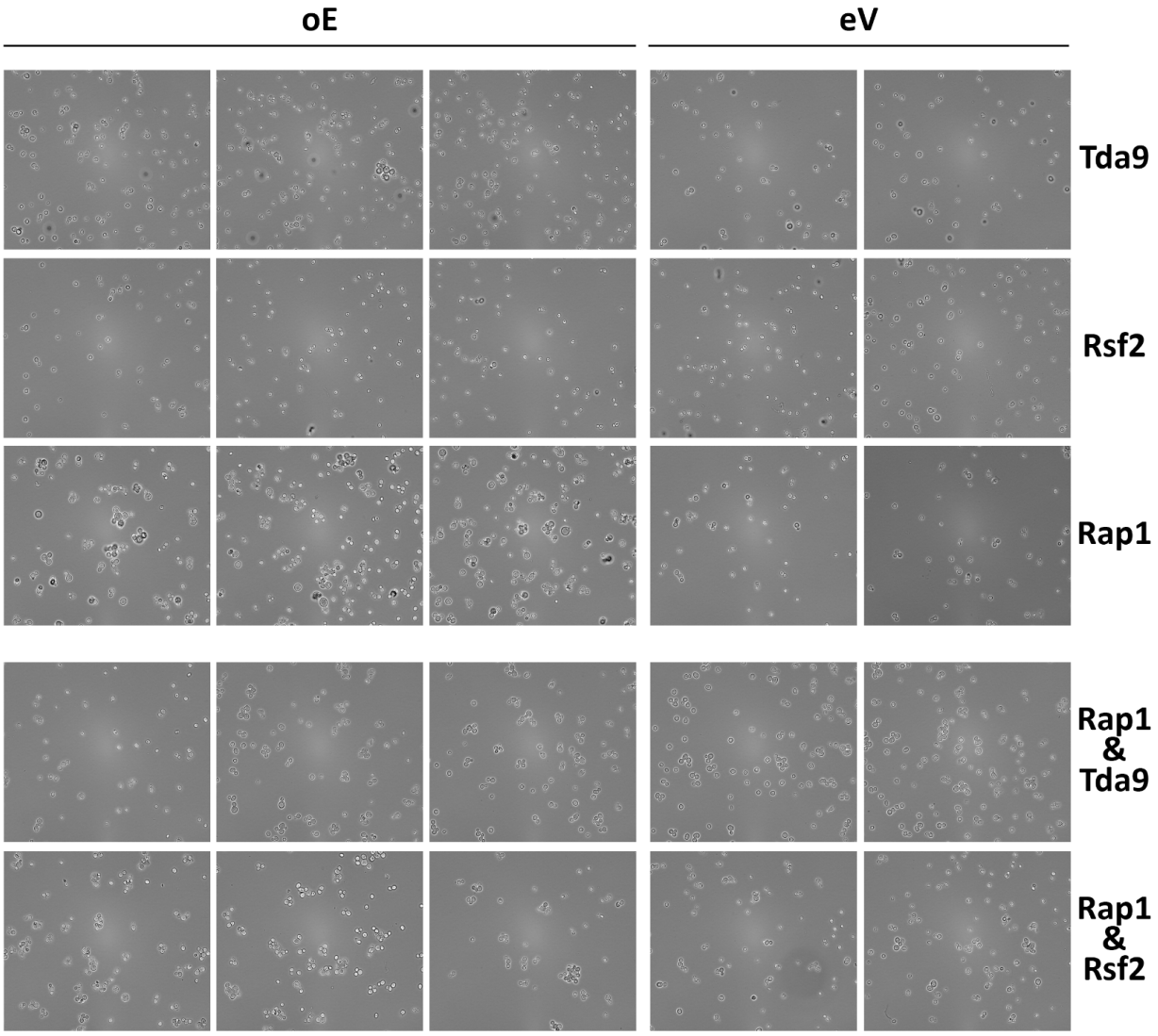

Figure 25. Cells Overexpressing TDA9, RSF2 & RAP1.
Cells were induced overnight in liquid culture (approximately, 10 PD). Magnification 40x.

Increase in cell size and change in morphology can serve as an indicator of senescence (**Ghanem *et al.,* 2019**). In addition, budding yeast cell size beyond its normal range was shown to impair gene induction, cell-cycle progression and cell signalling. Presumably, this is due to larger cells failing to scale nucleic acid and protein biosynthesis in respect to cytoplasm dilution, which eventually leads to reduced lifespan and contributes to aging (**Yang *et al.,* 2011; Neurohr *et al.,* 2019**).

When observed under a phase-contrast microscope, most cells overexpressing Rap1 alone appeared enlarged compared to those carrying the empty vector control (**Figure 25**). While occasionally some Tda9-overexpressing cells were also enlarged, the majority remained normal in size. Rsf2 overexpression had no observable effect on cell size or morphology.

Interestingly, cells co-overexpressing Rap1 & Tda9, did not seem to exhibit noticeable changes in cell sizes compared to control samples transformed with eVs (**Figure 25**). The same was observed for those co-overexpressing Rap1 & Rsf2.

These results suggest that overexpression or co-overexpression of the three proteins may not necessarily manifest in detectable morphological changes, despite the clear growth inhibition observed in the spotting assay. It is important to note, however, that the microscopy was performed after only overnight induction in liquid media (**Figure 25**), whereas the spotting plates were incubated for 72 hours (**Figure 24, A**). It is possible that a longer induction period might have revealed more pronounced morphological changes which could have aligned better with the spotting assay results potentially supporting them.

In addition to assessing cell morphology, cell cycle analysis revealed a normal distribution of cells across different phases: approximately 40% in G1, 20% in S and 40% in G2/M (visual assessment while taking photos in **Figure 25**, data not shown).

Next, I examined telomere length in cells overexpressing Tda9, Rsf2, Rap1 and combination of those (**Figure 26**). In cells overexpressing Rap1, Y' telomeres increased in length, consistent with the results observed in Southern blot analyses using XhoI-digested gDNA, as reported by Conrad *et al.* (1990). Additionally, a subset of telomeres also became heterogeneous, as indicated by the smeared signal in Rap1-oE samples (**Figure 26, A**). Overall, overexpression pattern of telomere length and heterogenicity analysed by Southern blot in this study resembles very well the one reported by Conrad *et al.* (1990).

Overexpression of Tda9 resulted in a significant increase in telomere length, approximately 1.5-fold compared to Rap1-overexpressing cells, yet without the heterogeneity observed in Rap1-oE samples (Southern blot and its quantification plot on the right in **Figure 26, A**). In contrast, overexpression of Rsf2 did not alter telomere length (same in **Figure 26, A**).

In samples co-overexpressing Rap1 and Rsf2, telomere length displayed a pattern similar to that observed in Rap1-only-overexpressing cells, as evidenced by the same pattern of smeared signal in both cases (**Figure 26, B**).

Cells co-overexpressing Rap1 and Tda9 exhibited poor growth, as shown in the spotting assay (**Figure 24, A**), and limited material was available, allowing only a single sample to be loaded in Southern blot (**Figure 26, B**). Nevertheless, in contrast, the smear pattern differed significantly from that of Rap1-oE samples and/or Rap1-Rsf2-co-oE samples – indicating that Y' telomeric restriction fragments were notably shorter, with a size range of approximately 1.3 to 2.6 kb, and exhibited moderate heterogeneity (**Figure 26, B**).

Collectively, these results indicate that overexpression of Tda9 – but not Rsf2 – impairs cell growth (**Figure 24, A**). Co-overexpression of Tda9 and Rap1 is toxic, resulting in minimal to no growth (**Figure 24, A**). In contrast, co-overexpression of Rsf2 and Rap1 has a similar impact on cell growth as overexpression of Rap1 alone (**Figure 24, A**).

In terms of telomere length, overexpression of Tda9 – but again, not Rsf2 – leads to the appearance of significantly shorter Y' telomeres, particularly when compared to Rap1-only-overexpressing cells (**Figure 26, A**). Interestingly, co-overexpression of Tda9 and Rap1 also results in shorter telomeres, but with a distinct pattern compared to that seen with Rap1 overexpression alone (**Figure 26, B**).

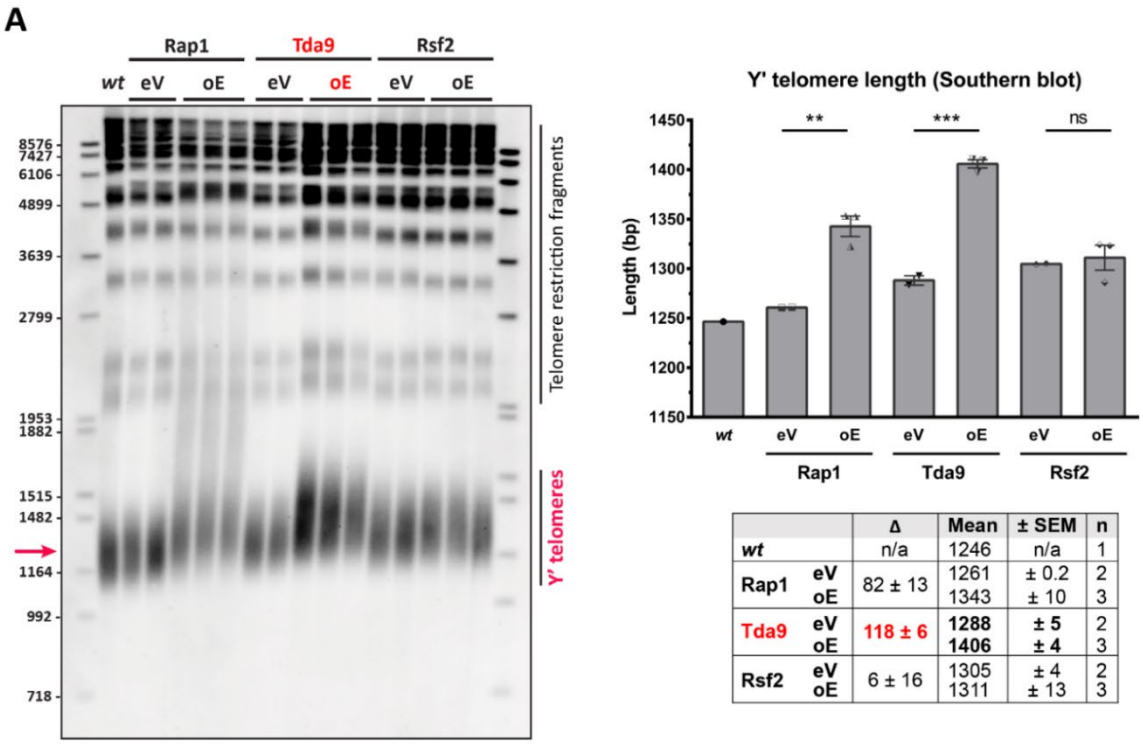

		Δ	Mean	± SEM	n
wt		n/a	1246	n/a	1
Rap1	eV	82 ± 13	1261	± 0.2	2
	oE		1343	± 10	3
Tda9	eV	118 ± 6	**1288**	**± 5**	2
	oE		**1406**	**± 4**	3
Rsf2	eV	6 ± 16	1305	± 4	2
	oE		1311	± 13	3

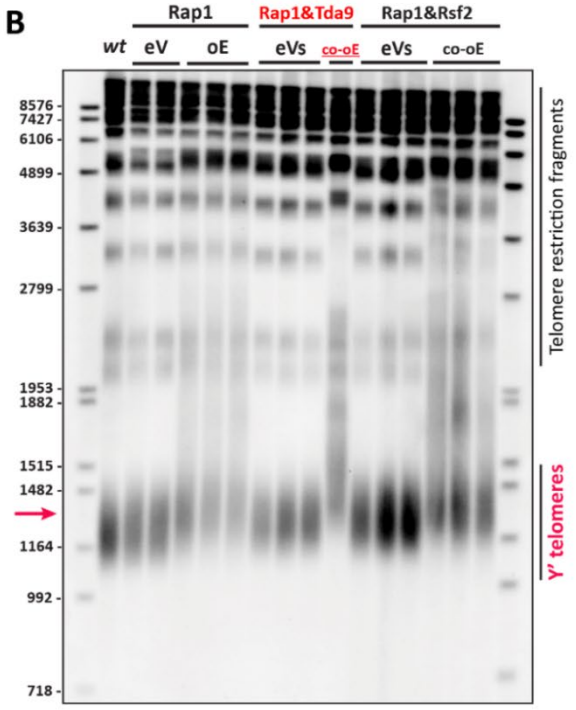

Figure 26. Overexpression of TDA9 Alters Telomere Length.

A. Telomere length analysis by Southern blot on the left, and its plotted Mean ± SEM quantification on the right (t test, **p < 0.01, ***p < 0.001) in cells overexpressing Tda9, Rsf2 and Rap1 for approximately 80 PD. XhoI-digested gDNA was run at 60V on 1.2% agarose gel overnight following hybridisation with telomeric DIG-probe. Red arrow indicates Y' telomeres smear quantified on the plot

on the right. **B.** Southern blot analysis of telomere length in samples co-overexpressing Rap1 & Tda9 and Rap1 & Rsf2 for approximately 80 PD. Here, no quantification was performed due to telomeres increased heterogeneity. Red arrow indicates Y' telomeres smear in *wt* and eV control samples. On both Southern blots under **A** and **B**, each sample is an individual colony derived from sequential 3 streaks on amino acid dropout galactose containing plate following incubation for 3 days between the streaks (which gives around 70 PD). To collect material for gDNA extraction, each colony was inoculated into dropout liquid media supplemented with galactose and incubated overnight (i.e., in total, samples were induced for approximately 80 PD). To collect enough material for gDNA extraction from Rap1-Tda9-oE sample, the cells were incubated for additional 2.5 days in liquid culture supplemented with galactose.

In contrast, co-overexpression of Rsf2 and Rap1 produces a telomere length profile nearly identical to that of Rap1-only-overexpression samples, as indicated by similar smear patterns on the Southern blot (**Figure 26, B**).

Notably, although Tda9 and Rsf2 are paralogs – and in line with the results of the aforementioned dissections and senescence curves (i.e., **Figure 20, 22, 23**) – they exert distinct effects on cell viability and telomere length upon overexpression, with Tda9 consistently having a greater impact.

RAP1 Depletion Causes a Slight Increase in the Levels of TDA9 and RSF2 at Telomeres

Building on the findings from the overexpression and co-overexpression experiments described in the previous chapter, and given that all three transcription factors – Tda9, Rsf2 and Rap1 – can bind to a similar and potentially overlapping telomeric sequence (**Figure 15, B and C** in chapter *"Paralogs TDA9 and RSF2 Bind Yeast Telomeric Sequences in vitro"*), we next sought to investigate whether the absence of Rap1 – achieved through its targeted depletion – might influence the levels of Tda9 and Rsf2 at telomeres. We hypothesised that in the absence of Rap1, the availability of binding sites could allow increased recruitment of Tda9 and Rsf2 to telomeres.

To test this, [redacted] employed ChIP using the AID* (Auxin-Inducible Degron 2) system (**Yesbolatova *et al.,* 2020; Morawska & Ulrich, 2013**), which enables rapid degradation of Rap1 upon treatment with indole-3-acetic acid (IAA). Three strains were analysed for efficient Rap1 depletion prior to performing ChIP (Western blot in **Figure 27, C**): *RAP1*-AID*-3MYC, *RAP1*-AID*-3MYC *TDA9*-3HA and *RAP1*-AID*-3MYC *RSF2*-3HA. Schematic representation of the experiment is depicted on **Figure 27, A**.

Depletion of Rap1 led to a modest increase in the levels of both Tda9 and Rsf2 at native telomeres. For Tda9, the enrichment ranged from a 0.5- to 1.1-fold change across the three telomeres tested, while Rsf2 showed a similar increase, ranging from 0.3- to 1.3-fold above background level (i.e., above dashed line in **Figure 27, B**).

Overall, though, Western blot analysis of band intensity revealed no significant increase in the expression levels of either protein upon Rap1 depletion (first sample in **Figure 27, C**). In addition, to opt for potential disruption due to galactose or auxin presence, and make sure the observed effect is due to Rap1 depletion alone, additional controls were included in the Western blot: "*TDA9*/*RSF2*-HA glucose" to ensure galactose has no additional

effect, and "*TDA9*/*RSF2*-3HA" to ensure auxin does not interfere with the depletion. The last sample – *RAP1*-AID*-3MYC – serves as a control confirming *RAP1*-AID* depletion system is working overall.

Additionally, when compared to the positive controls – pALD6 for Tda9 and pGUT2 for Rsf2 – the enrichment at the examined telomeres, although slightly increased upon Rap1 depletion, did not appear to be strongly telomere-specific.

Cumulatively, these results propose that even in the absence of Rap1, Tda9 and Rsf2 may not robustly associate with telomeres under native conditions. Thus, it is not feasible to draw a clear conclusion from ChIP experiment as to whether there is potential competition with Rap1, or whether the proteins can substitute for Rap1 at telomeres sufficiently upon its depletion. As suggested before (chapter *"Formation of Type II ALT-Survivors in the Absence of TDA9 and RSF2 is Delayed"*), it is yet possible that these proteins play a more prominent role at telomeres during the formation of the survivors, where their recruitment and functional importance at telomeres might be heightened.

Furthermore, Rap1 enrichment at the three control loci may not serve as an ideal reference point, as the depletion achieved might not have been sufficient to fully eliminate the cellular pool of Rap1. Apparently, given its abundance and versatility as a transcription factor, Rap1 may still be detectable at these genomic loci even after degradation (grey column, control plots in **Figure 27, B**). However, critically, the data indicate that Rap1 depletion at telomeres was sufficient, supporting the conclusions drawn from the telomere-specific ChIP results above (grey column, tested telomeres plots in **Figure 27, B**).

To explore this further, and to examine an additional possibility – that these proteins may interact additively or competitively with Rap1 at telomeres – I conducted an epistatic experiment involving protein overexpression in the absence of Rap1 interactors Rif1 and Rif2. The results are discussed in the following chapter.

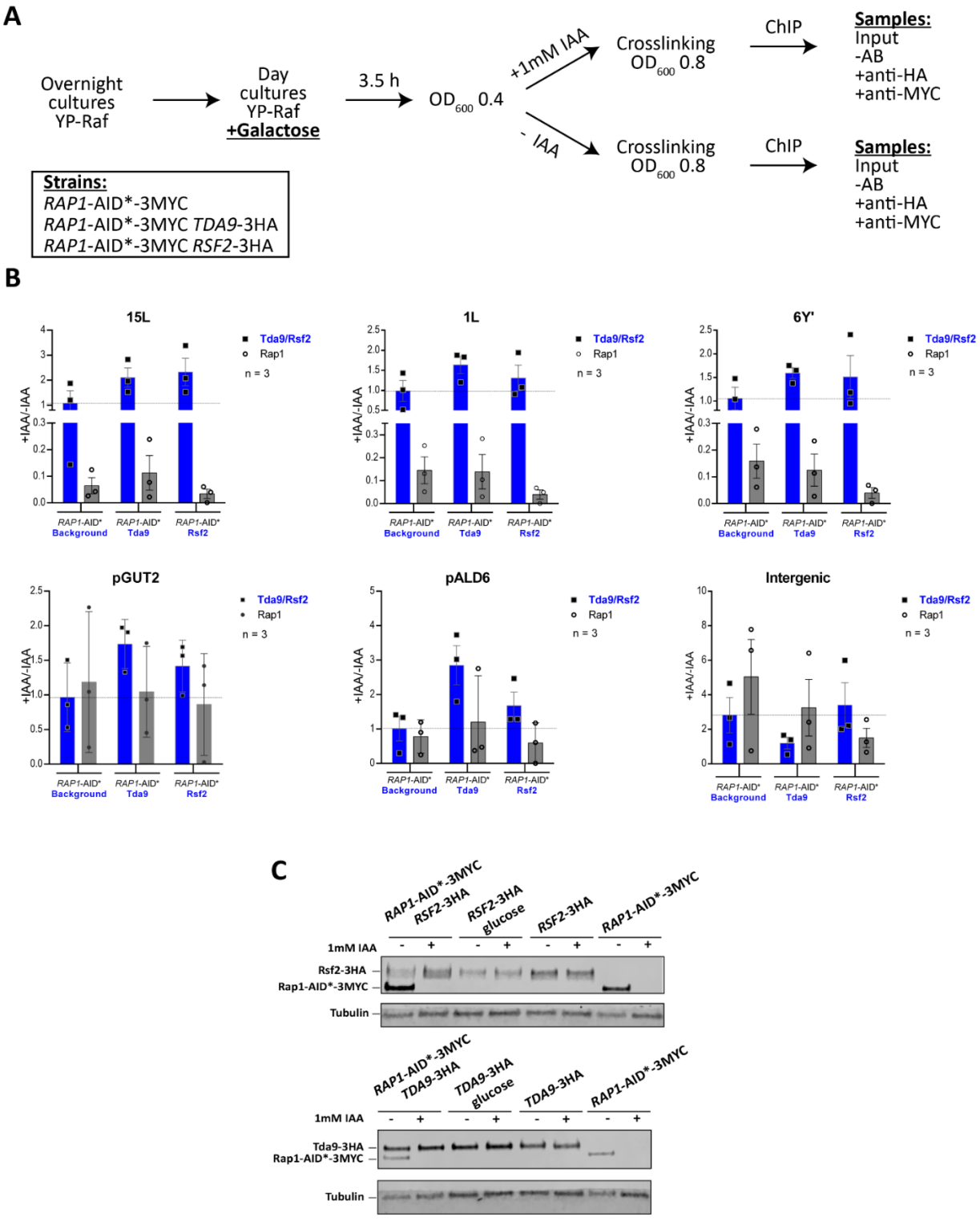

Figure 27. Depletion of RAP1 Causes a Modest Increase in the Levels of TDA9 and RSF2 at Telomeres.

A. Schematic representation of experiment involving Rap1 depletion via AID* system to assess levels of Tda9 and Rsf2 at telomeres (results of ChIP-qPCR are under **B**). YP-Raf – medium supplemented

with raffinose. Galactose is added to day cultures to induce ubiquitin OsTIR1 ligase expression in the AID2* degron system. **B.** ChIP-qPCR analysis of Tda9 and Rsf2 levels at three indicated telomeres upon Rap1 depletion. Rap1 is depleted to an indicated level (grey column) and levels of either Tda9 or Rsf2 at the three indicated telomeres – 15L, 1L and 6Y' – are assessed (blue column above dashed line). Dashed line indicates baseline signal coming from the background, for an easier visual comparison of the Tda9 and Rsf2 enrichment levels. pGUT2 is the positive control for Rsf2, pALD6 is the positive control for Tda9, Intergenic region is the negative control for Tda9, Rsf2 and Rap1. Plotted Mean ± SEM. **C.** Western blot analysis of Rap1-3MYC depletion, and analysis of Tda9-3HA and Rsf2-3HA band intensity upon Rap1 depletion. For samples description refer to the main text in this chapter. Tubulin serves as a loading control. **Indicators**: (-) no depletion, (+) depletion by adding 1mM IAA.

Overexpression of TDA9, but not RSF2, Alters Telomere Length in the Absence of RIF1 and RIF2

Building on the ChIP-qPCR findings from previous chapter showing a slight increase in Tda9 and Rsf2 binding to telomeres upon Rap1 depletion, and along with the results from chapter *"Overexpression of TDA9, but not RSF2, Alters Telomere Length"* demonstrating telomere elongation following Tda9 overexpression, we hypothesised that these proteins might compete with Rap1 for telomere binding sites when overexpressed.

To explore this possibility, Tda9 and Rsf2 were overexpressed as previously described (chapter *"Overexpression of TDA9, but not RSF2, Alters Telomere Length"*, also in *"Materials and Methods"*), but in strains lacking either Rif1 or Rif2 as a genetic background.

To recapitulate, in *S. cerevisiae*, Rif1 and Rif2 play crucial roles as negative regulators of telomere length. Rap1 recruits them thorough interaction with its C-terminal domain (**Figure 5** in chapter *"End-Protection Problem" and Composition of Telomeres in S. cerevisiae*).

While both proteins contribute to telomere length control, they operate via distinct mechanisms which are not yet fully elucidated. Their combined deletion leads to a synergistic effect on telomere elongation. Specifically, deletion of Rif1 results in extensive telomere lengthening, whereas deletion of Rif2, in comparison, leads to a moderate telomere extension. When both of the proteins are deleted, telomere length increases drastically indicating of the synergistic action of both of the proteins (**Wotton & Shore, 1997; Sreesankar *et al.,* 2012; Kaizer *et al.,* 2015**).

To date, two complementary models have been proposed to explain how the Rap1-Rif1-Rif2 complex contributes to telomere length equilibrium: the protein-counting model and the Velcro model. The latter posits that interlocking interaction among the three proteins forms a chromatin scaffold that physically restricts telomere elongation. The former, in contrast, suggests that the greater the number of Rap1-Rif1-Rif2 complexes bound along a telomere, the stronger the suppression of telomerase-mediated elongation of that telomere is. Notably, experiments in which Rif1 and Rif2 were artificially tethered to telomeres via fusion with other DNA-binding domains also resulted in limited telomere elongation, suggesting that the elongation-suppressive function is primarily mediated by Rif1 and Rif2, rather than Rap1 itself (**Levy & Blackburn, 2004; Teixeira *et al.,* 2004; Shi *et al.,* 2013; Kaizer *et al.,* 2015**).

In both *rif1* and *rif2* backgrounds, overexpression of Tda9 resulted in considerable telomere elongation compared to the corresponding empty vector controls, as shown by the smears in Southern blot on the left in **Figure 28, A**. Notably, consistent with observations in

the wild-type background (**Figure 26**), overexpression of Rsf2 in the absence of Rif1 or Rif2 had no detectable effect on telomere length (Southern blot on the right in **Figure 28, A)**.

To interpret these results, several possibilities can be considered:

i. If Tda9 acts by outcompeting Rap1 at telomeres, its overexpression in *rif1* or *rif2* backgrounds would reduce Rap1-bound Rif1 or Rif2, further diminishing repression and, thereby, allowing telomerase-mediated elongation. A hypothesis that would align well to what the data in **Figure 28, A** suggest. However, to further test whether Tda9 functions independently of the Rap1-Rif1-Rif2 axis, telomere length should ideally have been assessed in the *rif1rif2* double mutant upon Tda9 (and for that matter, Rsf2) overexpression as well – an experiment regrettably not pursued due to constraints in the progression of the project and prioritisation of experiments.

ii. Had Tda9 overexpression in the *rif1rif2* background still led to telomere elongation, it would suggest that Tda9 promotes telomere extension independently of the Rap1-Rif1-Rif2 complex. Possibly, by directly enhancing telomerase recruitment or activity.
Alternatively, it could suggest that Tda9 competes with Rap1 for binding to telomeres, and with the depletion of the Rap1 pool at telomeres, this competition may further disrupt telomere length regulation by reducing Rif1/Rif2 recruitment and leading to telomere elongation. This, then, could have further strengthen the results of ChIP-qPCR where a slight increase in protein levels at telomeres upon Rap1 depletion was demonstrated (chapter *“RAP1 Depletion Causes a Slight Increase in the Levels of TDA9 and RSF2 at Telomeres”*).
Conversely, if telomere length remained unchanged, it would imply that Tda9 possibly requires a functional Rap1-Rif1/Rif2 interface to exert its effect. For instance, through Rap1 binding stabilisation to either, Rif1 or Rif2.

iii. A third possibility, telomere shortening in the *rif1rif2* background or, most likely, any other effect – e.g., rearrangement, increased telomere length heterogeneity or end joining – would point toward a complex, context-dependent role for Tda9, possibly involving competition with, or replacement of, Rap1 upon its overexpression.

Taken together, findings presented in this chapter support the hypothesis that Tda9 positively regulates telomere length through a mechanism that is – at least partially – independent of Rif1 and Rif2, potentially by modulating telomerase access to the telomere ends.

This interpretation is further supported by the data presented in the chapter *"Deletion of TDA9 and RSF2 Leads to Shorter Telomeres"*, where telomere shortening in the *tda9rsf2* double knockout strain points to a telomerase-associated mechanism. Specifically, the observation that telomeres fail to gain approximately 1 nucleotide per population doubling in the absence of both, Tda9 and Rsf2, suggests reduced telomerase processivity or efficiency under these conditions (**Figure 18, 19**).

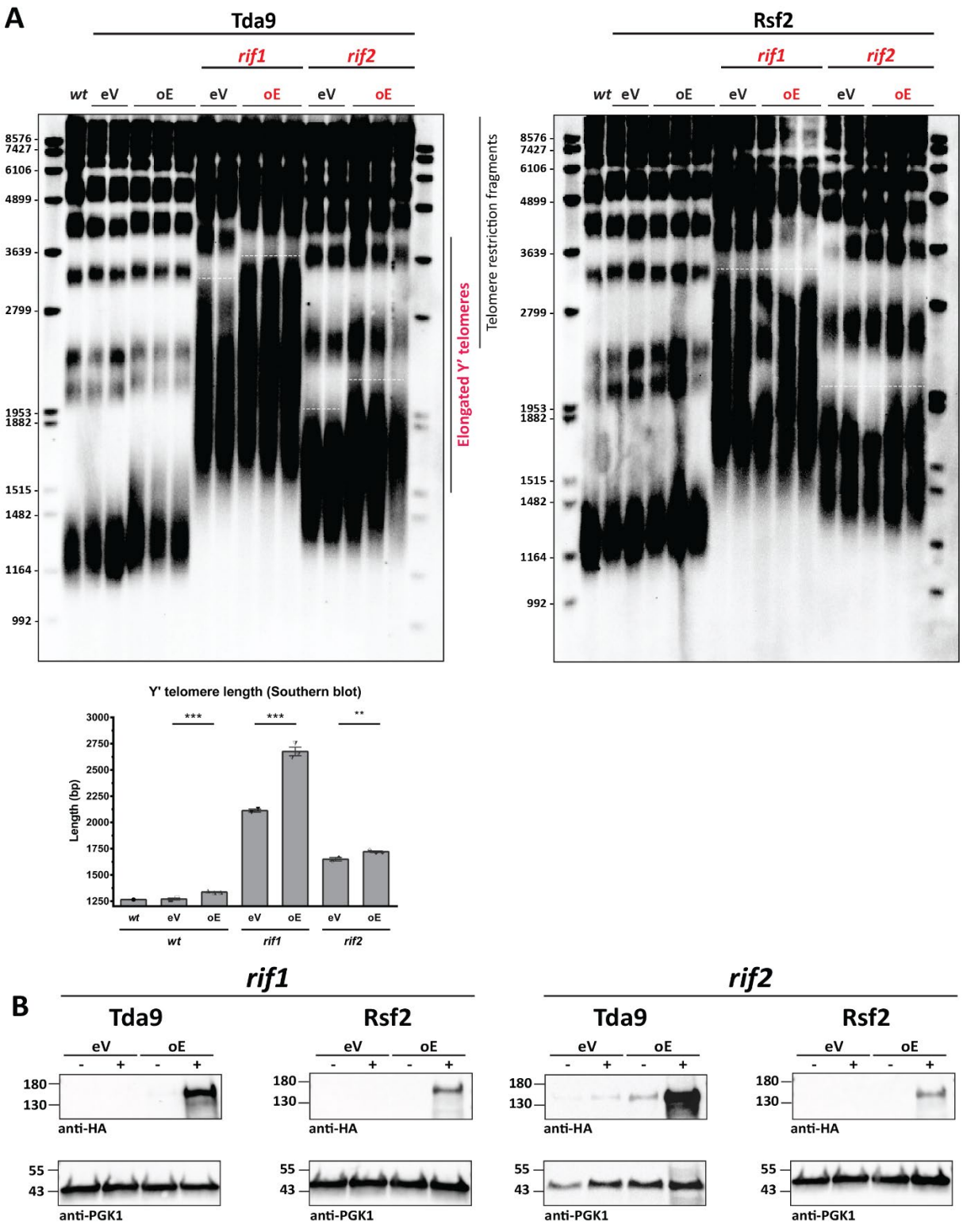

Figure 28. Overexpression of TDA9 in *rif1* and *rif2* Backgrounds Alters Telomere Length.

A. Southern blot analysis of telomere length upon Tda9 and Rsf2 overexpression in *rif1* and *rif2* backgrounds. Dashed line indicates the difference or similarity in telomere length. Plotted Mean ± SEM

quantification for Tda9 overexpressing cells (t test, **p < 0.01, ***p < 0.001). For Rsf2-oE samples no quantification is shown as the obtained values were inaccurate – due to poor quality transfer and inability to properly quantify the signal to estimate telomere length in these samples. Instead, compare the level of smears highlighted by the dashed line visually. Cells were overexpressing Tda9 and Rsf2 for approximately 80 PD. Sample under *wt* is the same that was used in **Figure 26, A** and is included for comparison and as a reference. XhoI-digested gDNA was run at 60V on 1.2% agarose gel overnight following hybridisation with telomeric DIG-probe. **B.** Western blot analysis of overexpression upon induction. Cells were grown overnight in selective media containing glucose, day cultures prepared in selective media containing raffinose, induction by adding galactose was permitted for 3.5 h prior to cells collection. **Abbreviations:** oE – overexpression (vector with the corresponding ORF under GAL1 promoter); eV – empty vector control (without cloned ORF). (-) no induction, (+) induction with galactose. Pgk1 serves as a loading control.

Effects of DNA Damaging Agents & TPE in Deletion Mutants

To assess whether the absence of Tda9 and/or Rsf2 affects cellular sensitivity to DNA damage, the respective deletion strains were exposed to DNA-damaging agents such as methyl methane sulfonate (MMS) and Zeocin™ (**Figure 29, A**).

MMS is a DNA alkylating, highly toxic chemical that methylates DNA at 7-deoxyguanine and 3-deoxyadenine causing base mispairing and replication fork stalling which, in turn, triggers activation of DDR pathways leading to cell cycle arrest (**Evensen & Seeberg, 1982**).

Zeocin™, on the other hand, is a commercial name of an antibiotic from bleomycin/phleomycin family group, a genotoxic radiomimetic DNA damaging compound that induces DSBs akin to those occurring after ionizing radiation (**www.thermofisher.com**). Both chemicals are frequently used in DNA damage studies (**e.g., Murakami-Sekimata *et al.,* 2010; Todorova *et al.,* 2019**).

Rad52 is one of the key HDR players. Its deletion hinders cell's ability to initiate DSB repair and DDR causing sensitivity of the deletion strain to DNA-damaging agents, specifically those mimicking damage caused by radiation, such as MMS and Zeocin™ (**reviewed in Kaytor & Livingston, 1994; Krol *et al.,* 2015**). Therefore, *rad52* strain is typically included in such spotting assay as a sensitivity control.

Neither the single deletion mutants of Tda9 or Rsf2, nor the *tda9rsf2* double knockout strain exhibited sensitivity to 0.02% MMS or to the tested concentrations of Zeocin™ (**Figure 29, A**). In contrast – and as expected – to the *rad52* control, which displayed loss of viability in both cases.

These findings suggest that neither Tda9, nor Rsf2 is likely involved in – or acts as a mediator of – canonical DDR and recombination pathways. However, their involvement in telomere-specific recombination cannot be excluded, particularly in light of the findings presented in the chapter *"Formation of Type II ALT-Survivors in the Absence of TDA9 and RSF2 is Delayed"*, where the double deletion in a telomerase-deficient background impaired formation of ALT-survivors.

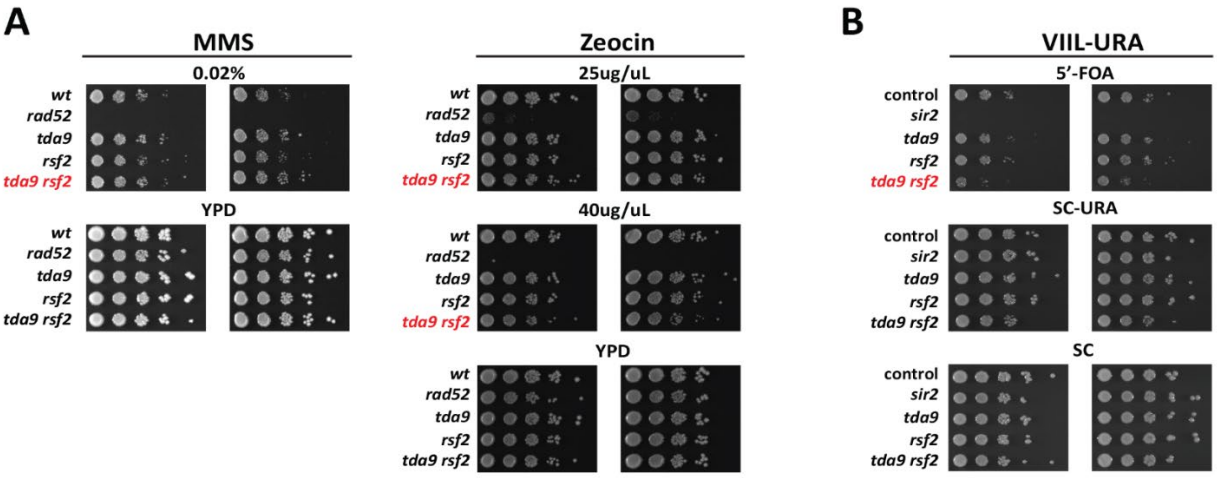

Figure 29. Assessment of Sensitivity to DNA Damaging Agents & TPE in Deletion Mutants.
A. Assessment of sensitivity to DNA-damaging agents in *tda9* and *rsf2* deletion mutants. Spotted on media containing 0.02% MMS or the respective concentrations of Zeocin™ 10-fold serial dilutions of indicated strains. Spotting on YPD medium serves as a control. Representative photos of two biological replicas at 72h. **B.** Assessment of the effect on subtelomeric transcription silencing (i.e., TPE) in the absence of Tda9 and Rsf2. Spotted 10-fold serial dilutions of indicated deletion strains in the VIIL-URA background. Representative photos of two biological replicas at 48h. Spotting on SC and SC-URA serves as a control. Here, "control" strain refers to the strain that has VIIL-URA background.

Next, formation of heterochromatin and silencing are initiated by Rap1-binding, which facilitates the recruitment of SIR complex (Sir2/3/4), whose distribution ensures epigenetic regulation of the transcription (**Figure 5**, chapter *"End-Protection Problem" and Composition of Telomeres in S. cerevisiae"*).

We then aimed to determine whether deletion of Tda9, Rsf2, or both affects telomeric silencing, a phenomenon known as the Telomere Position Effect (TPE). First described in yeast by Gottschling *et al.* (1990), TPE refers to the epigenetically regulated silencing of genes in the proximity to telomeres (**Sandell & Zakian, 1992**).

To monitor TPE in deletion mutants, I used strain carrying the *URA3* reporter gene integrated at a subtelomeric position (e.g., VIIL-URA) – a well-established system for studying gene silencing and chromatin structure (**e.g., Kimura *et al.*, 2002; Loney *et al.*, 2009**). In this system, *URA3* encodes orotidine-5'-phosphate decarboxylase (ODCase), which is required for pyrimidine biosynthesis. When *URA3* is transcriptionally active – i.e., when silencing is lost – ODCase converts the non-toxic compound 5-fluoroorotic acid (5'-FOA) into toxic 5-fluorouracil, leading to cell death.

Therefore, cells with intact TPE survive on medium supplemented with 5'-FOA, while those with impaired silencing – such as *sir2* mutant – cannot grow. The *sir2* strain, thus, serves as a positive control in spotting assay assessing telomeric silencing (**Figure 29, B**).

In this assay, the single deletion mutants of Tda9 and Rsf2 did not exhibit any apparent defects in TPE and silencing of the reporter gene (**Figure 29, B**). Interestingly and

in contrast, the *tda9rsf2* double knockout strain showed moderate growth impairment indicative of a partial TPE repression – i.e., lack of telomeric silencing in the absence of both proteins (**Figure 29, B**). These results might be indicative of altered chromatin structure at telomeres in the double knockout strain that is causing the decrease in silencing.

If so, one explanation might be that either or particularly in combination, Tda9 and Rsf2 contribute to epigenetic regulation occurring specifically at telomeres potentially acting as modulators of histones. Thus, Tda9 was proposed to be a recruiter of histone acetyltransferase (HAT) which enables its transcription activator abilities. These changes were mainly linked to the H3K18 modification – which in general appears to be favoured by a number of different TFs – as well as H3K27, H2BK11, H3K14 and H3K23 (**Pham *et al.*, 2007**; chapter *"Paralogs TDA9 and RSF2 Bind Yeast Telomeric Sequences in vitro"*). None of these histone modifications, however, are found at yeast telomeres as either eu- or heterochromatin-associated marks (**reviewed in Jezek & Green, 2019**).

To recapitulate, histone modifications such as acetylation and methylation, as well as distribution of the Sir proteins are important for the proper TPE. In particular, Sir2 – a NAD^+-dependent histone deacetylase – can remove acetyl group from lysin on histone H3 and H4 (i.e., H3K9, H3K14 and H4K16 modifications, respectively). Hypoacetylated form of H4K16 enhances binding of Sir3 to histone tails which in turn further promotes recruitment and association of Sir2 and Sir4. As a result, occupancy of Sir proteins and ***hypo***acetylation of H4K16 are highest near telomeres and gradually decrease with the distance from a chromosomal end, leading to a corresponding H4K16 ***hyper***acetylation and reduction in silencing (**Imai *et al.*, 2000; Landry *et al.*, 2000; Hoppe *et al.*, 2002; Kimura *et al.*, 2002; Rusche *et al.*, 2002; Katan-Khaykovich & Struhl, 2005; Rudner *et al.*, 2005; reviewed in Irizar *et al.*, 2010**).

Interestingly, though, while the majority of histone lysines are hypoacetylated or ubiquitinated enabling the proper TPE, in the study caried out by Zhou *et al.* (2011) the acetylation of H4K12 by NuA4 acetyltransferase complex at telomeric heterochromatin was linked to prevention of over-congregation and inappropriate binding of the Sir complex. Thus, preventing over-compaction of the subtelomeric region and ensuring its accessibility to transcription regulators and telomere-associated proteins.

Notably, loss of H4K12ac mark in this case was shown to cause similar effects on telomeres as concurrent deletion of Tda9 and Rsf2, including telomere shortening, reduced association of telomerase to telomeres due to the change in telomeric heterochromatin structure, and suppressive effect on HR at telomere ends causing disruption in the formation of Type II survivors (**Zhou *et al.*, 2011**).

Given the complexity of transcription factor regulatory networks, it is also possible that Tda9 and Rsf2 function as facilitators of histone modifications at a higher level, perhaps as transcription factors or co-factors regulating genes involved in chromatin remodelling and histone regulation. These, for instance, could include components of the Remodel the Structure of Chromatin (RSC) complex, the Histone Regulation (HIR) complex, or the Histone Deacetylase complex (RPD3S in yeast, homologous to SHREC in *S. pombe* and NuRD in humans). To test this hypothesis, it would be particularly interesting to investigate further whether expression levels of core histones or members of one of the abovementioned complexes are altered in the deletion mutants.

Additionally, considering the flexibility of transcription factors to bind an affinitive spectrum of sequences, it is also possible that Tda9 and Rsf2 interact with Subtelomeric Anti-silencing Regions, known as STARs (**Fourel *et al.,* 1999**). These sequences are naturally found in an immediate proximity to X and Y' elements and possess anti-silencing properties functioning as a barrier that prevents uncontrolled spread of silent chromatin. Notably, STARs contain Rap1-binding sites (**Fourel *et al.,* 1999**), which further supports this hypothesis given the similarity between binding sites of Rap1 and those predicted for Tda9/Rsf2.

Moreover, alterations in chromatin structure at telomeres have been linked to the regulation of a number of processes – including replication, DNA damage repair, recombination and transcription (**reviewed in Ottaviani *et al.,* 2007 and in Jezek & Green, 2019**).

In this case, the effect of Tda9 and Rsf2 on telomeres may also be more indirect, potentially reflecting a supportive or auxiliary role. For instance, their function could be analogous to that of the three ZnF-domain interactors of ZMYND8. While these proteins are thought to facilitate the activity of the ZMYND8-NuRD complex interaction in DDR and DSB, their precise contributions to these pathways remain incompletely understood (see **Figure 10** in the chapter *"Zinc Finger Proteins & Genome Integrity"*).

Next, transcribed from telomeres TERRA plays a role in modulation of telomerase activity, HDR and telomere capping in both yeast and human cells (**reviewed in Bettin *et al.,* 2019**). In yeast specifically, formed by TERRA RNA-DNA hybrids have been shown to accumulate at critically short telomeres thus regulating cycles of senescence in survivors known as Survivor Associated Senescence (SAS) (**Misino *et al.,* 2022**).

Therefore, given the results of compromised TPE and in addition to assessing histones and chromatin remodelling complexes expression levels in the deletion mutants, it would also be of significant interest to investigate towards potential changes in TERRA levels in deletion strains lacking active telomerase. In hindsight, the TERRA avenue should have been explored during the project but was regrettably overlooked due to my limited prior knowledge, despite my advisor's encouragement toward this line of inquiry.

Conclusion and Future Perspectives

This thesis aimed to identify novel telomere-associated binders across species within the *Ascomycota* yeast group. Two paralogs, the ZnF-domain-containing transcription factors Tda9 and Rsf2, emerged as the second most enriched proteins in nearly half of the species analysed, following the primary telomere binder Rap1, which was detected in the majority of species validating the approach.

Following the identification of these novel telomere-binding proteins (TBPs), an initial characterisation was undertaken to assess their association with telomeres in the budding yeast *Saccharomyces cerevisiae*. This involved phenotypic analyses related to telomere biology, including the effects of gene deletion and overexpression in different genetic backgrounds, impacts on replicative senescence and ALT-survivor formation, as well as alterations in chromatin structure at chromosomal termini.

Although the precise mechanism(s) by which these proteins act at telomeres were not fully elucidated in this study, the work presented establishes a solid foundation for future investigations into these novel ZnF telomere binders. Furthermore, the following chapter proposes their potential mode of action at telomeres, informed by the data generated in this study.

Overall, this work seeks to enhance our understanding of telomere biology and genome integrity in yeast as part of fundamental research, with the potential for translation into applied studies on human cancer, genome stability and healthy ageing.

Conclusion

In our screen for novel and conserved telomere-associated proteins across representatives of different clades within the *Saccharomycotina* subphylum, the main telomere binder Rap1 was successfully identified as one of the most highly enriched proteins.

Beyond well-characterised model organisms such as *S. cerevisiae*, it was particularly noteworthy to detect this protein in other yeast species across the phylogenetic tree (**Figure 13**, chapter *"Identifying Novel Telomere-Associated Proteins in Ascomycota Yeast Species"*). Especially given that genome databases for many of these less-studied species remain poorly annotated.

Rap1 is known to exhibit high tolerance towards variation in sequences it can bind, a property that underpins its versatility and functional uniqueness (as highlighted in chapters *"End-Protection Problem" and Composition of Telomeres in S. cerevisiae"* and *"Co-Evolution of Telomere-Associated Proteins and Telomeric DNA in Yeast"*). This, once again, provides Rap1 with a flexibility to act both as a major telomere binder and as a transcription factor throughout the genome.

It was, therefore, particularly interesting to identify Rap1 among the enriched proteins in species such as *C. lusitaniae*, the most phylogenetically distant species from the *Saccharomyces sensu stricto* group analysed in this study (**Figure 13, B**). This is particularly noteworthy given that *C. lusitaniae* harbours an unusual telomeric repeat sequence that contains only a single, apparent Rap1 half-site (**Steinberg-Neifach & Lue, 2015**).

Interestingly – though not entirely surprising given the well-established involvement of ZnF-domain containing proteins in genome stability and integrity – a substantial proportion of the identified in the screens across yeast phylogenetic tree proteins possess a ZnF domain (**Figure 14**, chapter *"Identifying Novel Telomere-Associated Proteins in Ascomycota Yeast Species"*).

Furthermore, ZnF protein Spt10 was identified in three species and ranked as the third most enriched hit following Rap1 and Tda9/Rsf2 (**Figure 13, C**). Its interacting partner, Spt21 – but not Spt10 itself – was previously reported in two high-throughput screens identifying deletion mutants with altered telomere length (**Askree *et al.,* 2004; Gatbonton *et al.,* 2006**).

Neither Spt21, nor Spt10 seem to interact with telomeres directly, however, mutations in or deletion of Spt10 were shown to have an effect on recruitment of Sir proteins and loss of silencing at telomeres. Nevertheless, in the respective study, authors could not elucidate the exact mechanism of action of these two factors (**Chang & Winston, 2011**).

Additionally, Npl6 appeared in one of these high-throughput screens (**Askree *et al.,* 2004**), while the pull-downs in this thesis identified Npl3 – recently characterised as a factor stabilising R-loops at short telomeres (**Perez-Martinez *et al.,* 2020**) – in two phylogenetically distant species (**Figure 13, C**).

Cumulatively, these findings further highlight the utility and robustness of the quantitative interactomics platform as an effective and powerful tool for reconstructing the evolutionary conservation of protein function, such as in case of Rap1. Moreover, this approach afforded us the opportunity to identify and investigate novel, previously uncharacterised telomere-associated proteins – ZnFs such as Tda9 and Rsf2.

***

Mass spectrometry analysis of proteins enriched in the *tda9rsf2* double knockout compared to wild type revealed several proteins from the same functional categories as those reported in the aforementioned high-throughput screens (**Supplementary 1**).

These include factors involved in phosphate metabolism – Pho89 and Pho5 in the double mutant, alongside reported hits Pho85, Pho80, Pho87, and Pho88 (**Askree *et al.,* 2004; Gatbonton *et al.,* 2006**). Similarly, in the category of nitrogen metabolism, Arg3 was enriched in the double knockout strain, while Arg2 had been reported in one of the previous screens (**Askree *et al.,* 2004**).

Furthermore, in the *tda9* mutant, mitochondrial protein Fmp40 and RNA metabolism factor Rrp46 were enriched, which resonates with previous reports identifying Fmp26 and Rrp8 (**Askree *et al.,* 2004**). Such correlations once again underscore the power of quantitative interactomics and mass spectrometry in supporting the reliability and interpretability of experimental data, reinforcing their importance for future research, evaluating anew previous studies and acting as foundational tools in basic science.

At the time of discovery, however, it may not always be evident why proteins with primary functions in seemingly unrelated processes – such as phosphate regulation, RNA processing, or mitochondrial activity – would have an impact on telomere biology. Often, such

connections are only elucidated later, sometimes explained by indirect mechanisms such as the “neighbouring gene effect” rather than direct telomere interaction.

For example, aforementioned Rrp8 – a gene involved in ribosomal pre-RNA processing, was initially reported in the 2004 screen as a deletion mutant causing slight telomere shortening (**Askree *et al.,* 2004**). However, a subsequent 2012 re-evaluation of gene annotation errors in frequently used mutant collections identified its proximity to Stn1 (**Ben-Shitrit *et al.,* 2012**). This insight, combined with more recent work, contributed to identifying epistatic effects on telomere length in the *elg1rrp8* double mutant, ultimately highlighting Elg1’s role via genetic and physical interactions with Stn1 (**Singh *et al.,* 2023**). In this case, the deletion of Rrp8 was disrupting expression of Stn1, an essential component of the CST telomeric ssDNA-binding complex, thereby indirectly affecting telomere maintenance and length as initially reported in high-throughput screen by Askree *et al.* (2004).

That said, unfortunately, neither Tda9 nor Rsf2 appeared in the aforementioned genetic screens, nor do they present obvious indicators such as a “neighbouring gene effect” to facilitate a straightforward interpretation of their roles at telomeres. Nevertheless, the data collected in the *Results and Discussion* section offer a basis for speculative model regarding their potential mechanisms of action at chromosomal termini.

***

In particular, findings discussed in the chapter *“Effects of DNA Damaging Agents & TPE in Deletion Mutants”* are indicative of altered chromatin structure at telomeres when Tda9 and Rsf2 are deleted.

Chapters *“Formation of Type II ALT-survivors in the Absence of TDA9 and RSF2 is Delayed”* and *“Growth and Senescence Profile Impairments in Deletion Mutants When Formation of Type I Survivors is Abolished (rad51 Background)”* highlight the importance and involvement of Tda9 and Rsf2 in the formation of survivors which utilise non-canonical telomere elongation mechanisms via homologous recombination.

In addition, in the absence of both Tda9 and Rsf2 telomerase processivity is seemingly reduced as discussed in the chapter *“Deletion of TDA9 and RSF2 Leads to Shorter Telomeres”*.

Collectively, these phenotypical observations point towards feasible involvement of Tda9 and Rsf2 as chromatin structure modulators at telomeres (**Figure 30**).

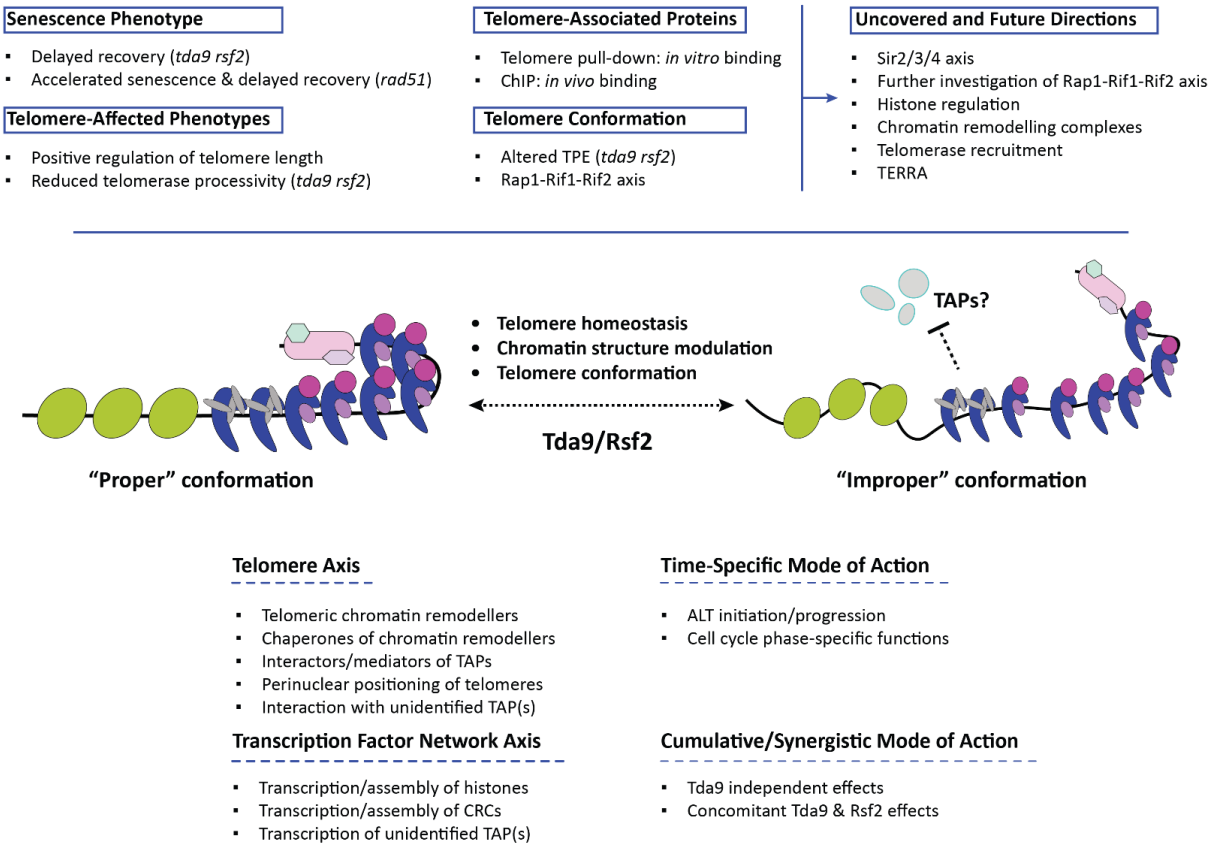

Figure 30. Summary of the experiments & Proposed Mode of Action for TDA9 and RSF2.
The **upper text section** summarises key findings of this thesis along with suggested directions for future experimental work.
The **middle scheme section** illustrates the proposed model for how Tda9 and Rsf2 may contribute to telomere regulation.
The **bottom text section** outlines specific roles and mechanisms of action in greater detail.
Dashed lines and dashed arrows indicate hypothetical relationships, proposed mechanism and function(s).
Proteins on the scheme as in **Figure 5**.
Abbreviations: TPE – telomere position effect; TAP – telomere-associated protein; CRC – chromatin remodelling complex; ALT – alternative lengthening of telomeres.

***

To strengthen this hypothesis, it is worth mentioning that the importance of proper conformation and structural stability of DNA at chromosomal termini has been highlighted by a number of studies.

For instance, disruption of this architecture has been shown to impair telomerase activity causing inhibition of telomeres extension, to lead to irregularities in telomeric structure and to reduce the formation of damage-induced foci at telomeres (Chow *et al.*, 2018).

In human telomeres, in addition to TPE which affects transcription within subtelomeric region, gene silencing can also be altered at a much greater distance from the heterochromatic subtelomeres due to the three-dimensional space positioning of the telomeres to otherwise transcriptionally active chromatin (i.e., looping onto a target gene) – a phenomenon referred to as TPE-OLD (telomere position effect over long distances; **reviewed in Misteli, 2014**). Notably, TPE-OLD has been proposed as a mechanism through which telomere shortening may influence ageing and the initiation or progression of disease prior to the activation of a critical DNA damage response (**Robin *et al.,* 2014**).

In addition to aforementioned H4K12 acetylation mediated by the NuA4 acetyltransferase complex at yeast telomeres – which produces phenotypes resembling those observed upon deletion of Tda9 and Rsf2, including suppression of HR and impairment of Type II survivor formation (**Zhou *et al.,* 2011** discussed in chapter *"Effects of DNA Damaging Agents & TPE in Deletion Mutants"*) – other histone-modifying enzymes have also been shown to influence telomere integrity.

For instance, deletion of the mouse histone methyltransferase DOT1L leads to a redistribution of epigenetic marks, including a reduction in H4K20me3 and an increase in euchromatic H3K9ac at DNA termini. Consequently, loss of DOT1L promotes activation of the ALT pathway, resulting in telomere elongation (**Jones *et al.,* 2008**).

In *S. cerevisiae*, deletion and overexpression of *DOT1*, as well as mutations affecting the euchromatin-associated H3K79 mark, were shown to cause loss of telomeric silencing. Presumably, this effect is mediated via altered interactions between Sir2/Sir3 and telomeres (**Ng *et al.,* 2002; van Leeuwen *et al.,* 2002**).

In general, H3K79 methylation can restrict the access of Sir proteins to heterochromatic regions (**reviewed in Ng *et al.,* 2003; Jones *et al.,* 2008**). The Dot1-deposited H3K79me mark has also been implicated in the control of the meiotic checkpoint by blocking DSB repair through a Rad54-dependent recombination pathway between sister chromatids.

Furthermore, Dot1 mutations have been shown to cause re-localisation of Sir3 away from telomeres, thereby resulting in loss of TPE (**San-Segundo *et al.,* 2000**). Additionally, Dot1 deletion has been demonstrated to impair activation of the yeast 53BP1 ortholog Rad9 or CHK2 homolog Rad53, leading to diminished Rad9 recruitment to DSBs following ionising radiation – findings indicative of Dot1's involvement in Rad9-dependent G1/S DNA damage checkpoint control in yeast (**Wysocki *et al.,* 2005**).

Nucleosomes are considered to be general inhibitors of transcription (**reviewed in Kornberg & Lorch, 2020; Lorch *et al.,* 1987**). Thus, it is plausible to assume that levels of transcription at subtelomeric and telomeric regions might be altered when chromatin structure is modified. This in turn might affect an important player in telomere maintenance – TERRA. Research into elucidation of TERRA transcription regulation is still ongoing, and current findings suggest a complex regulatory network of multiple mechanisms that vary depending on the model organism (**reviewed in Rivosecchi *et al.,* 2024**).

Interestingly, a recent study by Bauer *et al.* (2022) investigated how the essential protein and pioneer-transcription factor Reb1 – together with Sir2 – can function in opposing

pathways and antagonistically regulate TERRA transcription by modulating nucleosome positioning and occupancy at subtelomeric X-elements in yeast.

Specifically, the authors demonstrated that Sir2 and Reb1 compete for binding at the three nucleosomes located within the STR-D region of the X-element. Thus, Sir2 facilitates the stabilisation of the +1 nucleosome downstream of the TSS of TERRA, resulting in transcriptional repression. In Sir2-deficient cells, destabilisation of nucleosomes in this region was observed without changes in the TSS, leading to upregulation of TERRA transcription. Conversely, Reb1 binding at STR-D was shown to induce nucleosome destabilisation at the same loci, restricting cryptic and read-through transcription via a roadblock transcription termination mechanism, thereby reducing levels of telomeric RNA.

Collectively, these findings demonstrate that both transcription factor Reb1 and Sir2 can repress TERRA expression through distinct regulatory mechanisms, yet exert a cumulative effect on nucleosomal assembly at chromosomal termini.

Overall, TERRA transcripts play important roles in telomere maintenance. Among other functions, they have been shown to promote telomere instability through the formation of RNA:DNA hybrids (R-loops), which can result in replication fork stalling and collapse, as well as the activation of the DDR (**Aguilera & Gomez-Gonzalez, 2008; Balk *et al.,* 2013; Graf *et al.,* 2017**).

Conversely, TERRAs have also been demonstrated to facilitate ALT by promoting the recruitment of proteins involved in homologous recombination in telomerase-negative cells (**Arora *et al.,* 2014; Yu *et al.,* 2014**). In addition, these telomeric transcripts have been shown to associate to short telomeres, where they contribute to slowing the rate of survivor-associated senescence (SAS), thereby regulating short-telomere induced senescence disfunction that survivors undergo in cycles (**Misino *et al.,* 2022**).

The spatial configuration and organisation of telomeres to the nuclear periphery also considered to be an important feature contributing to genome stability, integrity and overall chromosomal architecture.

For instance, in *S. pombe* proper anchoring of telomeres to the nuclear envelope is mediated by the interaction between Rap1 and the inner nuclear membrane protein Bqt4. This peripheral localisation of telomeres creates a “buffer area” where gratuitous transcription and recombination are restricted ensuring telomere integrity in post-mitotic cells (**Maestroni *et al.,* 2020**).

***

Given the results presented and discussed in this thesis, in combination with the aforementioned studies – if Tda9 and Rsf2 indeed act as chromatin structure modulators at telomeres, they may exert this function through several possible mechanisms (middle scheme and bottom text sections in **Figure 30**).

One possibility is that they interact directly with telomeres. Supporting evidence includes ChIP results (**Figure 17, A** and additionally **Figure 16, D**), and the observation that in both – telomere pull-downs and mass spectrometry analyses of single and double deletion mutants (**Supplementary 1**) – no potential interactor was identified that showed a consistent enrichment (or depletion pattern) analogous to that of Rap1, Tda9 and Rsf2.

Moreover, the data presented and discussed in the chapter "*RAP1 Depletion Causes a Slight Increase in the Levels of TDA9 and RSF2 at Telomeres*" suggest that these proteins might directly associate with telomeres. Specifically, depletion of the major dsDNA telomere binder Rap1 led to a slight increase in the levels of Tda9 and Rsf2 at telomeric loci, implying a possible compensatory relationship. However, competitive one is also possible, yet less feasible at this point given the absence of overexpression in the *rif1rif2* results (discussed in the chapter *"Overexpression of TDA9, but not RSF2, in the Absence of RIF1 and RIF2 Alters Telomere Length*").

Additionally, both Tda9 and Rsf2 possess predicted binding sequences similar to the Rap1 recognition motif found at telomeres (**Figure 15, B (1) and C**). Although, neither matches the Rap1 binding site perfectly, it is well established that transcription factors can tolerate mismatches in their consensus sequences and exhibit varying levels of binding affinity, as is the case for Rap1 itself (**Wahlin & Cohn, 2000; Pina *et al.,* 2003; Steinberg-Neifach *et al.,* 2015**).

External findings in this case also support the potential for direct telomeric interaction, particularly for Tda9 – i.e., results of EMSA by Badis *et al.* (2008) (**Figure 15, B (2)**) and the proposed role of Tda9 in recruiting a histone acetyltransferase either individually or in a complex (**Pham *et al.,* 2007**) point towards its DNA-binding capability (chapter *"Paralogs TDA9 and RSF2 Bind Yeast Telomeric Sequences in vitro"*).

However, despite Tda9 and Rsf2 being ZnF-domain paralogs with the same predicted binding motif (**Figure 15, B (1)**), direct telomeric association is less clearly feasible for Rsf2. While presented in this study ChIP results do indicate telomeric presence (**Figure 17, A** and additionally **Figure 16, D**), overexpression and deletion of Rsf2 did not yield a notable telomeric phenotype as discussed in chapters *"Overexpression of TDA9, but not RSF2, Alters Telomere Length"*, *"Overexpression of TDA9, but not RSF2, in the Absence of RIF1 and RIF2 Alters Telomere Length"*, and *"Deletion of TDA9 and RSF2 Leads to Shorter Telomeres"*.

Furthermore, Lu *et al.* (2005) proposed that Rsf2 may not bind DNA directly, as no UASs were identified for the genes it supposedly regulates (discussed in chapter *"Paralogs TDA9 and RSF2 Bind Yeast Telomeric Sequences in vitro"*).

Taken together, these findings suggest that Tda9 is more likely to interact directly with telomeres, whereas Rsf2 may fiction upstream in the regulatory hierarchy.

However, it remains also possible that Tda9 and Rsf2 act in a synergistic or complementary manner at telomeres (bottom text section in **Figure 30**).

For example, while Tda9 exert a direct role at telomeres, Rsf2 can potentially act in an auxiliary or chaperone-like capacity – as a transcription factor influencing the expression of a core histone, chromatin remodelling complex, or currently unidentified telomere-associated protein.

It is also conceivable that both paralogs are capable of performing dual roles – acting as transcription factors and directly binding telomeres – each exhibiting distinct functional preferences or capacities for either or both activities.

These hypotheses are particularly supported by the more pronounced telomeric phenotypes observed in the double deletion mutant compared to the single deletions in a

number of tested backgrounds, suggesting a cumulative or cooperative effect (bottom text section of **Figure 30**).

Furthermore, in addition to results of overexpression in different genetic backgrounds data from ChIP experiments, measurements of colony diameter sizes of meiotic progenies, and senescence curve analyses consistently indicate that Tda9 exerts a more substantial influence on telomeres than Rsf2.

***

Overall, although the full mechanism by which Tda9 and Rsf2 may exert their influence on telomeres has not been elucidated within the scope of this study, the following section outlines potential follow-up experiments that could provide further insight into the roles of these proteins at telomeres, thereby building upon and strengthening the findings presented and discussed in this thesis.

Future Perspectives

To further investigate the hypothesis that Tda9 and Rsf2 function as modulators of telomeric chromatin structure, several additional to already have been mentioned follow-up experiments could be pursued (upper right text section in **Figure 30**).

Given the observed mild de-silencing effect upon deletion of both proteins which was discussed in chapter *"Effects of DNA Damaging Agents & TPE in Deletion mutants"*, it would be valuable to assess whether expression levels of core histones are altered in the double deletion mutant, but also in the single ones.

Moreover, as Tda9 and Rsf2 are transcription factors known to regulate metabolic pathways and given the complexity of TF's network, it is conceivable that one or both may also influence the expression of genes outside their known targets. Although mass spectrometry analysis of the deletion mutants did not reveal an obvious telomere-associated interactor affected by the deletions (**Supplementary 1**), global transcriptomic profiling could provide further insight. For instance, RNA sequencing could identify changes in the expression of chromatin remodelling or histone mark-regulating complexes such as RSC, HIR, RPD3S, or others, which might directly or indirectly impact telomeric structure and silencing.

Another approach would involve overexpression of individual Sir proteins to determine whether they can rescue the reduced TPE phenotype observed in the double knockout strain. Thus, Sir3 overexpression, in particular, has previously been shown to enhance the spreading of silencing chromatin at telomeres (**Renauld *et al.,* 1993; Hecht *et al.,* 1996; Luo *et al.,* 2002**). Such an experiment could clarify whether Tda9 and Rsf2 influence telomeric silencing not by directly competing with Rap1, but perhaps by modulating the activity or localisation of its associated silencing partners – Sir2, Sir3 and/or Sir4.

Depending on the results, one could also perform ChIP in a background where Sir proteins are depleted or deleted, to determine whether Tda9 and Rsf2 levels at telomeres are affected. Along this line, telomere length assessment via Southern blot could be carried out in one of the Sir deletion backgrounds.

Notably, deletion of either or both Sir3 and Sir4 is known to result in shorter telomeres and disrupt their perinuclear localisation (**Palladino *et al.,* 1993**). It would, therefore, be informative to examine whether the *tda9rsf2* deletion mutant exhibits even shorter telomeres in *sir3*, *sir4*, or *sir3sir4* double knockout backgrounds. This, again, could help clarify whether chromatin modulation by Tda9, Rsf2, or both, functions through an axis involving Sir proteins rather than the Rap1-Rif1-Rif2 assembly (upper right text section in **Figure 30**).

Next, given the results discussed in the chapter *"Deletion of TDA9 and RSF2 Leads to Shorter Telomeres"*, which suggest that telomerase is less processive in the *tda9rsf2* double knockout strain, it would also be worthwhile to perform ChIP using tagged telomerase to determine whether its recruitment is impaired.

If telomerase levels at telomeres remain unchanged, this could imply that Tda9 and Rsf2 are not directly involved in facilitating telomerase action. Instead, the shortened telomeres might be a consequence of their regulatory roles at a higher level within the transcription factor network.

Conversely, if telomerase levels are reduced in the double knockout, this would support the idea that Tda9 and Rsf2 influence chromatin structure at telomeres. In such a case, telomerase may either dissociate prematurely or be inadequately recruited due to altered telomeric conformation, leading to limited access to chromosomal termini and incomplete extension cycles. However, in this scenario, it remains possible that Tda9 and Rsf2 can affect telomerase recruitment indirectly, perhaps through interaction with another protein involved in facilitating telomerase access to telomeres.

In addition, recombination in Type I survivors has been shown to depend on the helicase Pif1 and the Ino80 chromatin remodelling complex (**Hu *et al.,* 2013**), underscoring the necessity of proper chromatin architecture for efficient HR. If Tda9 and Rsf2 act as telomeric chromatin modulators, the impaired survivor formation observed in their absence may be due to HR defects caused by disrupted chromatin organisation.

Therefore, building on findings from the chapters *"Formation of Type II ALT-survivors in the Absence of TDA9 and RSF2 is Delayed"* and *"Growth and Senescence Profile Impairments in Deletion Mutants When Formation of Type I Survivors is Abolished (rad51 Background)"* – which indicate compromised HR including evident accelerated senescence and severe survivor formation impairment in the *rad51* background, as well as survivor formation impairment in *tlc1* background – it would be valuable to assess senescence curves in the single and double deletion strains of Tda9 and Rsf2 in other genetic contexts.

Both Rad51 and Rad59 ensure the formation of survivors from ALT-precursor cells (see chapter *"Survivors of Replicative Senescence in Yeast"*). Notably, Rad59 promotes Rad52-mediated strand annealing and facilitates Rad51-independent Y' translocations – a mechanism of subtelomeric recombination in pre-senescent, telomerase-deficient cells. Deletion of Rad59 has been shown to impair Y' translocation efficiency, leading to accelerated senescence and prolonged crisis (**Churikov *et al.,* 2014**). It is, therefore, plausible to assume that such rearrangements could be compromised in case of impaired telomeric chromatin structure organisation, which can cause disruptions in the formation of ALT-precursor.

As the formation of any ALT survivor generally requires Rad52, which mediates HR (**Lundblad & Blackburn, 1993; Le *et al.,* 1999**), using *rad52* background would not be

possible. Instead, one could test Tda9 and Rsf2 deletions in a *rad59* background – this could help determine whether more pronounced epistatic effect on senescence arise and whether these cells remain viable or can form survivors at all, as was, rather surprisingly, observed in the *rad51* background in this study. Depending on the outcome, such an experiment could support the idea of compromised HR in the absence of Tda9 and Rsf2, thereby further reinforcing the hypothesis of their involvement in telomeric recombination and their potential influence on telomere conformation.

Additionally, to investigate whether Tda9 and Rsf2 influence telomeric chromatin through the Sir2/3/4 axis, senescence kinetics could also be analysed in deletion backgrounds of these proteins – particularly in the *sir4* background.

In addition to its role in silencing via Rap1-Sir2/3/4 interactions, Sir4 binding to Yku80 is required for telomerase recruitment in G1 (**Hass & Zappulla, 2015; Chen *et al.,* 2018**). Interestingly, telomere-capping-defective *yku70mre11* cells with active telomerase show senescence-like phenotype and senesce rapidly during the early growth of germinated spores but can recover and overcome the crisis efficiently (**Maringele & Lydall, 2004**).

Recently, Sir4 deficiency was shown to rescue telomere-shortening-induced senescence in *yku80mre11* cells by amplifying subtelomeric Y' elements via a Rad51-dependent pathway, leading to telomere lengthening (**Liu *et al.,* 2021**). That same study also demonstrated that this recombination-based rescue is inhibited by Sir4's interaction with Mps3, a perinuclear protein that ensures telomeres' anchoring to the nuclear envelope and repression of TERRA transcription.

Therefore, it would be valuable to assess Y' telomere length and senescence kinetics in the Tda9, Rsf2, and Sir2/3/4 deletion mutants to determine whether these genetic alterations enhance or further delay recovery and survivor formation.

***

In summary, the findings presented suggest a multifaceted role for Tda9 and Rsf2 in the modulation of telomeric chromatin – conceivably through both direct and indirect pathways. Their mechanism of action may operate at multiple levels and potentially involve transcriptional regulation, chromatin remodelling, and interactions with silencing complexes and/or other telomere-associated protein(s).

Further exploration using the outlined experimental approaches will be valuable in defining the precise molecular functions of these proteins at telomeres, as well as their broader impact on telomere homeostasis and cellular senescence.

Supplementary

Supplementary 1

wt
vs
tda9 rsf2

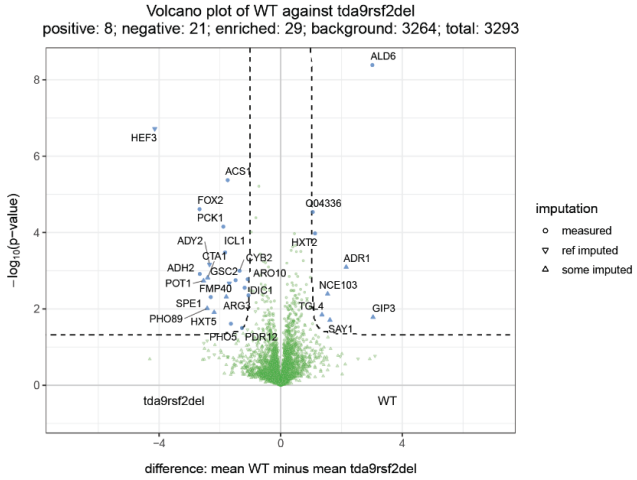

wt
vs
tda9

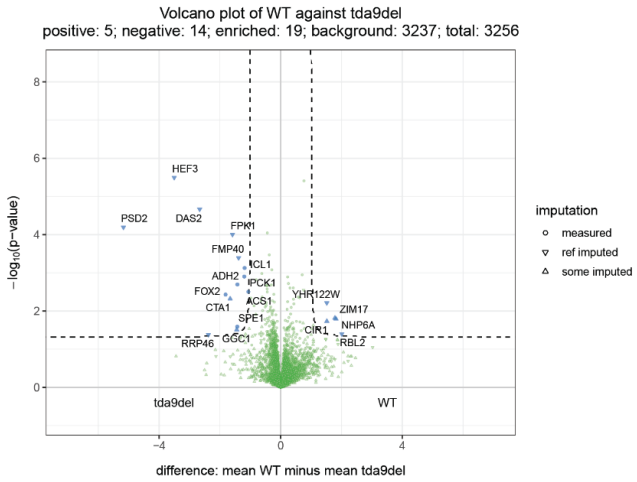

wt
vs
rsf2

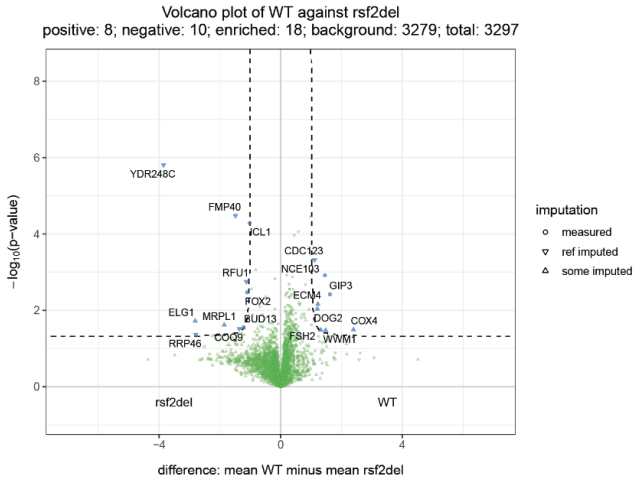

Materials and Methods

Materials

1. Yeast Strains

The yeast strains used in this study are derivatives of the BY4741 background (**Winston *et al.*, 1995**) with the *MATa his3Δ1 leu2Δ0 met15Δ0 ura3Δ0* genotype unless stated otherwise.

Strains used for the Telo pull-downs were obtained from the DSMZ-German Collection of Microorganisms and Cell Cultures GmbH (**www.dsmz.de**).

Strain ID	Description/ Genotype	Source
DSM 2791	*Schizosaccharomyces pombe var. pombe*	DSMZ
DSM 3774	*Saccharomyces bayanus (kudriavzevii)*	DSMZ
DSM 3795	*Kluyveromyces lactis*	DSMZ
DSM 11226	*Candida glabrata*	DSMZ
DSM 24508	*Candida orthopsilosis*	DSMZ
DSM 5784	*Candida parapsilosis*	DSMZ
DSM 11947	*Pichia guilliermondii (Candida guilliermondii)*	DSMZ
DSM 1345	*Yarrowia lipolytica*	DSMZ
DSM 70102	*Clavispora lusitaniae*	DSMZ
DSM 3428	*Debaryomyces hansenii*	DSMZ
DSM 3485	*Ashbya gossypii (Eremothecium gossypii)*	DSMZ
DSM 70320	*Lodderomyces elongisporus*	DSMZ
yAL95	*MATa/MATalpha his3Δ1/his3Δ1 leu2Δ0/leu2Δ0 ura3Δ0/ura3Δ0 MET15/met15Δ0 LYS2/lys2Δ0 TLC1/tlc1::NAT*	[redacted]
yBL7	*MATa his3Δ1 leu2Δ0 ura3Δ0 met15Δ0*	Euroscarf
yBL627	*MATa his3Δ1 leu2Δ0 ura3Δ0 met15Δ0 VIIL-URA3*	[redacted]
yBL629	*MATa his3Δ1 leu2Δ0 ura3Δ0 met15Δ0 sir2::KAN VIIL-URA3*	[redacted]
yBL229	*MATalpha his3Δ1 leu2Δ0 ura3Δ0 lys2Δ0 rad52::KAN*	Euroscarf
yBL354	*MATa his3Δ1 leu2Δ0 ura3Δ0 rif1::KAN*	[redacted]
yBL356	*MATa his3Δ1 leu2Δ0 ura3Δ0 rif2::KAN*	[redacted]
yBL627	*MATa his3Δ1 leu2Δ0 ura3Δ0 met15Δ0 VIIL-URA3*	[redacted]
yBL629	*MATa his3Δ1 leu2Δ0 ura3Δ0 met15Δ0 VIIL- URA3 sir2::KAN*	[redacted]
yCW7	*MATalpha his3Δ1 leu2Δ0 ura3Δ0 met15Δ0*	[redacted]
yFB115	*MATalpha his3Δ1 leu2Δ0 ura3Δ0 rad51::KAN*	[redacted]
yNL318, 319	*MATalpha his3Δ1 leu2Δ0 ura3Δ0 met15Δ0 LYS2 lyp1Δ::GAL1pr-OsTIR1(F74G)-NATMX RAP1-AID*-3MYC::HYG Tda9-3HA-KAN*	[redacted]
yNL323	*MATa his3Δ1 leu2Δ0 ura3Δ0 met15Δ0 LYS2 lyp1Δ::GAL1pr-OsTIR1(F74G)-NATMX RAP1-AID*-3MYC::HYG Tda9-3HA-KAN*	[redacted]
yNL324, 325	*MATalpha his3Δ1 leu2Δ0 ura3Δ0 met15Δ0 LYS2 lyp1Δ::GAL1pr-OsTIR1(F74G)-NATMX RAP1-AID*-3MYC::HYG Rsf2-3HA-KAN*	[redacted]
yNL329	*MATa his3Δ1 leu2Δ0 ura3Δ0 met15Δ0 LYS2 lyp1Δ::GAL1pr-OsTIR1(F74G)-NATMX RAP1-AID*-3MYC::HYG Rsf2-3HA-KAN*	[redacted]
yNL312, 313	*MATalpha his3Δ1 leu2Δ0 ura3Δ0 met15Δ0 LYS2 lyp1Δ::GAL1pr-OsTIR1(F74G)-NATMX RAP1-AID*-3MYC::HYG*	[redacted]
yNL317	*MATa his3Δ1 leu2Δ0 ura3Δ0 met15Δ0 LYS2 lyp1Δ::GAL1pr-OsTIR1(F74G)-NATMX RAP1-AID*-3MYC::HYG*	[redacted]

yRD302, 303	*his3Δ1 leu2Δ0 ura3Δ0 tda9::KAN rsf2::HYG*	[redacted]
yRD548	*MATa/MATalpha his3Δ1/his3Δ1 leu2Δ0/leu2Δ0 ura3Δ0/ura3Δ0 REV1/rev1::HIS REV7/rev7::KAN TLC1/tlc1::NAT*	[redacted]
yVV2	*MATa/MATalpha his3Δ1/his3Δ1 leu2Δ0/leu2Δ0 ura3Δ0/ura3Δ0 TDA9/tda9::KAN RSF2/rsf2::HYG TLC1/tlc1::NAT*	This study
yVV9; yVV10	*MATa his3Δ1 leu2Δ0 ura3Δ0 met15Δ0 tda9::KAN*	This study
yVV11; yVV12	*MATalpha his3Δ1 leu2Δ0 ura3Δ0 met15Δ0 tda9::KAN*	This study
yVV13; yVV14	*MATa his3Δ1 leu2Δ0 ura3Δ0 met15Δ0 rsf2::HYG*	This study
yVV15; yVV16	*MATalpha his3Δ1 leu2Δ0 ura3Δ0 met15Δ0 rsf2::HYG*	This study
yVV18	*MATa his3Δ1 leu2Δ0 ura3Δ0 met15Δ0 tda9::KAN rsf2::HYG*	This study
yVV19; yVV20	*MATalpha his3Δ1 leu2Δ0 ura3Δ0 met15Δ0 tda9::KAN rsf2::HYG*	This study
yVV150; yVV151	*MATalpha his3Δ1 leu2Δ0 ura3Δ0 met15Δ0 TDA9-TAP-HIS3MX6*	This study
yVV152; yVV154; yVV155	*MATalpha his3Δ1 leu2Δ0 ura3Δ0 met15Δ0 RSF2-TAP-HIS3MX6*	This study
yVV153; yVV156	*MATa his3Δ1 leu2Δ0 ura3Δ0 met15Δ0 RSF2-TAP-HIS3MX6*	This study
yVV188 – 190	*MATa his3Δ1 leu2Δ0 ura3Δ0 met15Δ0* + pBL183 (eV, overexpression control for pBG1805)	This study
yVV194 – 196	*MATa his3Δ1 leu2Δ0 ura3Δ0 met15Δ0* + pBG1805_TDA9 (TDA9 oE)	This study
yVV201 – 203	*MATa his3Δ1 leu2Δ0 ura3Δ0 met15Δ0* + pRS423_RSF2 (RSF2 oE)	This study
yVV204 – 206	*MATa his3Δ1 leu2Δ0 ura3Δ0 met15Δ0* + pRS423 (eV, overexpression control for pRS423)	This study
yVV207 – 209	*MATa his3Δ1 leu2Δ0 ura3Δ0 met15Δ0* + pRS425_RAP1 (RAP1 oE)	This study
yVV210 – 212	*MATa his3Δ1 leu2Δ0 ura3Δ0 met15Δ0* + pRS425 (eV, overexpression control for pRS425)	This study
yVV213 – 215	*MATa his3Δ1 leu2Δ0 ura3Δ0 met15Δ0* + pRS423_RSF2 + pRS425_RAP1 (co-oE of RSF2 and RAP1)	This study
yVV216 – 218	*MATa his3Δ1 leu2Δ0 ura3Δ0 met15Δ0* + pRS423 + pRS425 (eVs, overexpression control for pRS423 and pRS425)	This study
yVV219 – 221	*MATa his3Δ1 leu2Δ0 ura3Δ0 met15Δ0* + pBG1805_TDA9 + pRS425_RAP1 (co-oE of TDA9 and RAP1)	This study
yVV222 – 224	*MATa his3Δ1 leu2Δ0 ura3Δ0 met15Δ0* + pBL183 + pRS425 (eVs, overexpression control for pBG1805 and pRS425)	This study
yVV225, yVV226	*MATa/MATalpha his3Δ1/his3Δ1 leu2Δ0/leu2Δ0 ura3Δ0/ura3Δ0 met15Δ0/met15Δ0 VIIL/VIIL-URA3 TDA9/tda9::KAN*	This study
yVV227, yVV228	*MATa/MATalpha his3Δ1/his3Δ1 leu2Δ0/leu2Δ0 ura3Δ0/ura3Δ0 met15Δ0/met15Δ0 VIIL/VIIL-URA3 RSF2/rsf2::HYG*	This study
yVV229, yVV230	*MATa/MATalpha his3Δ1/his3Δ1 leu2Δ0/leu2Δ0 ura3Δ0/ura3Δ0 met15Δ0/met15Δ0 VIIL/VIIL-URA3 TDA9/tda9::KAN RSF2/rsf2::HYG*	This study
yVV231 – 234	*MATalpha his3Δ1 leu2Δ0 ura3Δ0 rad51::HIS*	This study
yVV237	*MATa his3Δ1 leu2Δ0 ura3Δ0 met15Δ0 VIIL-URA3 tda9::KAN*	This study
yVV238, yVV243	*MATalpha his3Δ1 leu2Δ0 ura3Δ0 met15Δ0 VIIL-URA3 tda9::KAN*	This study
yVV242	*MATa his3Δ1 leu2Δ0 ura3Δ0 met15Δ0 VIIL-URA3 tda9::KAN*	This study
yVV239, yVV245	*MATalpha his3Δ1 leu2Δ0 ura3Δ0 met15Δ0 VIIL-URA3 rsf2::HYG*	This study

yVV240, yVV246	*MATa his3Δ1 leu2Δ0 ura3Δ0 met15Δ0 VIIL-URA3 tda9::KAN rsf2::HYG*	This study
yVV241, yVV247	*MATalpha his3Δ1 leu2Δ0 ura3Δ0 met15Δ0 VIIL-URA3 tda9::KAN rsf2::HYG*	This study
yVV244	*MATa his3Δ1 leu2Δ0 ura3Δ0 met15Δ0 VIIL-URA3 rsf2::HYG*	This study
yVV252, yVV253	*MATalpha his3Δ1 leu2Δ0 ura3Δ0 lys2Δ0 rad52::KAN* + pBG1805_TDA9 (TDA9 oE)	This study
yVV254, yVV255	*MATalpha his3Δ1 leu2Δ0 ura3Δ0 lys2Δ0 rad52::KAN* + pBL183 (eV, overexpression control for pBG1805)	This study
yVV256, yVV257	*MATalpha his3Δ1 leu2Δ0 ura3Δ0 lys2Δ0 rad52::KAN* + pRS425_RAP1 (RAP1 oE)	This study
yVV258, yVV259	*MATalpha his3Δ1 leu2Δ0 ura3Δ0 lys2Δ0 rad52::KAN* + pRS425 (eV, overexpression control for pRS425)	This study
yVV260	*MATalpha his3Δ1 leu2Δ0 ura3Δ0 lys2Δ0 rad52::KAN* + pRS425_RAP1 + pBG1805_TDA9 (co-oE of TDA9 and RAP1)	This study
yVV261, yVV262	*MATalpha his3Δ1 leu2Δ0 ura3Δ0 lys2Δ0 rad52::KAN* + pRS425 + pBL183 (eVs, overexpression control for pRS425 and pBG1805)	This study
yVV263, yVV264	*MATa his3Δ1 leu2Δ0 ura3Δ0 rif1::KAN* + pBL183 (eV, overexpression control for pBG1805)	This study
yVV265, yVV266	*MATa his3Δ1 leu2Δ0 ura3Δ0 rif1::KAN* + pBG1805_TDA9 (TDA9 oE)	This study
yVV267, yVV268	*MATa his3Δ1 leu2Δ0 ura3Δ0 rif2::KAN* + pBL183 (eV, overexpression control for pBG1805)	This study
yVV269, yVV270	*MATa his3Δ1 leu2Δ0 ura3Δ0 rif2::KAN* + pBG1805_TDA9 (TDA9 oE)	This study
yVV271, yVV272	*MATa his3Δ1 leu2Δ0 ura3Δ0 rif1::KAN* + pRS423 (eV, overexpression control for pRS423)	This study
yVV273, yVV274	*MATa his3Δ1 leu2Δ0 ura3Δ0 rif1::KAN* + pRS423_RSF2 (pRS423 oE)	This study
yVV275, yVV276	*MATa his3Δ1 leu2Δ0 ura3Δ0 rif2::KAN* + pRS423 (eV, overexpression control for pRS423)	This study
yVV277, yVV278	*MATa his3Δ1 leu2Δ0 ura3Δ0 rif2::KAN* + pRS423_RSF2 (pRS423 oE)	This study

2. Plasmids

Plasmid ID	Description	Source
pBG1805_TDA9	pBG1805 carrying pGAL-TDA9 ORF-6xHIS3-HA-URA3, 2μ (AmpR)	Dharmacon
pBL183	BG1766 carrying pGAL-6xHIS3-HA-URA3 empty ORF control vector, 2μ (AmpR)	[redacted]
pRS423_RSF2	pRS423 carrying pGAL-RSF2 ORF-3HA-HIS3, 2μ (AmpR)	This study
pRS423	pRS423-pGAL-3HA-HIS3 empty ORF control vector, 2μ (AmpR)	[redacted]
pRS425_RAP1	pRS425 carrying pGAL-RAP1 ORF-3HA-LEU2, 2μ (AmpR)	This study
pRS425	pRS425 carrying pGAL-3HA-LEU2 empty ORF control vector, 2μ (AmpR)	[redacted]

3. Oligonucleotides

Oligo ID	Description	Sequence (5' -> 3')
Spombe_telo_fw	Fw; telomere bait oligo for *S. pombe* Telo pull-down	GTTACAGGTTACAGGGTTACAGGGGTTACAGGGGGTTACAGGGGGGTTACAGGGGGGGTTACAGGGGGGGG
Spombe_telo_rv	Rev; telomere bait oligo for *S. pombe* Telo pull-down	ACCCCCCCCCTGTAACCCCCCCTGTAACCCCCCTGTAACCCCCTGTAACCCCTGTAACCCTGTAACCTGTA
Scerevisiae_telo_fw	Fw; telomere bait oligo for *S. cerevisiae/kudriavzevii/bayanus* Telo pull-down	GTGGGTGTGTGGTGTGGGTGTGTGGGTGTGTGTGGTGTGGGTGTGTGTGGGTGTGTGTGTGGGTGTGGGTGTGGTGT
Scerevisiae_telo_rv	Rev; telomere bait oligo for *S. cerevisiae/kudriavzevii/bayanus* Telo pull-down	ACACACCACACCCACACCCACACACACACCCACACACCCACACCACACACACCCACACACCCACACCACACACCC
Klactis_telo_fw	Fw; telomere bait oligo for *K. lactis* Telo pull-down	ATTTGATTAGGTATGTGGTGTACGGATTTGATTAGGTATGTGGTGTACGGATTTGATTAGGTATGTGGTGTACGG
Klactis_telo_rv	Rev; telomere bait oligo for *K. lactis* Telo pull-down	ATCCGTACACCACATACCTAATCAAATCCGTACACCACATACCTAATCAAATCCGTACACCACATACCTAATCAA
Cglabrata_telo_fw	Fw; telomere bait oligo for *C. glabrata* Telo pull-down	CTGGGTGCTGTGGGGTCTGGGTGCTGTGGGGTCTGGGGTGCTGTGGGGTCTGGGTGCTGTGGGGT
Cglabrata_telo_rv	Rev; telomere bait oligo for *C. glabrata* Telo pull-down	AGACCCCACAGCACCCAGACCCCACAGCACCCAGACCCCACAGCACCCAGACCCCACAGCACCC
Corthopsilosis_telo_fw	Fw; telomere bait oligo for *C. orthopsilosis* Telo pull-down	GTTAGGATGTAGACAATACTGCGGTTAGGATGTAGACAATACTGCGGTTAGGATGTAGACAATACTGCG
Corthopsilosis_telo_rv	Rev; telomere bait oligo for *C. orthopsilosis* Telo pull-down	ACCGCAGTATTGTCTACATCCTAACCGCAGTATTGTCTACATCCTAACCGCAGTATTGTCTACATCCTA
Cparapsilosis_telo_fw	Fw; telomere bait oligo for *C. parapsilosis* Telo pull-down	GTCCGGATGTTGATTATACTGAGGTCCGGATGTTGATTATACTGAGGTCCGGATGTTGATTATACTGAG
Cparapsilosis_telo_rv	Rev; telomere bait oligo for *C. parapsilosis* Telo pull-down	ACCTCAGTATAATCAACATCCGGACCTCAGTATAATCAACATCCGGACCTCAGTATAATCAACATCCGG
Dhansenii_telo_fw	Fw; telomere bait oligo for *D. hansenii* Telo pull-down	ATGTTGAGGTGTAGGGATGTTGAGGTGTAGGGATGTTGAGGTGTAGGGATGTTGAGGTGTAGGG
Dhansenii_telo_rv	Rev; telomere bait oligo for *D. hansenii* Telo pull-down	ATCCCTACACCTCAACATCCCTACACCTCAACATCCCTACACCTCAACATCCCTACACCTCAAC
Agossypii_telo_fw	Fw; telomere bait oligo for *E. gossypii* Telo pull-down	GTGTGGTGTATGGGTCTCTCAGCGGTGTGGTGTATGGGTCTCTCAGCGGTGTGGTGTATGGGTCTCTCAGCG
Agossypii_telo_rv	Rev; telomere bait oligo for *E. gossypii* Telo pull-down	ACCGCTGAGAGACCCATACACCACACCGCTGAGAGACCCATACACCACACCGCTGAGAGACCCATACACCAC
Lelongisporus_telo_fw	Fw; telomere bait oligo for *L. elongisporus* Telo pull-down	GTGTAAGGATGCACTTGAAACTCGGTGTAAGGATGCACTTGAAACTCGGTGTAAGGATGCACTTGAAACTCG

Lelongisporus_telo_rv	Rev; telomere bait oligo for *L. elongisporus* Telo pull-down	ACCGAGTTTCAAGTGCATCCTTACACCGAGTTTCAAG TGCATCCTTACACCGAGTTTCAAGTGCATCCTTAC
Pguilliermondii_telo_fw	Fw; telomere bait oligo for *M. guilliermondii* Telo pull-down	CTGGTGTACTGGTGTACTGGTGTACTGGTGTACTGGT GTACTGGTGTACTGGTGTACTGGTGTA
Pguilliermondii_telo_rv	Rev; telomere bait oligo for *M. guilliermondii* Telo pull-down	AGTACACCAGTACACCAGTACACCAGTACACCAGTAC ACCAGTACACCAGTACACCAGTACACC
Ylipolytica_telo_fw	Fw; telomere bait oligo for *Y. lipolytica* Telo pull-down	ATTGGGACGATTGGGACGATTGGGACGATTGGGACG ATTGGGACGATTGGGACGATTGGGACG
Ylipolytica_telo_rv	Rev; telomere bait oligo for *Y. lipolytica* Telo pull-down	ATCGTCCCAATCGTCCCAATCGTCCCAATCGTCCCAA TCGTCCCAATCGTCCCAATCGTCCCA
Clusitaniae_telo_fw	Fw; telomere bait oligo for *C. lusitaniae* Telo pull-down	CTTTAGGGAGGTACTGATGTTCTTTAGGGAGGTACTG ATGTTCTTTAGGGAGGTACTGATGTT
Clusitaniae_telo_rv	Rev; telomere bait oligo for *C. lusitaniae* Telo pull-down	AGAACATCAGTACCTCCCTAAAGAACATCAGTACCTC CCTAAAGAACATCAGTACCTCCCTAA
Yeast_cont_fw	Fw; scrambled control sequence	GTCACAAACCACAAATTCCACAATTAACCACAATAACC TACAAATAACCACATAATAACCACTAATAATAA
Yeast_cont_rev	Rev; scrambled control sequence	ACTTATTATTAGTGGTTATTATGTGGTTATTTGTAGGTTA TTGTGGTTAATTGTGGAATTTGTGGTTTGTG
oBL29	Rev; anneals to TEF promoter	CTGCAGCGAGGAGCCGTAAT
oBL207	Rev; telomere-specific probe (Southern blot)	CACCACACCCACACACCACACCCACA
oBL258	Fw; anneals to 6R telomere region, ChIP (qPCR)	GTGTGTAGTGATCCGAACTCA
oBL259	Rev; anneals to 6R telomere region, ChIP (qPCR)	GCATATTGATATGGCGTACGCACACGT
oBL282	Rev; anneals to URA3	AGGCCTCTAGGTTCCTTTGTTAC
oBL283	Fw; anneals to URA3	GTCCCAAAATTTGTTTACTAAAAAC
oBL292	Fw; anneals to actin, ChIP (qPCR)	CCCAGGTATTGCCGAAAGAATGC
oBL293	Rev; anneals to actin, ChIP (qPCR)	TTTGTTGGAAGGTAGTCAAAGAAGCC
oBL295	Fw; anneals to 1L telomere region, ChIP (qPCR)	CGGTGGGTGAGTGGTAGTAAGTAGA
oBL296	Rev; anneals to 1L telomere region, ChIP (qPCR)	ACCCTGTCCCATTCAACCATAC
oBL358	Fw; Telo-PCR (1L telomere)	GCGGTACCAGGGTTAGATTAGGGCTG
oBL359	Rev; Telo-PCR (G tailing primer)	CGGGATCCGGGGGGGGGGGGGGGGG
oBL361	Fw; Telo-PCR (Y' telomere)	TTAGGGCTATGTAGAAGTGCTG
oRS39	Fw; anneals to presumably untranscribed intergenic region on ChrV	GGCTGTCAGAATATGGGGCCGTAGTA
oRS40	Rev; anneals to presumably untranscribed intergenic region on ChrV	CACCCCGAAGCTGCTTTCACAATAC
oLK49	Fw; anneals to 6Y' telomere region, ChIP (qPCR)	GGCTTGGAGGAGACGTACATG
oLK50	Rev; anneals to 6Y' telomere region, ChIP (qPCR)	CTCGCTGTCACTCCTTACCCG

oLK57	Fw; anneals to 15L telomere region, ChIP (qPCR)	GGGTAACGAGTGGGGAGGTAA
oLK58	Rev; anneals to 15L telomere region, ChIP (qPCR)	CAACACTACCCTAATCTAACCCTGT
oFB256	Rev RNA; TERRA control, FP-assay; **Nguyen *et al*., 2017**	GCAGCUGGCACGACAGGUAUGAAUC/36-FAM/
oFB260	Rev; ssDNA, FP-assay; **Nguyen *et al.,* 2017**	GCAGCTGGCACGACAGGTATGAATC/36-FAM/
oFB261	Fw; dsDNA, FP-assay; **Nguyen *et al.,* 2017**	GATTCATACCTGTCGTGCCAGCTGC
oFB436	Fw; ssDNA, FP-assay; **Nguyen *et al.,* 2017**	TGTGGGTGTGGTGTGTGGGTGTGGTG/36-FAM/
oFB437	Rev; ssDNA, FP-assay; **Nguyen *et al.,* 2017**	CACCACACCCACACACCACACCCACA
oFB438	Fw RNA; TERRA control, FP-assay; **Nguyen *et al.,* 2017**	UGUGGGUGUGGUGUGUGGGUGUGGUG/36-FAM/
oVV1	Fw; TDA9 tagging at 3’	GGGCTATTTACAATATCAACCACAGGAAATCTGTAAAC AGTGTACGTACGCTGCAGGTCGAC
oVV2	Rev; TDA9 tagging at 3’	CTAATATAATGTTACATACGGATATGCTAAATATCTATCT AAAGTATCGATGAATTCGAGCTCG
oVV3	Fw; anneals to TDA9 ORF, colony PCR check	CGATACACCAGTCTGGCCCG
oVV4	Fw; RSF2 tagging at 3’	GAGCTATCTATAGTGTTACGAAAAAAAGAAACACTAGA ATACGTACGCTGCAGGTCGAC
oVV5	Rev; RSF2 tagging at 3’	CTATAGTATAGAGACGGCCGCCATTATATATTTGTAAAT CGGACATCGATGAATTCGAGCTCG
oVV6	Fw; anneals to RSF2 ORF, colony PCR check	GGGCCATGGACCCGAATACCG
oVV7	Fw; TDA9 tagging with TAP at 3’	GGGCTATTTACAATATCAACCACAGGAAATCTGTAAAC AGTGTAGGTCGACGGATCCCCGGG
oVV8	Rev; TDA9 tagging with TAP at 3’	CTAATATAATGTTACATACGGATATGCTAAATATCTATCT AAAGTTCGATGAATTCGAGCTCG
oVV9	Fw; RSF2 tagging with TAP at 3’	GAGCTATCTATAGTGTTACGAAAAAAAGAAACACTAGA ATAGGTCGACGGATCCCCGGG
oVV10	Rev; RSF2 tagging with TAP at 3’	CTATAGTATAGAGACGGCCGCCATTATATATTTGTAAAT CGGACTCGATGAATTCGAGCTCG
oVV11	Rev; colony PCR check for tagged with TAP strain	TCACTGATGATTCGCGTCTACTTTCG
oVV13	Fw; anneals to pGUT2, ChIP (qPCR)	CTTTTCTCTGCTCCGATACG
oVV14	Rev; anneals to pGUT2, ChIP (qPCR)	CCTATTTGTGGCTGTTCTCTT
oVV15	Fw; anneals to pALD6, ChIP (qPCR); Walkey at al., 2012	AGGAACTGCCGTCACATACG
oVV16	Rev; anneals to pALD6, ChIP (qPCR); Walkey at al., 2012	CTGGCCATGCCCCTCATTTA
oVV17	Fw; anneals to TDA9 ORF, colony PCR check	TAGCGGGGTACATGAGGAGA
oVV18	Rev; anneals to TDA9 ORF, colony PCR check	TGTCCAGCGCTTGATTGGTA
oVV19	Rev; anneals to RSF2 ORF, colony PCR check	CTCTTGATTGCAAACCATGAGCGAA
oVV20	Rev; anneals to TDA9 ORF, Dharmacon’s pBG1805 check for TDA9 ORF presence	ACTGTTTACAGATTTCCTGTGGTTG

oVV21	Rev; anneals to TDA9 ORF, Dharmacon's pBG1805 check for TDA9 ORF presence	ATTGCAAACCATGAGCGAACGAT
oVV22	Fw; anneals to RSF2 ORF, Gibson's assembly	GCAGGCTTTAAAGGAACCAATTCAGTCGACTGGATCC ATGGAACCGTTCGCATTTGGACGAGGGGCGCCTGC
oVV23	Rev; anneals to RSF2 ORF, Gibson's assembly	CAACTTTGTACAAGAAAGCTGGGTCAAGAAAGCTGG GTCTAGATATCTCGAGTATTCTAGTGTTTCTTTTTTTCG TAACACTATAGATAGC
oVV24	Fw; anneals to RAP1 ORF, Gibson's assembly	CAAAAAAGCAGGCTGTACAAAAAAGCAGGCTTTAAAG GAACCAATTCAGTCGACTGGATCCATGTCTAGTCCAG ATGATTTTGAAACTGCACCAGC
oVV25	Rev; anneals to RAP1 ORF, Gibson's assembly	CTTTGTACAAGAAAGCTGGGTCAAGAAAGCTGGGTCT AGATATCTCGAGTAACAGGTCCTTCTCAAAAAATCTTT TCCTCATTTC

4. Media

Liquid Media

Medium	Composition	
Yeast peptone dextrose (YPD)	2 % (w/v) 1 % (w/v) 2 % (w/v)	Peptone Yeast extract Glucose
Synthetic complete w/o amino acids (SC)	0.192 % (w/v) 0.67 % (w/v) 2 % (w/v)	Yeast synthetic dropout medium w/o amino acids Yeast nitrogen base w/o amino acids Glucose/ Raffinose/ Galactose
Sporulation (SPO)	0.005 % (w/v) 1 % (w/v)	Zinc acetate Potassium acetate
Lysogeny broth (LB)	1 % (w/v) 1 % (w/v) 0.5 % (w/v)	NaCl Tryptone Yeast extract

Solid Media

Medium	Composition	
YPD agar	10 % (w/v) 5 % (w/v) 10 % (w/v) 2 % (w/v)	Peptone Yeast extract Agar Glucose
SC complete agar	0.192 % (w/v) 0.67 % (w/v) 2.4 % (w/v) 2 % (w/v) 1 % (w/v)	Yeast synthetic dropout medium w/o amino acids Yeast nitrogen base w/o amino acids Agar Glucose 100x amino acid
SC w/o acid agar	0.192 % (w/v) 0.67 % (w/v) 2.4 % (w/v) 2 % (w/v)	Yeast synthetic dropout medium w/o amino acids Yeast nitrogen base w/o amino acids Agar Glucose/ Raffinose/ Galactose
SC agar	0.67 % (w/v) 2.4 % (w/v) 2 % (w/v)	Yeast nitrogen base w/o amino acids Agar Glucose
SC w/o acid + 5-FOA agar	0.192 % (w/v) 0.67 % (w/v) 0.005% (w/v) 2.4 % (w/v) 2 % (w/v) 0.1% (w/v) 0.2% (v/v)	Yeast synthetic dropout medium w/o amino acids uracil Yeast nitrogen base w/o amino acids Uracil Agar Glucose 5-FOA in ddH2O at 65˚C Required amino acids

LB agar	0.5 % (w/v) 1 % (w/v) 1 % (w/v) 1.5 % (w/v)	Yeast extract Tryptone NaCl Agar
Pre-sporulation (pre-SPO)	3 % (w/v) 1 % (w/v) 2 % (w/v) 5 % (w/v)	Standard nutrient broth Yeast extract Agar Glucose

5. Antibiotics (Added After Autoclaving)

Antibiotic	Final (working) concentration
Carbenicillin (disodium salt)	100 µg/mL
Kanamycin (G418 disulfate solution)	100 to 300 µg/mL
Hygromycin B	100 to 300 µg/mL
Zeocin	10 µg/µL, 25 µg/µL, 40 µg/µL

6. Buffers and Solutions (Filter Sterilisation 0.22 µm; Autoclaving 15-20 min at 121^{0}C)

Buffer/ Solution	Composition	
1x PBST	1x PBS in ddH2O 0.1 %	in ddH_2O Tween-20
2x Laemmli Buffer	125 mM 4 % 20 % 0.004 % 10 %	Tris-HCl pH 6.8 SDS Glycerol Bromophenol blue β-mercaptoethanol
5x DIG wash buffer pH 7.5 (Dot blot, Southern blot)	100 mM 0.75 M 1.5 % (v/v)	Maleic acid buffer pH 7.5 NaCl Tween-20 Filter sterilised
6x DNA orange loading dye	15 % 10 mM Orange G	Ficoll EDTA pH 8.0 To colour
10x PBS	1.37 M 30 mM 80 mM 20 mM	NaCl KCl Na_2HPO_4 x $2H_2O$ KH_2PO_4 pH adjusted to 7.4 Autoclaved
10x Blocking solution (Dot blot, Southern blot)	10% (w/v) 100 mM	Blocking reagent Maleic acid buffer pH 7.5
10x TBE, filter sterilised	0.89 M 0.89 M 20 mM	Tris-HCl pH 8.0 Boric acid Na_2EDTA pH 8.0

10x TE	100 mM 10 mM	Tris-HCl pH 7.5 EDTA pH 8.0
10x SDS-PAGE running buffer	1 % (w/v) 250 mM 1.92 M	SDS Tris-HCl pH 8.0 Glycine pH adjusted to 8.3 Filter sterilised
20x SSC	3 M 0.3 M	NaCl Sodium citrate tribasic dihydrate pH adjusted to 7.0
Annealing buffer (Telo pull-down)	200 mM 100 mM 1 M	Tris-HCl pH 8.0 $MgCl_2$ KCl
Blocking buffer (Western blot)	5 % (w/v)	Skim milk powder Dissolved in 1x PBST
Buffer III	10 mM 1 mM 250 mM 1 % (v/v) 1 % (w/v)	Tris-HCl pH 8.0 EDTA pH 8.0 LiCl NP-40 Sodium deoxycholate (SOD)
DBB	1 M 10 mM 1 mM	NaCl Tris-HCl pH 8.0 EDTA pH 8.0
DML buffer	10 mM 10 mM	Na_2HPO_4 NaH_2PO_4 Dissolved in LC-grade water
DIG-detection buffer pH 9.5	130 mM 75 mM	Tris-HCl NaCl pH adjusted to 9.5 Filter sterilised
EDTA	500 mM	Disodium EDTA x2 H_2O pH adjusted to 7.5 or 8.0
Elution Buffer B (ChIP)	50 mM 1 % (v/v) 10 mM	Tris-HCl pH 7.5 SDS EDTA pH 8.0
Elution buffer (Telo pull-down)	2M 100mM 10mM	Urea Ammoniumbicarbonate DTT
FA lysis buffer (ChIP)	50 mM 140 mM 1 mM 1 % (v/v)	HEPES pH 7.5 NaCl EDTA pH 8.0 Triton X-100 Filter sterilised

FA Lysis Buffer -SOD	140 mM 50 mM 1 % 1mM	NaCl HEPES pH 7.5 Triton X-100 EDTA (pH 8.0)
FA lysis buffer + SOD (ChIP)	50 mM 140 mM 1 mM 1 % (v/v) 0.1% (w/v)	HEPES pH 7.5 NaCl EDTA pH 8.0 Triton X-100 Sodium deoxycholate (SOD) Filter sterilised
FA lysis buffer 500 (ChIP)	50 mM 0.5 M 1 mM 1 % (v/v) 0.1 % (w/v)	HEPES pH 7.5 NaCl EDTA pH 8.0 Triton X-100 Sodium deoxycholate (SOD) Filter sterilised
FP Buffer + Zn^{2+}	100 mM/ 150 mM/ 200 mM 20 mM 5 % 0.025 % 100 mM/ 150 mM/ 200 mM	NaCl HEPES pH 7.5 Glycerol Triton X-100 $ZnCl_2$
Hybridisation solution (Dot blot, Southern blot)	50% (v/v) 5x 5x 5 mM 10 mM 0.04 % (w/v) 1 % (v/v)	Formamide SSC Denhardt's EDTA PIPES pH 6.4 Yeast RNA SDS Filter sterilised
Hybridisation buffer for oligos (FP-assay)	90mM 10mM 50mM	Tris-HCl pH 7.5 $MgCl_2$ NaCl
LiAc-Mix	100 mM	Lithium acetate Dissolved in 1x TE
Lysis buffer base (whole protein extraction in Telo pull-down)	100 mM 50 mM 10 mM	NaCl Tris-HCl pH 7.5 $MgCl_2$ Filter sterilised
Malic acid buffer pH 7.5	100 mM 150 mM	Maleic acid NaCl pH adjusted to 7.5 Filter sterilised

PEG-Mix	40 % (v/v)	Polyethylene glycol 400 Dissolve in LiAc-Mix Filter sterilised
Potassium phosphate buffer pH 7.4 (100 mM)	80.2 mM 19.8 mM	K_2HPO_4 KH_2PO_4
PIB	150 mM 50 mM	NaCl Tris-HCl pH 8.0
Sorbitol	2 M	Sorbitol Dissolved in ddH_2O Filter sterilised
Solution 1 (Protein extraction, Western blot)	1.85 M 1.09 M	NaOH β-mercaptoethanol
Solution 2 (Protein extraction, Western blot)	50 % (v/v) in	Trichloroacetic acid Dissolved in ddH_2O
Solution 3 (Protein extraction, Western blot)	100 % (v/v)	Acetone
Stripping buffer (Western blot)	62.5 mM 2 % (v/v) 100.4 mM	Tris pH 6.8 SDS β-mercaptoethanol
Transfer buffer (Western blot)	1x 2 % (v/v)	Bio-Rad transfer buffer in ddH_2O Absolute ethanol
Triton X-100	10 % (v/v)	Triton X-100 Dissolved in ddH_2O
Urea Buffer (Protein extraction, Western blot)	120 mM 5 % (v/v) 8 M 143 mM 8 % (v/v) Bromophenol blue	Tris-HCL pH 6.8 Glycerol Urea β-mercaptoethanol SDS To colour
Washing solution I (Dot blot, Southern blot)	0.1 % (v/v)	SDS Dissolved in 2x SSC
Washing solution II (Dot blot, Southern blot)	0.1 % (v/v)	SDS Dissolved in 0.5x SSC

7. Antibodies

Antibody	Working dilution	Identifier	Source
Rabbit monoclonal peroxidase anti-peroxidase (PAP)	1:3000	Cat. No. P1291	Sigma-Aldrich
Mouse monoclonal anti-HA	1:2000	N/A	IMB CF
Goat monoclonal anti-mouse (HRP conjugate)	1:3000	Cat. No. 170-5047	Bio-Rad
Goat monoclonal anti-rabbit (HRP conjugate)	1:3000	Cat. No. 170-5046	Bio-Rad
Mouse monoclonal anti-Myc (clone 9B11)	1:1000	Cat. No. 2276S	Cell Signalling/ NEB
Mouse monoclonal anti-PGK1	1:20000	Cat. No. 459250	Thermo Fisher
Rabbit polyclonal anti-sheep (HRP conjugate)	1:5000	Cat. No. AB97130	Abcam
Anti-Digoxigenin-AP Fab fragments 150U	1:5000	Cat. No. 11093274910	Roche

8. Commercially Available Kits, Reagents, Enzymes and Additional Materials

Kit	Identifier	Supplier
DIG Oligonucleotide 3′-End Labelling Kit, 2nd generation	Cat. No. 3353575910	Roche
MiniElute PCR Purification Kit	Cat. No. 28004	Qiagen
QIAprep Spin Miniprep Kit	Cat. No. 27106	Qiagen
QIAquick Gel Extraction Kit	Cat. No. 28706	Qiagen
QIAquick PCR Purification Kit	Cat. No. 28106	Qiagen
Qubit® dsDNA HS Assay Kit	Cat. No. 10606433	Fisher Scientific
RNeasy Mini Elute Cleanup Kit	Cat. No. 74204	Qiagen
ZymoPrep Yeast Plasmid Miniprep II kit	Cat. No. D2004	Zymo Research
Trans-blot® Turbo™ RTA Midi Nitrocellulose Transfer Kit	Cat. No. 1704271	Bio-Rad
Enzyme	**Identifier**	**Supplier**
2x Gibson assembly enzyme mix	N/A	IMB CF
2x Phusion HF PCR Master Mix	Cat. No. M0531	NEB
2x Q5® High-Fidelity Master Mix	Cat. No. M0492	NEB
Q5® Hot Start High-Fidelity DNA Polymerase	Cat. No. M0493	NEB
2x Taq PCR Master Mix	Cat. No. M0270	NEB
Alu I	Cat. No. R0137	NEB
DNase I	Cat. No. 79254	Qiagen
Exo I (E. coli)	Cat. No. M0293	NEB
Hae III	Cat. No. R0108	NEB
Hinf I	Cat. No. R0155	NEB

Lyticase	Cat. No. L4025	Sigma Aldrich
LR Clonase	N/A	IMB CF
Msp I	Cat. No. R0106	NEB
Proteinase K	Cat. No. 1151ML010	Myneolab
RNase A	Cat. No. EN0531	Thermo Scientific
Terminal Transferase	Cat. No. M0315	NEB
Xho I	Cat. No. R0146	NEB
Zymolyase T100	Cat. No. E1005	Zymo Research
Chemical/ Additional Material	**Identifier**	**Supplier**
0.5mm Zirconia/Silica beads	Cat. No. 11079105Z	BioSpec
1kb DNA ladder	Cat. No. N3232	NEB
5-FOA	Cat. No. F9001-1	Zymo Research
6x Blue DNA loading dye	Cat. No. B7024S	NEB
10x Exo I Reaction Buffer	Cat. No. B0293S	NEB
15 mL BioRuptor® Pico tubes and sonication beads	Cat. No. C01020031	Diagenode
100bp DNA ladder	Cat. No. N3231	NEB
Agar	Cat. No. 05040	Sigma-Aldrich
Agarose	Cat. No. A9539	Sigma-Aldrich
Amersham Hybond-NX Nylon Membrane	Cat. No. 10712237	GE Healthcare
Amersham Protran Premium Nitrocellulose Membrane	Cat. No. 15219804	GE Healthcare
Bacto tryptone	Cat. No. 211705	BD Biosciences
Bacto yeast extract	Cat. No. 212750	BD Biosciences
Bradford solution	Cat. No. A6932	AppliChem
Bromophenol blue	Cat. No. B0126	Sigma-Aldrich
Black/Clear flat bottom 384-well low volume plate	Cat. No. 3544	Corning
Carbenicillin disodium salt	Cat. No. C1389	Sigma-Aldrich
CDP-Star™	Cat. No.12041677001	Roche
cOmplete Mini EDTA-free Protease Inhibitor Cocktail tablets	Cat. No. 4693159001	Roche
CutSmart® buffer	Cat. No. B7204S	NEB
dATP [α-^{32}P]	Cat. No. SRP-203	Hartmann Analytic
DMSO	Cat. No. D8418	Sigma-Aldrich
DTT	Cat. No. 43816	Sigma-Aldrich
Dynabeads™ Protein G	Cat. No. 10607605	Invitrogen
EDTA	Cat. No. 03620	Sigma-Aldrich
Falcon™ 96-well Clear Flat Bottom TC-treated Culture Microplate	Cat. No. 353072	Corning

Multiscreen™ 96-Well-plate, hydrophile PVDF-Membrane	Cat. No. 41104923	Millipore
Formaldehyde Solution, 37%	Cat. No. F8775	Sigma-Aldrich
G418 disulfate solution	Cat. No. A6798	AppliChem
Galactose (D+)	Cat. No. 1421731211	AppliChem
Glucose (D+)	Cat. No. A1422	AppliChem
Glycerol	Cat. No. 11433297	Fisher Scientific
Glycine	Cat. No. A1067	AppliChem
Hard-Shell 384-well PCR plates	Cat. No. HSP3805	Bio-Rad
HEPES buffer pH 7.5	Cat. No. A6916	Applichem
Hydroxyurea	Cat. No. H8627	Sigma-Aldrich
Hygromycin B gold solution	Cat. No. ANT-HG-5	InvivoGen
IgG Sepharose™ 6-Fast-Flow-Medium	Cat. No. 11574955	GE Healthcare
IgG Sepharose	Cat. No. 11574955	Thermo Scientific
Lysing Matrix C tubes	Cat. No. 11492410	MP Biomedicals
Microscopic Cover Glasses 22 x 22 mm	Cat. No. 01-2222/x	Novoglas
Microscope slides	Cat. No. 1-6274	Neo Lab
Microseal 'B' PCD Adhesive seal	Cat. No. MSB1001	Bio-Rad
Mini-Protean® TGX Stain-Free™ Protein Gels 4-15% (10/15 well)	Cat. No. 4568086	Bio-Rad
Na_2EDTA	Cat. No. A3553	AppliChem
NuPAGE™ 10% Bis-Tris precast gel	Cat. No. NP0301	Thermo Scientific
NuPAGE™ 20x MES buffer	Cat. No. NP0002	Thermo Scientific
NuPAGE™ 4x LDS sample buffer	Cat. No. NP0008	Thermo Scientific
NuPAGE™ LDS Sample Buffer 4x	Cat. No. NP0008	Life Technologies
Orange G	Cat. No. A1404	Applichem
PhosSTOP tablets	Cat. No. 04906845001	Roche
PEG 400	Cat. No. 81240	Sigma-Aldrich
Ponceau S solution	Cat. No. P7170	Sigma-Aldrich
Prestained protein marker, Broad Range (11-190 kDa)	Cat. No. P7706	NEB
Protein A Sepharose	Cat. No. 11359931	Thermo Scientific
Raffinose	Cat. No. A6882	AppliChem
Skim milk powder	Cat. No. 70166	Sigma-Aldrich
SDS - 20 % solution	Cat. No. A0675	AppliChem
Streptavidin sepharose high performance beads	Cat. No. 90100484	Cytiva
Sorbitol (D+)	Cat. No. 51876	Sigma-Aldrich

Sucrose	Cat. No. S0389	Sigma-Aldrich
SuperSignal West Pico PLUS Chemiluminescent Substrate	Cat. No. 34578	Thermo Scientific
SYBR Safe DNA gel stain	Cat. No. 10328162	Fisher Scientific
Trichloroacetic acid (TCA)	Cat. No. 27242	Sigma-Aldrich
Trizma base	Cat. No. T1503	Sigma-Aldrich
Triton X-100	Cat. No. X100	Sigma-Aldrich
Trypsin	Cat. No. T6567	Sigma-Aldrich
Tween-20	Cat. No. P1379	Sigma-Aldrich
Urea	Cat. No. U5378	Sigma-Aldrich
Yeast extract	Cat. No. 16259781	Thermo Scientific
Yeast nitrogen base w/o amino acids	Cat. No. Y0626	Sigma-Aldrich
Yeast synthetic dropout medium supplement w/o amino acid (SC or SD)	Cat. No. 1145112-CF	MP Biomedicals
Yeast synthetic dropout medium w/o uracil	Cat. No. Y1501	Sigma-Aldrich
Yeastmaker™ carrier DNA	Cat. No. 630440	Clontech
Zinc chloride	Cat. No. 383317	Sigma-Aldrich

9. Equipment and Software

Equipment	**Supplier**
Bioruptor Pico & Water Cooler Mini-chiller	Diagenode
ChemiDoc Touch Imaging System	Bio-Rad
Dissection microscope SporePlay+	Singer Instruments
EASY-n LC 1000 system	Thermo Scientific
Electrospray ion source (Nanospray Flex™)	Thermo Scientific
Hybridisation Oven OV3	Biometra
FastPrep-25	MP Biomedicals
NanoDrop 2000	Thermo Scientific
Q Exactive Orbitrap Plus mass spectrometer	Thermo Scientific
Qubit 2.0 Fluorometer	Thermo Scientific
Real Time PCD Detection System CFX384 Touch	Bio-Rad
Sonifier 450	Branson
Spark 20M multimode microplate reader	Tecan
Spectrophotometer UltraSPARC 2100 pro	Biochron
Thermal Cycler C1000 Touch	Bio-Rad
Trans-Blot Turbo Transfer System	Bio-Rad
UV Stratalinker 2400	Stratagene
Widefield microscope	Leica/ The ECHO Revolve
Software	**Supplier**
Adobe Illustrator	Adobe
GraphPad Prism 6	GraphPad
Illustrator CC2020	Adobe

ImageJ Fiji	https://fiji.sc/
ImageLab V5	Bio-Rad
MaxQuant	Max Planck Institute of Biochemistry
MS Office 2016	Microsoft
R	The R Foundation
SnapGene 4	GSL Biotech

Methods

1. *S. cerevisiae* Strains and Culture Manipulation

Strains were cultivated as liquid cultures in either YPD, SC or SPO media at 30^0C and 200rpm agitation. Supplementation of SC with appropriate amino acids and/or sugar source was carried out in accordance with the needs of an experiment to ensure appropriate selection and/or induction. Overnight cultures were incubated for 12-17h as 5mL liquid medium inoculated with a single colony or a spore-colony. For exponential growth culture (day culture), on the following day the overnight culture was diluted to an appropriate OD_{600} (0.1 – 0.2) in a new flask with fresh medium and cultivated further to a desired OD_{600} (0.8 – 1.0) in the same conditions. For induction experiments, the overnight cultures were incubated with 2% raffinose-selective media, and the day cultures of those were induced by addition of 2% final concentration galactose for the required period of time (typically, 2-4h unless stated otherwise).

2. *S. cerevisiae* Mating, Sporulation and Dissection

To mate, strains of opposite mating type (*MATa* or *MATalpha*) were streaked on top of each other as ca. 1x1 cm patch onto pre-SPO plate and incubated overnight at 30^0C. The next day, the patch was scraped from the plate and inoculated into 3-5mL of SPO medium following incubation for 4 – 14 days at 23^0C until sufficient amount of asci was observed under the microscope. For dissection, the 1:1 mix of sporulated culture and Lyticase (2.5mg/mL, Sigma-Aldrich) was incubated for 15min on a bench following a drop-like inoculation of a Petri YPD plate and dissection with the SporePlay+ micromanipulation microscope. Dissected plates were then incubated at 30^0C for 3 days, replica plated if necessary and patched onto selective media for genotyping and mating type assessments.

3. *S. cerevisiae* Transformation

Transformation of yeast cultures was carried out as described in Gietz & Schiestl (2007) except that 35% (w/v) PEG 3350 was substituted with 35% (w/v) PEG 400 for availability reasons, and the heat shock was done for 15min instead of 40min as in the published protocol without the effect on transformation efficacy. If transformation was done for integration of PCR fragments or plasmids, after the heat shock the cultures were allowed for 1 to 6 hours recovery at 30^0C before being plated onto selection media following incubation for several days at the same temperature until visible colonies were observed. To ensure no false-positive colonies selected, single colonies of transformed culture were re-steaked again onto selective media before cryo stock preservation.

4. Bacterial Transformation

Commercially available, chemically competent *E. coli* DH5alpha cells as “Mix & Go!” set from Zymo Research were used for bacterial transformation. The transformation steps were carried out in accordance to manufacture’s protocol.

5. Spotting Assay

Overnight cultures were diluted to an initial OD_{600} of 0.5 (10^0) in a 2mL-tube following four sequential 10-fold step dilutions to the final dilution of 10^{-4} in a 96-well cell culture plate. All five dilutions were then spotted onto selective media plates with a frogger and incubated for

72h at 30^0C. If required, pictures of plates were taken every 24h, otherwise, on the last day of incubation.

6. Senescence Curve and Senescence Spotting Assay

After the dissection of strains with telomerase deficiency and their spores genotyping, those of interest were inoculated into 5mL of YPD to the final OD_{600} of 0.01 and left for exactly 24h at 30^0C and 200rpm agitation. The following day the OD_{600} were measured again and the cultures diluted to the final OD_{600} of 0.01 in 5mL of fresh YPD; this process was repeated in general for the total of 10-14 days. The collected OD_{600} were used to calculate a relative growth potential (% viability) of each strain/genotype as the relative to the first day measured OD_{600} (considered as 100% viability), and plotted over the time course as $\log_2(OD_{600}/0.01)$ and population doublings (PD). If PDs were calculated from the moment of dissection rather than liquid culture inoculation, it is indicated in the figure and is estimated as ca. 7.5-8PD per each 24h on a solid medium (thus, 3 days of dissection plate incubation results in the additional of ca. 25PD from the moment haploid progeny started to grow). Graphs were plotted with GraphPad Prism 6 software.

For the senescence assay on solid media, the spores of each desired genotype were diluted to the final OD_{600} of 0.5 and spotted in 10-fold dilutions onto YPD plates with a frogger as described above (spotting assay method). The plates were then incubated for 72h and passaged in the same way as the first spotting each time for the duration of the assay (typically, 4-6 passages); additionally, to avoid cross-contamination, each time the cells were being passaged a small fraction was spotted onto selective media. Photos of plates were taken each 72h unless stated otherwise.

7. Telomere-PCR (Telo-PCR)

The genomic DNA was obtained by collecting 0.2 OD_{600} units of a culture, washing it with ddH_2O, resuspending in 20µL of 0.02M NaOH following incubation for 10min at 100^0C, after that samples were kept on ice. Two µL of the sample were further mixed with 3µL of ddH_2O and used for each telomere length measurement including the controls. The diluted gDNA was incubated for 10min at 96^0C and gradually cooled down to 4^0C, meanwhile 5µL of the C-tailing mix were added to each reaction (per sample: 3.7µL ddH_2O, 1µL 10x NEB 4 buffer, 0.1µL 10mM dCTP, 0.2µL 20u/uL terminal transferase). Then, samples were incubated at 37^0C for 30min, at 65^0C for 10min, at 96^0C for 5min and cooled to 65^0C again at which point 30µL of PCR master mix were added to each reaction tube (per sample: 21µL ddH_2O, 4µL 10x PCR buffer (670mM Tris-HCl pH 8.8, 160mM $(NH_4)_2SO4$, 50% glycerol, 0.1% Tween-20, prepared in water), 4µL 2mM dNTPs, 0.3µL 100µM either oBL358 (1L telomere), oBL361 (Y' telomere) or oBL360 (6R telomere), 0.3µL 100µM oBL359 (G18-BamHI primer), 0.4µL 2U/µL Q5 Hot Start NEB DNA polymerase). The following PCR program was used: 98^0C for 3min, 98^0C for 30s, 63^0C for 15s, 72^0C for 20s (last three steps repeated 45 times in total), 72^0C for 5min. After that, samples were run on 1.8% agarose gel until proper separation of the PCR product. Bands' size corresponding to different telomere length was estimated with ImageLab calculator (Bio-Rad software). Graphs for each telomere were plotted with GraphPad Prism 6 software.

8. Protein Extraction and Western Blot

Two OD_{600} units of exponentially growing culture were precipitated and resuspended in 150µL of cold Solution 1 and kept on ice for 10min. After that, 150µL of cold Solution 2 were added and the sample was vortexed briefly following additional 10min incubation on ice. One mL of ice-cold Solution 3 was added to the precipitated for 2min at top-speed bench centrifuge pre-cooled to $+4^0$C pellet. The S_N was removed and the pellet resuspended in 100µL of urea buffer and incubated for 5min at 95^0C and 500rpm shaking. If loaded on the gel immediately afterwards, the sample was centrifuged briefly for about 10s at top-speed bench centrifuge prior to loading its 5-10µL per well onto precast SDS-PAGE gel. Otherwise, a sample could be kept at -20^0C until further use and prior to loading on a gel was brought to room temperature following denaturation for 5min at 95^0C and brief centrifugation. Samples were typically run at 110V with 1x SDS running buffer in Bio-Rad vertical electrophoresis gel chamber until the front line gave a signal of required separation range. To transfer samples onto nitrocellulose membrane afterwards, the TurboBlot Bio-Rad system and the "High Molecular Weight" preset program were used. The membrane was then stained with Ponceau solution to monitor protein transfer, washed with PBS-0.1%Tween solution until the signs of the staining were gone, and blocked for 1h in Blocking buffer on a rocking platform at room temperature. The membrane was incubated with a primary antibody diluted to a desired concentration in Blocking buffer overnight in a cold room (4^0C). The next day, the membrane was washed 3 times with PBS-0.1%Tween, incubated with a secondary antibody diluted in Blocking buffer for 1h at room temperature on a rocking platform, washed again 3 times with PBS-0.1%Tween, rinsed with PBS and incubated with chemiluminescence substrate enhancing signal solution following imaging with Bio-Rad ChemiDoc™ Touch Imaging System.

9. Southern Blot

A pellet of 20mL exponentially growing culture, 5mL of overnight culture or up to 500mL of deeply senesced culture was collected for gDNA extraction following cells lysis with 1mL solution of 900mM sorbitol, 100mM EDTA pH 8.0, 14mM β-mercaptoethanol, 15U of 100T Lyticase (Sigma-Aldrich) by incubation for up to 3h at 37^0C. Once sphaeroplasts were observed under the microscope, the samples were pelleted at top-speed bench centrifuge for 2min at room temperature, resuspended in TE buffer containing 2.5mM EDTA pH 8, 222mM Tris, and 2.2% SDS, incubated for 30min at 65^0C and 600rpm, following addition of potassium acetate to the final concentration of 0.7M and immediate incubation for at least 1h on ice. Cell residues were eliminated by centrifugation at top-speed for 15min at 4^0C and nucleic acid containing S_N was precipitated with ethanol after what resuspended in TE buffer overnight without pipetting but on a rotating-wheel in cold room (4^0C). The next day, samples were treated with 25µg RNAse A for 30-60min at 37^0C following isopropanol precipitation and resuspension in TE buffer without pipetting. The extracted gDNA was assessed by agarose gel electrophoresis and quantified via Bio-Rad ImageLab calculator and ImageJ Fiji software tools. One µg of gDNA was digested for 3h at 37^0C with either 20U of XhoI or a cocktail of enzymes including 20U AluI, 20U HaeIII, 20U HinfI and 20U MspI. DNA fragments were separated on 1% agarose gel running overnight (15-16h) at 50V. The next day, the gel was denatured in solution containing 400mM NaOH and 600mM NaCl for 1h, following its neutralisation in 1M Trizma base and 1.5M NaCl pH 7.4 solution for 1h. The DNA was capillary transferred onto nylon positively charged membrane (GE Healthcare) in 10x SSC

overnight (17-20h) and cross-linked to the membrane with UV light for 30s and 1200J on auto program. The membrane was then blocked for 1h in hybridisation solution on a rotating platform at 47.5^{0}C following overnight incubation with DIG-labelled telomere specific probe (oBL207). The next day, the membrane was washed twice with pre-warmed to 47.5^{0}C 2x SSC, 0.1% SDS solution (5min/wash) and twice with 0.5x SSC, 0.1% SDS solution (20min/wash). After that, it was blocked with 1x Roche blocking solution for 30min at room temperature, incubated with Anti-DIG-AP Fab fragments antibody, rinsed and imaged with ChemiDoc^{TM} Touch Imaging System (Bio-Rad) after signal enhancing with CDP-Star solution.

10. Fluorescence Polarisation Assay (FP-assay)

Substrates of telomere-mimicking dsDNA (oFB260/261; oFB436/437) and ssDNA (oFB260; oFB436) or TERRA RNA (oFB256; oFB438) labelled with 3'-FAM were annealed in Hybridisation buffer for oligos in a thermocycle at 95^{0}C for 3min with ramping cooling down to 4^{0}C at 1^{0}C/s. After that, 10nM of substrate was incubated with a serial dilution of protein (range of 2.56nM to 200μM) in FP-buffer with different concentrations of NaCl and $ZnCl_2$ for 15min at room temperature (see table with Buffers & Solutions above) in a black 384-well Corning plate. Next, fluorescence polarisation was measured using Spark 20M multimode microplate reader with auto gain mode. Graphs were plotted with GraphPad Prism 6 software.

11. Chromatin Immunoprecipitation (TAP-ChIP)

Exponentially growing cell cultures were cross-linked with 1.2% final concentration formaldehyde for 12min at room temperature and subsequently quenched with 115mM final concentration glycine for 5min at room temperature. After that, the cultures were kept on ice for at least 30min and handled at 4^{0}C later on, being pelleted at 3000rpm for 5min following 2-times washing with ice-cold 20mL PBS. If not used immediately, the pellets were stored at -80^{0}C until further use. Pellets were resuspended in 400μL FA-SOD buffer supplemented with protease inhibitor tablet (Roche), transferred to lysing Matrix C tubes and lysed in FastPrep-25 (3 sequential runs at 6.5M/s as 30s/run, 30s/rest on ice each time). Extracts were recovered by adding 800μL ice-cold FA+SOD buffer supplemented with protease inhibitor tablet and, after mixing well, pelleted at 4^{0}C for 15min top-speed; the pellets were resuspended in 1.5mL of the same buffer supplemented with 20μL of 20% SDS/sample afterwards. Next, samples were sonicated for 30s on/off (5 cycles total) in BioRuptor Pico sonicator at 4^{0}C and pelleted at 4^{0}C for 15min top-speed. To ensure sonication efficiency, 100μL of S_N containing shared chromatin were mixed with 100μL of elution buffer, incubated at 65^{0}C overnight, treated with Proteinase K and RNase A following loading of 2-5μL on 1.5% agarose gel. Protein concentration of the ChIP extract was assessed by Bradford assay, and brought to 1mg/mL with ice-cold FA+SOD+protease inhibitor buffer; from that sample, 50μL were taken as 5% input for de-cross-linking and Proteinase K/RNase A treatment as above so that the final volume of the sample was 200μL in Elution buffer B). And 1mL was incubated with 50μL of blocked with 5% BSA in PBS and pre-washed IgG Sepharose beads on a rotating wheel at 4^{0}C in a cold room overnight. The following day, beads were washed once with ice-cold FA+SOD lysis buffer, once with FA lysis buffer 500, once with Buffer III, and once with TE pH 8.0 buffer before being eluted twice in total 200μL volume of Elution buffer B for 8min at 65^{0}C each time. The IP samples as well as 5% input ones were then subjected to qPCR analysis.

12. Telomere Pull-down (Telo Pull-down)

- *Whole Protein Extract of Yeast Cell Cultures Preparation*

Depending on how well yeast culture grew, 100 to 500mL of exponentially growing cells were collected as a pellet at 3000rpm for 5min, washed twice with 10mL PBS and kept at -80^{0}C until further use. For the pull-down, cell pellet was dissolved in ice-cold lysis buffer base supplemented with protein inhibitor cocktail shortly before use, transferred to 2mL-tubes with 0.5mm Zirconia/Silica beads and lysed in FastPrep-25 (3 sequential runs at 6.5M/s as 30s/run and 30s/rest on ice each time). Protein concentration of S_N was assessed with Bradford assay, 1mg of total protein extract was used for the Telo pull-down.

- *Concatomerisation of Telomere and Control DNA Baits*

To anneal, 100µL of each oligo were mixed in annealing buffer and heated up to 80^{0}C in a thermoblock for 5min following gradual cooling after switching it off. To phosphorylate and polymerise, annealed oligos were first incubated with 100U of T4 PNK for 2h at 37^{0}C following overnight incubation at room temperature with 40U of T4 DNA ligase. The next day, polymerisation was checked on 2% agarose gel, and concatomerised oligos were purified by phenol/chloroform and ethanol precipitation. For biotinylation, the oligos were incubated overnight at 37^{0}C with N6-(6-Amino) hexyl-dATP - Biotin (Biotin-7-dATP) (Jena Bioscience) and 30 units of DNA polymerase Klenow fragment exo- (Thermo Scientific). Finally, the oligos were purified with MicroSpin Sephadex G50 columns (GE Healthcare) before being used for the pull-down.

- *Telo Pull-down in a 96-well Filter Plate*

All steps are in a cold room (4^{0}C), a Multiscreen 96-well plate was washed with 70% ethanol and DBB supplemented with 0.05% IGEPAL, after that 20µL of Streptavidin sepharose beads in a total of 200µL of DBB was mixed with 50µL of oligos from the step above and incubated on the plate for 1h at 850rpm to immobilise oligos to the beads. Next, the beads were washed once with DBB and twice with PIB supplemented with 0.25% IGEPAL, 1mM DTT and protease inhibitor cocktail. One mg of whole protein extract was mixed with the beads and 1µg of salmon sperm in a total volume of 150µL of PIB and incubated for 2h at 850rpm. The plate was then washed 3 times with PIB and PBS before being taken out of a cold room. At room temperature in a humidified dark chamber, for reduction of disulfide bonds of the pulled proteins the plate was incubated with 50µL of Elution buffer for 30min. To alkylate the disulfide bonds, 5µL of 0.5M IAA were added per each sample allowing incubation for 10min following trypsin digestion by adding 2.5µg trypsin per sample and incubating for 1h. The peptides were eluted from the plate in 50µL of Elution buffer.

- *Dimethyl Labelling (DML) and Mass Spectrometry (MS) Samples Preparation*

Eluted proteins were subjected to dimethyl labelling with either light (37% CH_2O) or medium (20% CD_2O) compound prepared in DML buffer supplemented with $NaBH_3CN$. After that, peptides were desalted on a C18 stagetip as described in Rappsilber & Ishihama, 2007 and analysed by nanoflow liquid chromatography on EASY-nL C 1000 system (Thermo Scientific) coupled to Orbitrap Exploris Mass spectrometer (Thermo Scientific).

- *MS Data Processing and Bioinformatic Analysis*

MS output raw data files were initially analysed with MaxQuant software (release 1.6.11.0) using ENSEMBL protein database (for each strain used in this study individually, Release49 from December 2020); the MaxQuant output files were then analysed with an in-house R script for DML MS data (written by [redacted] and modified by [redacted]).

Further, the comparative analysis of orthologous groups (OGs) across yeast clades was done with ProteinOrtho tool (v5.16b) and reciprocal best hit (RBH) method. A minimum of 3 orthologs was required to form each OG, and the relationship within a set of two OGs was established based on a hit score calculated from the sum of all aligned regions of each protein pair in this set. RBHs was used to build foundation of each OGs where the higher the algebraic connectivity values were the stronger the orthologous relationships appeared. To build protein-protein interactions (PPIs) network, orthologs of different yeast species were matched to those in *S. cerevisiae*, with functional annotation being done using Gene orthology (GO) terms enrichment and STRING protein domain analysis database. The interaction score threshold was set to 0.700 confidence level. The PPI network enrichment scores were computed with Benjamini-Hochberg corrected p-value method (*S. cerevisiae* as the background organism) and underwent k-means clustering with 3 clusters for up- and 5 clusters for down-regulated networks. The bioinformatical analysis was performed by [redacted].

References

A

Afzal O, Kumar S, Haider MR, Ali MR, Kumar R, Jaggi M, Bawa S. A review on anticancer potential of bioactive heterocycle quinoline. Eur J Med Chem. 2015 Jun 5;97:871-910. doi: 10.1016/j.ejmech.2014.07.044. Epub 2014 Jul 24. PMID: 25073919.

Aguilera A, Gómez-González B. Genome instability: a mechanistic view of its causes and consequences. Nat Rev Genet. 2008 Mar;9(3):204-17. doi: 10.1038/nrg2268. PMID: 18227811.

Ahel I, Rass U, El-Khamisy SF, Katyal S, Clements PM, McKinnon PJ, Caldecott KW, West SC. The neurodegenerative disease protein aprataxin resolves abortive DNA ligation intermediates. Nature. 2006 Oct 12;443(7112):713-6. doi: 10.1038/nature05164. Epub 2006 Sep 10. PMID: 16964241.

Alexander MK, Zakian VA. Rap1p telomere association is not required for mitotic stability of a C(3)TA(2) telomere in yeast. EMBO J. 2003 Apr 1;22(7):1688-96. doi: 10.1093/emboj/cdg154. PMID: 12660174; PMCID: PMC152898**.**

Amelina H, Subramaniam S, Moiseeva V, Armstrong CA, Pearson SR, Tomita K. Telomere protein Rap1 is a charge resistant scaffolding protein in chromosomal bouquet formation. BMC Biol. 2015 Jun 10;13:37. doi: 10.1186/s12915-015-0149-x. PMID: 26058898; PMCID: PMC4660835.

Aravind L, Iyer LM, Koonin EV. Scores of RINGS but no PHDs in ubiquitin signaling. Cell Cycle. 2003 Mar-Apr;2(2):123-6. doi: 10.4161/cc.2.2.335. PMID: 12695663.

Arora R, Lee Y, Wischnewski H, Brun CM, Schwarz T, Azzalin CM. RNaseH1 regulates TERRA-telomeric DNA hybrids and telomere maintenance in ALT tumour cells. Nat Commun. 2014 Oct 21;5:5220. doi: 10.1038/ncomms6220. PMID: 25330849; PMCID: PMC4218956.

Askree SH, Yehuda T, Smolikov S, Gurevich R, Hawk J, Coker C, Krauskopf A, Kupiec M, McEachern MJ. A genome-wide screen for Saccharomyces cerevisiae deletion mutants that affect telomere length. Proc Natl Acad Sci U S A. 2004 Jun 8;101(23):8658-63. doi: 10.1073/pnas.0401263101. Epub 2004 May 25. PMID: 15161972; PMCID: PMC423251.

Azad GK, Tomar RS. The multifunctional transcription factor Rap1: a regulator of yeast physiology. Front Biosci (Landmark Ed). 2016 Jun 1;21(5):918-30. doi: 10.2741/4429. PMID: 27100480.

B

Badis G, Chan ET, van Bakel H, Pena-Castillo L, Tillo D, Tsui K, Carlson CD, Gossett AJ, Hasinoff MJ, Warren CL, Gebbia M, Talukder S, Yang A, Mnaimneh S, Terterov D, Coburn D, Li Yeo A, Yeo ZX, Clarke ND, Lieb JD, Ansari AZ, Nislow C, Hughes TR. A library of yeast transcription factor motifs reveals a widespread function for Rsc3 in targeting nucleosome exclusion at promoters. Mol Cell. 2008 Dec 26;32(6):878-87. doi: 10.1016/j.molcel.2008.11.020. PMID: 19111667; PMCID: PMC2743730.

Balk B, Maicher A, Dees M, Klermund J, Luke-Glaser S, Bender K, Luke B. Telomeric RNA-

DNA hybrids affect telomere-length dynamics and senescence. Nat Struct Mol Biol. 2013 Oct;20(10):1199-205. doi: 10.1038/nsmb.2662. Epub 2013 Sep 8. PMID: 24013207.

Basta J, Rauchman M. The nucleosome remodeling and deacetylase complex in development and disease. Transl Res. 2015 Jan;165(1):36-47. doi: 10.1016/j.trsl.2014.05.003. Epub 2014 May 10. PMID: 24880148; PMCID: PMC4793962.

Bauer SL, Grochalski TNT, Smialowska A, Åström SU. Sir2 and Reb1 antagonistically regulate nucleosome occupancy in subtelomeric X-elements and repress TERRAs by distinct mechanisms. PLoS Genet. 2022 Sep 22;18(9):e1010419. doi: 10.1371/journal.pgen.1010419. PMID: 36137093; PMCID: PMC9531808.

Ben-Shitrit T, Yosef N, Shemesh K, Sharan R, Ruppin E, Kupiec M. Systematic identification of gene annotation errors in the widely used yeast mutation collections. Nat Methods. 2012 Feb 5;9(4):373-8. doi: 10.1038/nmeth.1890. PMID: 22306811.

Bettin N, Oss Pegorar C, Cusanelli E. The Emerging Roles of TERRA in Telomere Maintenance and Genome Stability. Cells. 2019 Mar 15;8(3):246. doi: 10.3390/cells8030246. PMID: 30875900; PMCID: PMC6468625.

Bianchi A, Negrini S, Shore D. Delivery of yeast telomerase to a DNA break depends on the recruitment functions of Cdc13 and Est1. Mol Cell. 2004 Oct 8;16(1):139-46. doi: 10.1016/j.molcel.2004.09.009. PMID: 15469829.

Bluhm A, Viceconte N, Li F, Rane G, Ritz S, Wang S, Levin M, Shi Y, Kappei D, Butter F. ZBTB10 binds the telomeric variant repeat TTGGGG and interacts with TRF2. Nucleic Acids Res. 2019 Feb 28;47(4):1896-1907. doi: 10.1093/nar/gky1289. PMID: 30629181; PMCID: PMC6393293.

Bonnell E, Pasquier E, Wellinger RJ. Telomere replication: solving multiple end replication problems. Front Cell Dev Biol. 2021 Apr 1;9:668171. doi: 10.3389/fcell.2021.668171. PMID: 33869233; PMCID: PMC8047117.

Boulton SJ, Jackson SP. Components of the Ku-dependent non-homologous end-joining pathway are involved in telomeric length maintenance and telomeric silencing. EMBO J. 1998 Mar 16;17(6):1819-28. doi: 10.1093/emboj/17.6.1819. PMID: 9501103; PMCID: PMC1170529.

Braun H, Xu Z, Chang F, Viceconte N, Rane G, Levin M, Lototska L, Roth F, Hillairet A, Fradera-Sola A, Khanchandani V, Sin ZW, Yong WK, Dreesen O, Yang Y, Shi Y, Li F, Butter F, Kappei D. ZNF524 directly interacts with telomeric DNA and supports telomere integrity. Nat Commun. 2023 Dec 12;14(1):8252. doi: 10.1038/s41467-023-43397-7. PMID: 38086788; PMCID: PMC10716145.

Brevet V, Berthiau AS, Civitelli L, Donini P, Schramke V, Géli V, Ascenzioni F, Gilson E. The number of vertebrate repeats can be regulated at yeast telomeres by Rap1-independent mechanisms. EMBO J. 2003 Apr 1;22(7):1697-706. doi: 10.1093/emboj/cdg155. PMID: 12660175; PMCID: PMC152899.

Bryan TM. G-Quadruplexes at Telomeres: Friend or Foe? Molecules. 2020 Aug 13;25(16):3686. doi: 10.3390/molecules25163686. PMID: 32823549; PMCID: PMC7464828.

Cappadocia L, Pichler A, Lima CD. Structural basis for catalytic activation by the human ZNF451 SUMO E3 ligase. Nat Struct Mol Biol. 2015 Dec;22(12):968-75. doi: 10.1038/nsmb.3116. Epub 2015 Nov 2. PMID: 26524494; PMCID: PMC4709122.

Carvalho J, Mergny JL, Salgado GF, Queiroz JA, Cruz C. G-quadruplex, Friend or Foe: the role of the G-quartet in Anticancer Strategies. Trends Mol Med. 2020 Sep;26(9):848-861. doi: 10.1016/j.molmed.2020.05.002. Epub 2020 May 25. PMID: 32467069.

Cassandri M, Smirnov A, Novelli F, Pitolli C, Agostini M, Malewicz M, Melino G, Raschellà G. Zinc-finger proteins in health and disease. Cell Death Discov. 2017 Nov 13;3:17071. doi: 10.1038/cddiscovery.2017.71. PMID: 29152378; PMCID: PMC5683310.

Cervenak F, Sepsiova R, Nosek J, Tomaska L. Step-by-step evolution of telomeres: lessons from yeasts. Genome Biol Evol. 2021 Feb 3;13(2):evaa268. doi: 10.1093/gbe/evaa268. PMID: 33537752; PMCID: PMC7857110.

Cesare AJ, Reddel RR. Alternative lengthening of telomeres: models, mechanisms and implications. Nat Rev Genet. 2010 May;11(5):319-30. doi: 10.1038/nrg2763. Epub 2010 Mar 30. PMID: 20351727.

Chakravarti D, LaBella KA, DePinho RA. Telomeres: history, health, and hallmarks of aging. Cell. 2021 Jan 21;184(2):306-322. doi: 10.1016/j.cell.2020.12.028. Epub 2021 Jan 14. PMID: 33450206; PMCID: PMC8081271.

Chan A, Boulé JB, Zakian VA. Two pathways recruit telomerase to Saccharomyces cerevisiae telomeres. PLoS Genet. 2008 Oct;4(10):e1000236. doi: 10.1371/journal.pgen.1000236. Epub 2008 Oct 24. PMID: 18949040; PMCID: PMC2567097.

Chang JS, Winston F. Spt10 and Spt21 are required for transcriptional silencing in Saccharomyces cerevisiae. Eukaryot Cell. 2011 Jan;10(1):118-29. doi: 10.1128/EC.00246-10. Epub 2010 Nov 5. PMID: 21057056; PMCID: PMC3019801.

Chen Q, Ijpma A, Greider CW. Two survivor pathways that allow growth in the absence of telomerase are generated by distinct telomere recombination events. Mol Cell Biol. 2001 Mar;21(5):1819-27. doi: 10.1128/MCB.21.5.1819-1827.2001. PMID: 11238918; PMCID: PMC86745.

Chen H, Xue J, Churikov D, Hass EP, Shi S, Lemon LD, Luciano P, Bertuch AA, Zappulla DC, Géli V, Wu J, Lei M. Structural Insights into Yeast Telomerase Recruitment to Telomeres. Cell. 2018 Jan 11;172(1-2):331-343.e13. doi: 10.1016/j.cell.2017.12.008. Epub 2017 Dec 28. PMID: 29290466; PMCID: PMC5839504.

Chow TT, Shi X, Wei JH, Guan J, Stadler G, Huang B, Blackburn EH. Local enrichment of HP1alpha at telomeres alters their structure and regulation of telomere protection. Nat Commun. 2018 Sep 4;9(1):3583. doi: 10.1038/s41467-018-05840-y. PMID: 30181605; PMCID: PMC6123478.

Churikov D, Charifi F, Simon MN, Géli V. Rad59-facilitated acquisition of Y' elements by short telomeres delays the onset of senescence. PLoS Genet. 2014 Nov 6;10(11):e1004736. doi: 10.1371/journal.pgen.1004736. PMID: 25375789; PMCID: PMC4222662.

Conomos D, Reddel RR, Pickett HA. NuRD-ZNF827 recruitment to telomeres creates a molecular scaffold for homologous recombination. Nat Struct Mol Biol. 2014 Sep;21(9):760-70. doi: 10.1038/nsmb.2877. Epub 2014 Aug 24. PMID: 25150861.

D

Dan J, Rousseau P, Hardikar S, Veland N, Wong J, Autexier C, Chen T. Zscan4 Inhibits Maintenance DNA Methylation to Facilitate Telomere Elongation in Mouse Embryonic Stem Cells. Cell Rep. 2017 Aug 22;20(8):1936-1949. doi: 10.1016/j.celrep.2017.07.070. PMID: 28834755; PMCID: PMC5595351.

Dai Z, Dai X, Xiang Q, Feng J, Wang J, Deng Y, He C. Genome-wide analysis of interactions between ATP-dependent chromatin remodeling and histone modifications. BMC Genomics. 2009 Jul 8;10:304. doi: 10.1186/1471-2164-10-304. PMID: 19586523; PMCID: PMC2713269.

Diakun GP, Fairall L, Klug A. EXAFS study of the zinc-binding sites in the protein transcription factor IIIA. Nature. 1986 Dec 18-31;324(6098):698-9. doi: 10.1038/324698a0. PMID: 3796733.

Dionne I, Wellinger RJ. Processing of telomeric DNA ends requires the passage of a replication fork. Nucleic Acids Res. 1998 Dec 1;26(23):5365-71. doi: 10.1093/nar/26.23.5365. PMID: 9826760; PMCID: PMC148004.

Dilley RL, Greenberg RA. ALTernative Telomere Maintenance and Cancer. Trends Cancer. 2015 Oct 1;1(2):145-156. doi: 10.1016/j.trecan.2015.07.007. PMID: 26645051; PMCID: PMC4669901.

Doksani Y, de Lange T. The role of double-strand break repair pathways at functional and dysfunctional telomeres. Cold Spring Harb Perspect Biol. 2014 Sep 16;6(12):a016576. doi: 10.1101/cshperspect.a016576. PMID: 25228584; PMCID: PMC4292156.

Dujon B. Yeast evolutionary genomics. Nat Rev Genet. 2010 Jul;11(7):512-24. doi: 10.1038/nrg2811. PMID: 20559329.

Dunham MA, Neumann AA, Fasching CL, Reddel RR. Telomere maintenance by recombination in human cells. Nat Genet. 2000 Dec;26(4):447-50. doi: 10.1038/82586. PMID: 11101843.

E

Evensen G, Seeberg E. Adaptation to alkylation resistance involves the induction of a DNA glycosylase. Nature. 1982 Apr 22;296(5859):773-5. doi: 10.1038/296773a0. PMID: 7040984.

F

Fourel G, Revardel E, Koering CE, Gilson E. Cohabitation of insulators and silencing elements in yeast subtelomeric regions. EMBO J. 1999 May 4;18(9):2522-37. doi: 10.1093/emboj/18.9.2522. PMID: 10228166; PMCID: PMC1171334.

Freeman K, Gwadz M, Shore D. Molecular and genetic analysis of the toxic effect of RAP1 overexpression in yeast. Genetics. 1995 Dec;141(4):1253-62. doi: 10.1093/genetics/141.4.1253. PMID: 8601471; PMCID: PMC1206864.

Gamsjaeger R, Liew CK, Loughlin FE, Crossley M, Mackay JP. Sticky fingers: zinc-fingers as protein-recognition motifs. Trends Biochem Sci. 2007 Feb;32(2):63-70. doi: 10.1016/j.tibs.2006.12.007. Epub 2007 Jan 8. PMID: 17210253.

Gatbonton T, Imbesi M, Nelson M, Akey JM, Ruderfer DM, Kruglyak L, Simon JA, Bedalov A. Telomere length as a quantitative trait: genome-wide survey and genetic mapping of telomere length-control genes in yeast. PLoS Genet. 2006 Mar;2(3):e35. doi: 10.1371/journal.pgen.0020035. Epub 2006 Mar 17. Erratum in: PLoS Genet. 2006 Jun;2(6):e104. PMID: 16552446; PMCID: PMC1401499.

Ge Y, Wu Z, Chen H, Zhong Q, Shi S, Li G, Wu J, Lei M. Structural insights into telomere protection and homeostasis regulation by yeast CST complex. Nat Struct Mol Biol. 2020 Aug;27(8):752-762. doi: 10.1038/s41594-020-0459-8. Epub 2020 Jul 13. PMID: 32661422.

Ghanem NZ, Malla SRL, Araki N, Lewis LK. Quantitative assessment of changes in cell growth, size and morphology during telomere-initiated cellular senescence in Saccharomyces cerevisiae. Exp Cell Res. 2019 Aug 1;381(1):18-28. doi: 10.1016/j.yexcr.2019.05.005. Epub 2019 May 7. PMID: 31075257; PMCID: PMC6563841.

Gietz RD, Schiestl RH. High-efficiency yeast transformation using the LiAc/SS carrier DNA/PEG method. Nat Protoc. 2007;2(1):31-4. doi: 10.1038/nprot.2007.13. PMID: 17401334.

Gilson E, Roberge M, Giraldo R, Rhodes D, Gasser SM. Distortion of the DNA double helix by RAP1 at silencers and multiple telomeric binding sites. J Mol Biol. 1993 May 20;231(2):293-310. doi: 10.1006/jmbi.1993.1283. PMID: 8510148.

Gong F, Chiu LY, Cox B, Aymard F, Clouaire T, Leung JW, Cammarata M, Perez M, Agarwal P, Brodbelt JS, Legube G, Miller KM. Screen identifies bromodomain protein ZMYND8 in chromatin recognition of transcription-associated DNA damage that promotes homologous recombination. Genes Dev. 2015 Jan 15;29(2):197-211. doi: 10.1101/gad.252189.114. PMID: 25593309; PMCID: PMC4298138.

Gong F, Clouaire T, Aguirrebengoa M, Legube G, Miller KM. Histone demethylase KDM5A regulates the ZMYND8-NuRD chromatin remodeler to promote DNA repair. J Cell Biol. 2017 Jul 3;216(7):1959-1974. doi: 10.1083/jcb.201611135. Epub 2017 Jun 1. PMID: 28572115; PMCID: PMC5496618.

Gottschling DE, Aparicio OM, Billington BL, Zakian VA. Position effect at S. cerevisiae telomeres: reversible repression of Pol II transcription. Cell. 1990 Nov 16;63(4):751-62. doi: 10.1016/0092-8674(90)90141-z. PMID: 2225075.

Graf M, Bonetti D, Lockhart A, Serhal K, Kellner V, Maicher A, Jolivet P, Teixeira MT, Luke B. Telomere Length Determines TERRA and R-Loop Regulation through the Cell Cycle. Cell. 2017 Jun 29;170(1):72-85.e14. doi: 10.1016/j.cell.2017.06.006. PMID: 28666126.

Grandin N, Damon C, Charbonneau M. Ten1 functions in telomere end protection and length regulation in association with Stn1 and Cdc13. EMBO J. 2001 Mar 1;20(5):1173-83. doi: 10.1093/emboj/20.5.1173. PMID: 11230140; PMCID: PMC145504.

Greider CW, Blackburn EH. Identification of a specific telomere terminal transferase activity

in Tetrahymena extracts. Cell. 1985 Dec;43(2 Pt 1):405-13. doi: 10.1016/0092-8674(85)90170-9. PMID: 3907856.

Guarente L. Diverse and dynamic functions of the Sir silencing complex. Nat Genet. 1999 Nov;23(3):281-5. doi: 10.1038/15458. PMID: 10545947.

Gunisova S, Elboher E, Nosek J, Gorkovoy V, Brown Y, Lucier JF, Laterreur N, Wellinger RJ, Tzfati Y, Tomaska L. Identification and comparative analysis of telomerase RNAs from Candida species reveal conservation of functional elements. RNA. 2009 Apr;15(4):546-59. doi: 10.1261/rna.1194009. Epub 2009 Feb 17. PMID: 19223441; PMCID: PMC2661832.

H

Hardy CF, Sussel L, Shore D. A RAP1-interacting protein involved in transcriptional silencing and telomere length regulation. Genes Dev. 1992 May;6(5):801-14. doi: 10.1101/gad.6.5.801. PMID: 1577274.

Hass EP, Zappulla DC. The Ku subunit of telomerase binds Sir4 to recruit telomerase to lengthen telomeres in S. cerevisiae. Elife. 2015 Jul 28;4:e07750. doi: 10.7554/eLife.07750. PMID: 26218225; PMCID: PMC4547093.

Hayflick L, Moorhead PS. The serial cultivation of human diploid cell strains. Exp Cell Res. 1961 Dec;25:585-621. doi: 10.1016/0014-4827(61)90192-6. PMID: 13905658.

Hecht A, Strahl-Bolsinger S, Grunstein M. Spreading of transcriptional repressor SIR3 from telomeric heterochromatin. Nature. 1996 Sep 5;383(6595):92-6. doi: 10.1038/383092a0. PMID: 8779721.

Hughes TR, Weilbaecher RG, Walterscheid M, Lundblad V. Identification of the single-strand telomeric DNA binding domain of the Saccharomyces cerevisiae Cdc13 protein. Proc Natl Acad Sci U S A. 2000 Jun 6;97(12):6457-62. doi: 10.1073/pnas.97.12.6457. PMID: 10841551; PMCID: PMC18624.

Hu Y, Tang HB, Liu NN, Tong XJ, Dang W, Duan YM, Fu XH, Zhang Y, Peng J, Meng FL, Zhou JQ. Telomerase-null survivor screening identifies novel telomere recombination regulators. PLoS Genet. 2013;9(1):e1003208. doi: 10.1371/journal.pgen.1003208. Epub 2013 Jan 17. PMID: 23390378; PMCID: PMC3547846.

Hoppe GJ, Tanny JC, Rudner AD, Gerber SA, Danaie S, Gygi SP, Moazed D. Steps in assembly of silent chromatin in yeast: Sir3-independent binding of a Sir2/Sir4 complex to silencers and role for Sir2-dependent deacetylation. Mol Cell Biol. 2002 Jun;22(12):4167-80. doi: 10.1128/MCB.22.12.4167-4180.2002. PMID: 12024030; PMCID: PMC133845.

I

Imai S, Armstrong CM, Kaeberlein M, Guarente L. Transcriptional silencing and longevity protein Sir2 is an NAD-dependent histone deacetylase. Nature. 2000 Feb 17;403(6771):795-800. doi: 10.1038/35001622. PMID: 10693811.

Irizar A, Yu Y, Reed SH, Louis EJ, Waters R. Silenced yeast chromatin is maintained by Sir2 in preference to permitting histone acetylations for efficient NER. Nucleic Acids Res. 2010 Aug;38(14):4675-86. doi: 10.1093/nar/gkq242. Epub 2010 Apr 12. PMID: 20385597; PMCID: PMC2919727.

J

Jezek M, Green EM. Histone Modifications and the Maintenance of Telomere Integrity. Cells. 2019 Feb 25;8(2):199. doi: 10.3390/cells8020199. PMID: 30823596; PMCID: PMC6407025.

Jones B, Su H, Bhat A, Lei H, Bajko J, Hevi S, Baltus GA, Kadam S, Zhai H, Valdez R, Gonzalo S, Zhang Y, Li E, Chen T. The histone H3K79 methyltransferase Dot1L is essential for mammalian development and heterochromatin structure. PLoS Genet. 2008 Sep 12;4(9):e1000190. doi: 10.1371/journal.pgen.1000190. PMID: 18787701; PMCID: PMC2527135.

Jurikova K, Gajarsky M, Hajikazemi M, Nosek J, Prochazkova K, Paeschke K, Trantirek L, Tomaska L. Role of folding kinetics of secondary structures in telomeric G-overhangs in the regulation of telomere maintenance in *Saccharomyces cerevisiae*. J Biol Chem. 2020 Jul 3;295(27):8958-8971. doi: 10.1074/jbc.RA120.012914. Epub 2020 May 8. PMID: 32385108; PMCID: PMC7335780.

K

Kaizer H, Connelly CJ, Bettridge K, Viggiani C, Greider CW. Regulation of Telomere Length Requires a Conserved N-Terminal Domain of Rif2 in Saccharomyces cerevisiae. Genetics. 2015 Oct;201(2):573-86. doi: 10.1534/genetics.115.177899. Epub 2015 Aug 20. PMID: 26294668; PMCID: PMC4596670.

Kamaliyan Z, Clarke TL. Zinc finger proteins: guardians of genome stability. Front Cell Dev Biol. 2024 Jul 25;12:1448789. doi: 10.3389/fcell.2024.1448789. PMID: 39119040; PMCID: PMC11306022.

Kanev PB, Atemin A, Stoynov S, Aleksandrov R. PARP1 roles in DNA repair and DNA replication: The basi(c)s of PARP inhibitor efficacy and resistance. Semin Oncol. 2024 Feb-Apr;51(1-2):2-18. doi: 10.1053/j.seminoncol.2023.08.001. Epub 2023 Sep 6. PMID: 37714792.

Kappei D, Butter F, Benda C, Scheibe M, Draškovič I, Stevense M, Novo CL, Basquin C, Araki M, Araki K, Krastev DB, Kittler R, Jessberger R, Londoño-Vallejo JA, Mann M, Buchholz F. HOT1 is a mammalian direct telomere repeat-binding protein contributing to telomerase recruitment. EMBO J. 2013 Jun 12;32(12):1681-701. doi: 10.1038/emboj.2013.105. Epub 2013 May 17. PMID: 23685356; PMCID: PMC3680732.

Kappei D, Scheibe M, Paszkowski-Rogacz M, Bluhm A, Gossmann TI, Dietz S, Dejung M, Herlyn H, Buchholz F, Mann M, Butter F. Phylointeractomics reconstructs functional evolution of protein binding. Nat Commun. 2017 Feb 8;8:14334. doi: 10.1038/ncomms14334. PMID: 28176777; PMCID: PMC5309834.

Katan-Khaykovich Y, Struhl K. Heterochromatin formation involves changes in histone modifications over multiple cell generations. EMBO J. 2005 Jun 15;24(12):2138-49. doi: 10.1038/sj.emboj.7600692. Epub 2005 May 26. PMID: 15920479; PMCID: PMC1150886.

Kataria A, Tyagi S. Domain architecture and protein-protein interactions regulate KDM5A recruitment to the chromatin. Epigenetics. 2023 Dec;18(1):2268813. doi: 10.1080/15592294.2023.2268813. Epub 2023 Oct 15. PMID: 37838974; PMCID: PMC10578193.

Kaytor MD, Livingston DM. Saccharomyces cerevisiae RAD52 alleles temperature-sensitive for the repair of DNA double-strand breaks. Genetics. 1994 Aug;137(4):933-44. doi: 10.1093/genetics/137.4.933. PMID: 7982574; PMCID: PMC1206070.

Kimura A, Umehara T, Horikoshi M. Chromosomal gradient of histone acetylation established by Sas2p and Sir2p functions as a shield against gene silencing. Nat Genet. 2002 Nov;32(3):370-7. doi: 10.1038/ng993. Epub 2002 Oct 15. PMID: 12410229.

Klug A. The discovery of zinc fingers and their applications in gene regulation and genome manipulation. Annu Rev Biochem. 2010;79:213-31. doi: 10.1146/annurev-biochem-010909-095056. PMID: 20192761.

Kockler ZW, Comeron JM, Malkova A. A unified alternative telomere-lengthening pathway in yeast survivor cells. Mol Cell. 2021 Apr 15;81(8):1816-1829.e5. doi: 10.1016/j.molcel.2021.02.004. Epub 2021 Feb 26. PMID: 33639094; PMCID: PMC8052312.

Konig P, Giraldo R, Chapman L, Rhodes D. The crystal structure of the DNA-binding domain of yeast RAP1 in complex with telomeric DNA. Cell. 1996 Apr 5;85(1):125-36. doi: 10.1016/s0092-8674(00)81088-0. PMID: 8620531.

Kordyukova M, Olovnikov I, Kalmykova A. Transposon control mechanisms in telomere biology. Curr Opin Genet Dev. 2018 Apr;49:56-62. doi: 10.1016/j.gde.2018.03.002. Epub 2018 Mar 20. PMID: 29571043.

Kornberg RD, Lorch Y. Primary Role of the Nucleosome. Mol Cell. 2020 Aug 6;79(3):371-375. doi: 10.1016/j.molcel.2020.07.020. PMID: 32763226.

Kozak ML, Chavez A, Dang W, Berger SL, Ashok A, Guo X, Johnson FB. Inactivation of the Sas2 histone acetyltransferase delays senescence driven by telomere dysfunction. EMBO J. 2010 Jan 6;29(1):158-70. doi: 10.1038/emboj.2009.314. Epub 2009 Oct 29. PMID: 19875981; PMCID: PMC2808364.

Kramara J, Willcox S, Gunisova S, Kinsky S, Nosek J, Griffith JD, Tomaska L. Tay1 protein, a novel telomere binding factor from Yarrowia lipolytica. J Biol Chem. 2010 Dec 3;285(49):38078-92. doi: 10.1074/jbc.M110.127605. Epub 2010 Oct 5. PMID: 20923774; PMCID: PMC2992242.

Krol K, Brozda I, Skoneczny M, Bretner M, Skoneczna A. A genomic screen revealing the importance of vesicular trafficking pathways in genome maintenance and protection against genotoxic stress in diploid Saccharomyces cerevisiae cells. PLoS One. 2015 Mar 10;10(3):e0120702. doi: 10.1371/journal.pone.0120702. Erratum in: PLoS One. 2015 Apr 07;10(4):e0124186. doi: 10.1371/journal.pone.0124186.. Bretne, Maria [corrected to Bretner, Maria]. PMID: 25756177; PMCID: PMC4355298.

Kupiec M. Biology of telomeres: lessons from budding yeast. FEMS Microbiol Rev. 2014 Mar;38(2):144-71. doi: 10.1111/1574-6976.12054. PMID: 24754043.

Kyrion G, Liu K, Liu C, Lustig AJ. RAP1 and telomere structure regulate telomere position effects in Saccharomyces cerevisiae. Genes Dev. 1993 Jul;7(7A):1146-59. doi: 10.1101/gad.7.7a.1146. PMID: 8319907.

Kwapisz M, Morillon A. Subtelomeric Transcription and its Regulation. J Mol Biol. 2020 Jul 10;432(15):4199-4219. doi: 10.1016/j.jmb.2020.01.026. Epub 2020 Feb 6. PMID: 32035903; PMCID: PMC7374410.

L

Landry J, Sutton A, Tafrov ST, Heller RC, Stebbins J, Pillus L, Sternglanz R. The silencing protein SIR2 and its homologs are NAD-dependent protein deacetylases. Proc Natl Acad Sci U S A. 2000 May 23;97(11):5807-11. doi: 10.1073/pnas.110148297. PMID: 10811920; PMCID: PMC18515.

Larrivee M, LeBel C, Wellinger RJ. The generation of proper constitutive G-tails on yeast telomeres is dependent on the MRX complex. Genes Dev. 2004 Jun 15;18(12):1391-6. doi: 10.1101/gad.1199404. PMID: 15198981; PMCID: PMC423190.

Le S, Moore JK, Haber JE, Greider CW. RAD50 and RAD51 define two pathways that collaborate to maintain telomeres in the absence of telomerase. Genetics. 1999 May;152(1):143-52. doi: 10.1093/genetics/152.1.143. PMID: 10224249; PMCID: PMC1460580.

Lendvay TS, Morris DK, Sah J, Balasubramanian B, Lundblad V. Senescence mutants of Saccharomyces cerevisiae with a defect in telomere replication identify three additional EST genes. Genetics. 1996 Dec;144(4):1399-412. doi: 10.1093/genetics/144.4.1399. PMID: 8978029; PMCID: PMC1207693.

Levis RW, Ganesan R, Houtchens K, Tolar LA, Sheen FM. Transposons in place of telomeric repeats at a Drosophila telomere. Cell. 1993 Dec 17;75(6):1083-93. doi: 10.1016/0092-8674(93)90318-k. PMID: 8261510.

Levy DL, Blackburn EH. Counting of Rif1p and Rif2p on Saccharomyces cerevisiae telomeres regulates telomere length. Mol Cell Biol. 2004 Dec;24(24):10857-67. doi: 10.1128/MCB.24.24.10857-10867.2004. PMID: 15572688; PMCID: PMC533994.

Li N, Li Y, Lv J, Zheng X, Wen H, Shen H, Zhu G, Chen TY, Dhar SS, Kan PY, Wang Z, Shiekhattar R, Shi X, Lan F, Chen K, Li W, Li H, Lee MG. ZMYND8 Reads the Dual Histone Mark H3K4me1-H3K14ac to Antagonize the Expression of Metastasis-Linked Genes. Mol Cell. 2016 Aug 4;63(3):470-84. doi: 10.1016/j.molcel.2016.06.035. Epub 2016 Jul 28. PMID: 27477906; PMCID: PMC4975651.

Li Y, Steenwyk JL, Chang Y, Wang Y, James TY, Stajich JE, Spatafora JW, Groenewald M, Dunn CW, Hittinger CT, Shen XX, Rokas A. A genome-scale phylogeny of the kingdom Fungi. Curr Biol. 2021 Apr 26;31(8):1653-1665.e5. doi: 10.1016/j.cub.2021.01.074. Epub 2021 Feb 18. PMID: 33607033; PMCID: PMC8347878.

Li JS, Miralles Fusté J, Simavorian T, Bartocci C, Tsai J, Karlseder J, Lazzerini Denchi E. TZAP: A telomere-associated protein involved in telomere length control. Science. 2017 Feb 10;355(6325):638-641. doi: 10.1126/science.aah6752. Epub 2017 Jan 12. PMID: 28082411; PMCID: PMC5518674.

Liu LF, Desai SD, Li TK, Mao Y, Sun M, Sim SP. Mechanism of action of camptothecin. Ann N Y Acad Sci. 2000;922:1-10. doi: 10.1111/j.1749-6632.2000.tb07020.x. PMID: 11193884.

Liu J, Wang L, Wang Z, Liu JP. Roles of Telomere Biology in Cell Senescence, Replicative and Chronological Ageing. Cells. 2019 Jan 15;8(1):54. doi: 10.3390/cells8010054. PMID: 30650660; PMCID: PMC6356700.

Liu J, Hong X, Wang L, Liang CY, Liu JP. Sir4 Deficiency Reverses Cell Senescence by Sub-Telomere Recombination. Cells. 2021 Apr 1;10(4):778. doi: 10.3390/cells10040778. PMID: 33915984; PMCID: PMC8066019.

Liu CC, Chan HR, Su GC, Hsieh YZ, Lei KH, Kato T, Yu TY, Kao YW, Cheng TH, Chi P, Lin JJ. Flap endonuclease Rad27 cleaves the RNA of R-loop structures to suppress telomere recombination. Nucleic Acids Res. 2023 May 22;51(9):4398-4414. doi: 10.1093/nar/gkad236. PMID: 36999631; PMCID: PMC10201435.

Loney ER, Inglis PW, Sharp S, Pryde FE, Kent NA, Mellor J, Louis EJ. Repressive and non-repressive chromatin at native telomeres in Saccharomyces cerevisiae. Epigenetics Chromatin. 2009 Dec 2;2(1):18. doi: 10.1186/1756-8935-2-18. PMID: 19954519; PMCID: PMC3225887.

López-Otín C, Blasco MA, Partridge L, Serrano M, Kroemer G. The hallmarks of aging. Cell. 2013 Jun 6;153(6):1194-217. doi: 10.1016/j.cell.2013.05.039. PMID: 23746838; PMCID: PMC3836174.

López-Otín C, Blasco MA, Partridge L, Serrano M, Kroemer G. Hallmarks of aging: An expanding universe. Cell. 2023 Jan 19;186(2):243-278. doi: 10.1016/j.cell.2022.11.001. Epub 2023 Jan 3. PMID: 36599349**.**

Lorch Y, LaPointe JW, Kornberg RD. Nucleosomes inhibit the initiation of transcription but allow chain elongation with the displacement of histones. Cell. 1987 Apr 24;49(2):203-10. doi: 10.1016/0092-8674(87)90561-7. PMID: 3568125.

Lu L, Roberts GG, Oszust C, Hudson AP. The YJR127C/ZMS1 gene product is involved in glycerol-based respiratory growth of the yeast Saccharomyces cerevisiae. Curr Genet. 2005 Oct;48(4):235-46. doi: 10.1007/s00294-005-0023-4. Epub 2005 Nov 4. PMID: 16208474.

Lue NF. Plasticity of telomere maintenance mechanisms in yeast. Trends Biochem Sci. 2010 Jan;35(1):8-17. doi: 10.1016/j.tibs.2009.08.006. Epub 2009 Oct 19. PMID: 19846312; PMCID: PMC2818170.
Lue NF, Chan J. Duplication and functional specialization of the telomere-capping protein Cdc13 in Candida species. J Biol Chem. 2013 Oct 4;288(40):29115-23. doi: 10.1074/jbc.M113.506519. Epub 2013 Aug 21. PMID: 23965999; PMCID: PMC3790010.

Lue NF. Duplex telomere-binding proteins in fungi with canonical telomere repeats: new lessons in the rapid evolution of telomere proteins. Front Genet. 2021 Feb 26;12:638790. doi: 10.3389/fgene.2021.638790. PMID: 33719348; PMCID: PMC7952879.

Lundblad V, Blackburn EH. An alternative pathway for yeast telomere maintenance rescues est1- senescence. Cell. 1993 Apr 23;73(2):347-60. doi: 10.1016/0092-8674(93)90234-h. PMID: 8477448.

Lundblad V, Szostak JW. A mutant with a defect in telomere elongation leads to senescence in yeast. Cell. 1989 May 19;57(4):633-43. doi: 10.1016/0092-8674(89)90132-3. PMID:

2655926.

Luo K, Vega-Palas MA, Grunstein M. Rap1-Sir4 binding independent of other Sir, yKu, or histone interactions initiates the assembly of telomeric heterochromatin in yeast. Genes Dev. 2002 Jun 15;16(12):1528-39. doi: 10.1101/gad.988802. PMID: 12080091; PMCID: PMC186350.

Lydeard JR, Jain S, Yamaguchi M, Haber JE. Break-induced replication and telomerase-independent telomere maintenance require Pol32. Nature. 2007 Aug 16;448(7155):820-3. doi: 10.1038/nature06047. Epub 2007 Aug 1. PMID: 17671506.

M

Maestroni L, Matmati S, Coulon S. Solving the Telomere Replication Problem. Genes (Basel). 2017 Jan 31;8(2):55. doi: 10.3390/genes8020055. PMID: 28146113; PMCID: PMC5333044.

Maestroni L, Reyes C, Vaurs M, Gachet Y, Tournier S, Géli V, Coulon S. Nuclear envelope attachment of telomeres limits TERRA and telomeric rearrangements in quiescent fission yeast cells. Nucleic Acids Res. 2020 Apr 6;48(6):3029-3041. doi: 10.1093/nar/gkaa043. PMID: 31980821; PMCID: PMC7102995.

Marcand S, Gilson E, Shore D. A protein-counting mechanism for telomere length regulation in yeast. Science. 1997 Feb 14;275(5302):986-90. doi: 10.1126/science.275.5302.986. PMID: 9020083.

Marcand S, Brevet V, Gilson E. Progressive cis-inhibition of telomerase upon telomere elongation. EMBO J. 1999 Jun 15;18(12):3509-19. doi: 10.1093/emboj/18.12.3509. PMID: 10369690; PMCID: PMC1171430.

Maringele L, Lydall D. EXO1 plays a role in generating type I and type II survivors in budding yeast. Genetics. 2004 Apr;166(4):1641-9. doi: 10.1534/genetics.166.4.1641. PMID: 15126386; PMCID: PMC1470825.

Matthews JM, Bhati M, Lehtomaki E, Mansfield RE, Cubeddu L, Mackay JP. It takes two to tango: the structure and function of LIM, RING, PHD and MYND domains. Curr Pharm Des. 2009;15(31):3681-96. doi: 10.2174/138161209789271861. PMID: 19925420.

Maxwell PH, Coombes C, Kenny AE, Lawler JF, Boeke JD, Curcio MJ. Ty1 mobilizes subtelomeric Y' elements in telomerase-negative Saccharomyces cerevisiae survivors. Mol Cell Biol. 2004 Nov;24(22):9887-98. doi: 10.1128/MCB.24.22.9887-9898.2004. PMID: 15509791; PMCID: PMC525482.

McClintock B. The Stability of Broken Ends of Chromosomes in Zea Mays. Genetics. 1941 Mar;26(2):234-82. doi: 10.1093/genetics/26.2.234. PMID: 17247004; PMCID: PMC1209127.

Miller J, McLachlan AD, Klug A. Repetitive zinc-binding domains in the protein transcription factor IIIA from Xenopus oocytes. EMBO J. 1985 Jun;4(6):1609-14. doi: 10.1002/j.1460-2075.1985.tb03825.x. PMID: 4040853; PMCID: PMC554390.

Misino S, Bonetti D, Luke-Glaser S, Luke B. Increased TERRA levels and RNase H sensitivity are conserved hallmarks of post-senescent survivors in budding yeast.

Differentiation. 2018 Mar-Apr;100:37-45. doi: 10.1016/j.diff.2018.02.002. Epub 2018 Feb 16. PMID: 29494831.

Misino S, Busch A, Wagner CB, Bento F, Luke B. TERRA increases at short telomeres in yeast survivors and regulates survivor associated senescence (SAS). Nucleic Acids Res. 2022 Dec 9;50(22):12829-12843. doi: 10.1093/nar/gkac1125. PMID: 36513120; PMCID: PMC9825167.

Misteli T. The long reach of telomeres. Genes Dev. 2014 Nov 15;28(22):2445-6. doi: 10.1101/gad.254573.114. PMID: 25403176; PMCID: PMC4233237.

Morawska M, Ulrich HD. An expanded tool kit for the auxin-inducible degron system in budding yeast. Yeast. 2013 Sep;30(9):341-51. doi: 10.1002/yea.2967. Epub 2013 Jul 23. PMID: 23836714; PMCID: PMC4171812.

Moye AL, Porter KC, Cohen SB, Phan T, Zyner KG, Sasaki N, Lovrecz GO, Beck JL, Bryan TM. Telomeric G-quadruplexes are a substrate and site of localization for human telomerase. Nat Commun. 2015 Jul 9;6:7643. doi: 10.1038/ncomms8643. PMID: 26158869; PMCID: PMC4510649.

Mozdy AD, Cech TR. Low abundance of telomerase in yeast: implications for telomerase haploinsufficiency. RNA. 2006 Sep;12(9):1721-37. doi: 10.1261/rna.134706. Epub 2006 Aug 7. PMID: 16894218; PMCID: PMC1557690.

Muller HJ. The Production of Mutations by X-Rays. Proc Natl Acad Sci U S A. 1928 Sep;14(9):714-26. doi: 10.1073/pnas.14.9.714. PMID: 16587397; PMCID: PMC1085688.

Murakami-Sekimata A, Huang D, Piening BD, Bangur C, Paulovich AG. The Saccharomyces cerevisiae RAD9, RAD17 and RAD24 genes are required for suppression of mutagenic post-replicative repair during chronic DNA damage. DNA Repair (Amst). 2010 Jul 1;9(7):824-34. doi: 10.1016/j.dnarep.2010.04.007. Epub 2010 May 15. PMID: 20472512; PMCID: PMC2893243.

N

Negrini S, Ribaud V, Bianchi A, Shore D. DNA breaks are masked by multiple Rap1 binding in yeast: implications for telomere capping and telomerase regulation. Genes Dev. 2007 Feb 1;21(3):292-302. doi: 10.1101/gad.400907. PMID: 17289918; PMCID: PMC1785115.

Neumann AA, Reddel RR. Telomere maintenance and cancer – look, no telomerase. Nat Rev Cancer. 2002 Nov;2(11):879-84. doi: 10.1038/nrc929. PMID: 12415258.

Neurohr GE, Terry RL, Lengefeld J, Bonney M, Brittingham GP, Moretto F, Miettinen TP, Vaites LP, Soares LM, Paulo JA, Harper JW, Buratowski S, Manalis S, van Werven FJ, Holt LJ, Amon A. Excessive Cell Growth Causes Cytoplasm Dilution And Contributes to Senescence. Cell. 2019 Feb 21;176(5):1083-1097.e18. doi: 10.1016/j.cell.2019.01.018. Epub 2019 Feb 7. PMID: 30739799; PMCID: PMC6386581.

Ng HH, Feng Q, Wang H, Erdjument-Bromage H, Tempst P, Zhang Y, Struhl K. Lysine methylation within the globular domain of histone H3 by Dot1 is important for telomeric silencing and Sir protein association. Genes Dev. 2002 Jun 15;16(12):1518-27. doi: 10.1101/gad.1001502. PMID: 12080090; PMCID: PMC186335.

Ng HH, Ciccone DN, Morshead KB, Oettinger MA, Struhl K. Lysine-79 of histone H3 is hypomethylated at silenced loci in yeast and mammalian cells: a potential mechanism for position-effect variegation. Proc Natl Acad Sci U S A. 2003 Feb 18;100(4):1820-5. doi: 10.1073/pnas.0437846100. Epub 2003 Feb 6. PMID: 12574507; PMCID: PMC149917.

Nguyen HD, Yadav T, Giri S, Saez B, Graubert TA, Zou L. Functions of Replication Protein A as a Sensor of R Loops and a Regulator of RNaseH1. Mol Cell. 2017 Mar 2;65(5):832-847.e4. doi: 10.1016/j.molcel.2017.01.029. PMID: 28257700; PMCID: PMC5507214.

Nielsen L, Edström JE. Complex telomere-associated repeat units in members of the genus Chironomus evolve from sequences similar to simple telomeric repeats. Mol Cell Biol. 1993 Mar;13(3):1583-9. doi: 10.1128/mcb.13.3.1583-1589.1993. PMID: 8441399; PMCID: PMC359470.

Nischwitz E, Schoonenberg VAC, Fradera-Sola A, Dejung M, Vydzhak O, Levin M, Luke B, Butter F, Scheibe M. DNA damage repair proteins across the Tree of Life. iScience. 2023 Apr 29;26(6):106778. doi: 10.1016/j.isci.2023.106778. PMID: 37250769; PMCID: PMC10220248.

O

Ohle C, Tesorero R, Schermann G, Dobrev N, Sinning I, Fischer T. Transient RNA-DNA Hybrids Are Required for Efficient Double-Strand Break Repair. Cell. 2016 Nov 3;167(4):1001-1013.e7. doi: 10.1016/j.cell.2016.10.001. Epub 2016 Oct 27. PMID: 27881299.

Oliner JD, Saiki AY, Caenepeel S. The Role of MDM2 Amplification and Overexpression in Tumorigenesis. Cold Spring Harb Perspect Med. 2016 Jun 1;6(6):a026336. doi: 10.1101/cshperspect.a026336. PMID: 27194168; PMCID: PMC4888815.

Olovnikov AM. A theory of marginotomy. The incomplete copying of template margin in enzymic synthesis of polynucleotides and biological significance of the phenomenon. J Theor Biol. 1973 Sep 14;41(1):181-90. doi: 10.1016/0022-5193(73)90198-7. PMID: 4754905.

Ottaviani A, Gilson E, Magdinier F. Telomeric position effect: from the yeast paradigm to human pathologies? Biochimie. 2008 Jan;90(1):93-107. doi: 10.1016/j.biochi.2007.07.022. Epub 2007 Aug 6. PMID: 17868970.

P

Paigen K, Petkov PM. PRDM9 and Its Role in Genetic Recombination. Trends Genet. 2018 Apr;34(4):291-300. doi: 10.1016/j.tig.2017.12.017. Epub 2018 Jan 21. PMID: 29366606; PMCID: PMC5878713.

Palladino F, Laroche T, Gilson E, Axelrod A, Pillus L, Gasser SM. SIR3 and SIR4 proteins are required for the positioning and integrity of yeast telomeres. Cell. 1993 Nov 5;75(3):543-55. doi: 10.1016/0092-8674(93)90388-7. PMID: 8221893.

Persikov AV, Singh M. De novo prediction of DNA-binding specificities for Cys2His2 zinc finger proteins. Nucleic Acids Res. 2014 Jan;42(1):97-108. doi: 10.1093/nar/gkt890. Epub 2013 Oct 3. PMID: 24097433; PMCID: PMC3874201.

Petreaca RC, Chiu HC, Eckelhoefer HA, Chuang C, Xu L, Nugent CI. Chromosome end protection plasticity revealed by Stn1p and Ten1p bypass of Cdc13p. Nat Cell Biol. 2006

Jul;8(7):748-55. doi: 10.1038/ncb1430. Epub 2006 Jun 11. PMID: 16767082.

Petreaca RC, Chiu HC, Nugent CI. The role of Stn1p in Saccharomyces cerevisiae telomere capping can be separated from its interaction with Cdc13p. Genetics. 2007 Nov;177(3):1459-74. doi: 10.1534/genetics.107.078840. Epub 2007 Oct 18. PMID: 17947422; PMCID: PMC2147953.

Perez-Martínez L, Öztürk M, Butter F, Luke B. Npl3 stabilizes R-loops at telomeres to prevent accelerated replicative senescence. EMBO Rep. 2020 Mar 4;21(3):e49087. doi: 10.15252/embr.201949087. Epub 2020 Feb 6. PMID: 32026548; PMCID: PMC7054685.

Pham H, Ferrari R, Cokus SJ, Kurdistani SK, Pellegrini M. Modeling the regulatory network of histone acetylation in Saccharomyces cerevisiae. Mol Syst Biol. 2007;3:153. doi: 10.1038/msb4100194. Epub 2007 Dec 18. PMID: 18091724; PMCID: PMC2174627.

Pickett HA, Cesare AJ, Johnston RL, Neumann AA, Reddel RR. Control of telomere length by a trimming mechanism that involves generation of t-circles. EMBO J. 2009 Apr 8;28(7):799-809. doi: 10.1038/emboj.2009.42. Epub 2009 Feb 12. PMID: 19214183; PMCID: PMC2670870.

Pina B, Fernández-Larrea J, García-Reyero N, Idrissi FZ. The different (sur)faces of Rap1p. Mol Genet Genomics. 2003 Mar;268(6):791-8. doi: 10.1007/s00438-002-0801-3. Epub 2003 Jan 25. PMID: 12655405.

Platt JM, Ryvkin P, Wanat JJ, Donahue G, Ricketts MD, Barrett SP, Waters HJ, Song S, Chavez A, Abdallah KO, Master SR, Wang LS, Johnson FB. Rap1 relocalization contributes to the chromatin-mediated gene expression profile and pace of cell senescence. Genes Dev. 2013 Jun 15;27(12):1406-20. doi: 10.1101/gad.218776.113. Epub 2013 Jun 11. PMID: 23756653; PMCID: PMC3701195.

Pommier Y. Drugging topoisomerases: lessons and challenges. ACS Chem Biol. 2013 Jan 18;8(1):82-95. doi: 10.1021/cb300648v. Epub 2013 Jan 4. PMID: 23259582; PMCID: PMC3549721.

Q

R

Rass U, Ahel I, West SC. Actions of aprataxin in multiple DNA repair pathways. J Biol Chem. 2007 Mar 30;282(13):9469-9474. doi: 10.1074/jbc.M611489200. Epub 2007 Feb 2. PMID: 17276982.

Rappsilber J, Mann M, Ishihama Y. Protocol for micro-purification, enrichment, pre-fractionation and storage of peptides for proteomics using StageTips. Nat Protoc. 2007;2(8):1896-906. doi: 10.1038/nprot.2007.261. PMID: 17703201.

Reid RJ, González-Barrera S, Sunjevaric I, Alvaro D, Ciccone S, Wagner M, Rothstein R. Selective ploidy ablation, a high-throughput plasmid transfer protocol, identifies new genes affecting topoisomerase I-induced DNA damage. Genome Res. 2011 Mar;21(3):477-86. doi: 10.1101/gr.109033.110. Epub 2010 Dec 20. PMID: 21173034; PMCID: PMC3044861.

Renauld H, Aparicio OM, Zierath PD, Billington BL, Chhablani SK, Gottschling DE. Silent

domains are assembled continuously from the telomere and are defined by promoter distance and strength, and by SIR3 dosage. Genes Dev. 1993 Jul;7(7A):1133-45. doi: 10.1101/gad.7.7a.1133. PMID: 8319906.

Rivera T, Haggblom C, Cosconati S, Karlseder J. A balance between elongation and trimming regulates telomere stability in stem cells. Nat Struct Mol Biol. 2017 Jan;24(1):30-39. doi: 10.1038/nsmb.3335. Epub 2016 Dec 5. PMID: 27918544; PMCID: PMC5215970.

Rivosecchi J, Jurikova K, Cusanelli E. Telomere-specific regulation of TERRA and its impact on telomere stability. Semin Cell Dev Biol. 2024 Apr;157:3-23. doi: 10.1016/j.semcdb.2023.11.001. Epub 2023 Dec 11. PMID: 38088000.

Robin JD, Ludlow AT, Batten K, Magdinier F, Stadler G, Wagner KR, Shay JW, Wright WE. Telomere position effect: regulation of gene expression with progressive telomere shortening over long distances. Genes Dev. 2014 Nov 15;28(22):2464-76. doi: 10.1101/gad.251041.114. PMID: 25403178; PMCID: PMC4233240.

Rosas Bringas FR, Stinus S, de Zoeten P, Cohn M, Chang M. Rif2 protects Rap1-depleted telomeres from MRX-mediated degradation in *Saccharomyces cerevisiae*. Elife. 2022 Jan 19;11:e74090. doi: 10.7554/eLife.74090. PMID: 35044907; PMCID: PMC8791636.

Rudner AD, Hall BE, Ellenberger T, Moazed D. A nonhistone protein-protein interaction required for assembly of the SIR complex and silent chromatin. Mol Cell Biol. 2005 Jun;25(11):4514-28. doi: 10.1128/MCB.25.11.4514-4528.2005. PMID: 15899856; PMCID: PMC1140625.

Rusché LN, Kirchmaier AL, Rine J. Ordered nucleation and spreading of silenced chromatin in Saccharomyces cerevisiae. Mol Biol Cell. 2002 Jul;13(7):2207-22. doi: 10.1091/mbc.e02-03-0175. PMID: 12134062; PMCID: PMC117306.

S

Sandell LL, Zakian VA. Telomeric position effect in yeast. Trends Cell Biol. 1992 Jan;2(1):10-4. doi: 10.1016/0962-8924(92)90138-d. PMID: 14731632.

Sandell LL, Zakian VA. Loss of a yeast telomere: arrest, recovery, and chromosome loss. Cell. 1993 Nov 19;75(4):729-39. doi: 10.1016/0092-8674(93)90493-a. PMID: 8242745.

San-Segundo PA, Roeder GS. Role for the silencing protein Dot1 in meiotic checkpoint control. Mol Biol Cell. 2000 Oct;11(10):3601-15. doi: 10.1091/mbc.11.10.3601. PMID: 11029058; PMCID: PMC15018.

Savitsky P, Krojer T, Fujisawa T, Lambert JP, Picaud S, Wang CY, Shanle EK, Krajewski K, Friedrichsen H, Kanapin A, Goding C, Schapira M, Samsonova A, Strahl BD, Gingras AC, Filippakopoulos P. Multivalent Histone and DNA Engagement by a PHD/BRD/PWWP Triple Reader Cassette Recruits ZMYND8 to K14ac-Rich Chromatin. Cell Rep. 2016 Dec 6;17(10):2724-2737. doi: 10.1016/j.celrep.2016.11.014. PMID: 27926874; PMCID: PMC5177622.

Schellenberg MJ, Lieberman JA, Herrero-Ruiz A, Butler LR, Williams JG, Muñoz-Cabello AM, Mueller GA, London RE, Cortés-Ledesma F, Williams RS. ZATT (ZNF451)-mediated resolution of topoisomerase 2 DNA-protein cross-links. Science. 2017 Sep

29;357(6358):1412-1416. doi: 10.1126/science.aam6468. Epub 2017 Sep 14. PMID: 28912134; PMCID: PMC5623066.

Seidle HF, Bieganowski P, Brenner C. Disease-associated mutations inactivate AMP-lysine hydrolase activity of Aprataxin. J Biol Chem. 2005 Jun 3;280(22):20927-31. doi: 10.1074/jbc.M502889200. Epub 2005 Mar 23. PMID: 15790557; PMCID: PMC2556069.

Sepsiova R, Necasova I, Willcox S, Prochazkova K, Gorilak P, Nosek J, Hofr C, Griffith JD, Tomaska L. Evolution of Telomeres in Schizosaccharomyces pombe and Its Possible Relationship to the Diversification of Telomere Binding Proteins. PLoS One. 2016 Apr 21;11(4):e0154225. doi: 10.1371/journal.pone.0154225. PMID: 27101289; PMCID: PMC4839565.

Singer MS, Gottschling DE. TLC1: template RNA component of Saccharomyces cerevisiae telomerase. Science. 1994 Oct 21;266(5184):404-9. doi: 10.1126/science.7545955. PMID: 7545955.

Singh JK, van Attikum H. DNA double-strand break repair: Putting zinc fingers on the sore spot. Semin Cell Dev Biol. 2021 May;113:65-74. doi: 10.1016/j.semcdb.2020.09.003. Epub 2020 Sep 19. PMID: 32962915.

Singh P, Gazy I, Kupiec M. Control of telomere length in yeast by SUMOylated PCNA and the Elg1 PCNA unloader. Elife. 2023 Aug 2;12:RP86990. doi: 10.7554/eLife.86990. PMID: 37530521; PMCID: PMC10396338.

Slichenmyer WJ, Rowinsky EK, Donehower RC, Kaufmann SH. The current status of camptothecin analogues as antitumor agents. J Natl Cancer Inst. 1993 Feb 17;85(4):271-91. doi: 10.1093/jnci/85.4.271. PMID: 8381186.

Smith MA, Blankman E, Deakin NO, Hoffman LM, Jensen CC, Turner CE, Beckerle MC. LIM domains target actin regulators paxillin and zyxin to sites of stress fiber strain. PLoS One. 2013 Aug 21;8(8):e69378. doi: 10.1371/journal.pone.0069378. PMID: 23990882; PMCID: PMC3749209.

Soudet J, Jolivet P, Teixeira MT. Elucidation of the DNA end-replication problem in Saccharomyces cerevisiae. Mol Cell. 2014 Mar 20;53(6):954-64. doi: 10.1016/j.molcel.2014.02.030. PMID: 24656131.

Sreesankar E, Senthilkumar R, Bharathi V, Mishra RK, Mishra K. Functional diversification of yeast telomere associated protein, Rif1, in higher eukaryotes. BMC Genomics. 2012 Jun 19;13:255. doi: 10.1186/1471-2164-13-255. PMID: 22712556; PMCID: PMC3410773.

Shi T, Bunker RD, Mattarocci S, Ribeyre C, Faty M, Gut H, Scrima A, Rass U, Rubin SM, Shore D, Thomä NH. Rif1 and Rif2 shape telomere function and architecture through multivalent Rap1 interactions. Cell. 2013 Jun 6;153(6):1340-53. doi: 10.1016/j.cell.2013.05.007. PMID: 23746845.

Spruijt CG, Luijsterburg MS, Menafra R, Lindeboom RG, Jansen PW, Edupuganti RR, Baltissen MP, Wiegant WW, Voelker-Albert MC, Matarese F, Mensinga A, Poser I, Vos HR, Stunnenberg HG, van Attikum H, Vermeulen M. ZMYND8 Co-localizes with NuRD on Target Genes and Regulates Poly(ADP-Ribose)-Dependent Recruitment of GATAD2A/NuRD to

Sites of DNA Damage. Cell Rep. 2016 Oct 11;17(3):783-798. doi: 10.1016/j.celrep.2016.09.037. PMID: 27732854.

T

Taggart AK, Teng SC, Zakian VA. Est1p as a cell cycle-regulated activator of telomere-bound telomerase. Science. 2002 Aug 9;297(5583):1023-6. doi: 10.1126/science.1074968. PMID: 12169735.

Takata H, Tanaka Y, Matsuura A. Late S phase-specific recruitment of Mre11 complex triggers hierarchical assembly of telomere replication proteins in Saccharomyces cerevisiae. Mol Cell. 2005 Feb 18;17(4):573-83. doi: 10.1016/j.molcel.2005.01.014. PMID: 15721260.

Tammaro M, Barr P, Ricci B, Yan H. Replication-dependent and transcription-dependent mechanisms of DNA double-strand break induction by the topoisomerase 2-targeting drug etoposide. PLoS One. 2013 Nov 7;8(11):e79202. doi: 10.1371/journal.pone.0079202. PMID: 24244448; PMCID: PMC3820710.

Teixeira MT, Arneric M, Sperisen P, Lingner J. Telomere length homeostasis is achieved via a switch between telomerase- extendible and -nonextendible states. Cell. 2004 Apr 30;117(3):323-35. doi: 10.1016/s0092-8674(04)00334-4. PMID: 15109493.

Teixeira MT, Gilson E. Telomere maintenance, function and evolution: the yeast paradigm. Chromosome Res. 2005;13(5):535-48. doi: 10.1007/s10577-005-0999-0. PMID: 16132818.

Teng SC, Chang J, McCowan B, Zakian VA. Telomerase-independent lengthening of yeast telomeres occurs by an abrupt Rad50p-dependent, Rif-inhibited recombinational process. Mol Cell. 2000 Oct;6(4):947-52. doi: 10.1016/s1097-2765(05)00094-8. PMID: 11090632.

Teng SC, Zakian VA. Telomere-telomere recombination is an efficient bypass pathway for telomere maintenance in Saccharomyces cerevisiae. Mol Cell Biol. 1999 Dec;19(12):8083-93. doi: 10.1128/MCB.19.12.8083. PMID: 10567534; PMCID: PMC84893.

Todorova T, Miteva D, Chankova S. DNA susceptibility of Saccharomyces cerevisiae to Zeocin depends on the growth phase. Int Microbiol. 2019 Dec;22(4):419-428. doi: 10.1007/s10123-019-00065-5. Epub 2019 Mar 14. PMID: 30875034.

Torres IO, Kuchenbecker KM, Nnadi CI, Fletterick RJ, Kelly MJ, Fujimori DG. Histone demethylase KDM5A is regulated by its reader domain through a positive-feedback mechanism. Nat Commun. 2015 Feb 17;6:6204. doi: 10.1038/ncomms7204. PMID: 25686748; PMCID: PMC5080983.

Tumbale P, Appel CD, Kraehenbuehl R, Robertson PD, Williams JS, Krahn J, Ahel I, Williams RS. Structure of an aprataxin-DNA complex with insights into AOA1 neurodegenerative disease. Nat Struct Mol Biol. 2011 Oct 9;18(11):1189-95. doi: 10.1038/nsmb.2146. PMID: 21984210; PMCID: PMC3210380.

U

V

van Leeuwen F, Gafken PR, Gottschling DE. Dot1p modulates silencing in yeast by methylation of the nucleosome core. Cell. 2002 Jun 14;109(6):745-56. doi: 10.1016/s0092-

8674(02)00759-6. PMID: 12086673.

Vega LR, Mateyak MK, Zakian VA. Getting to the end: telomerase access in yeast and humans. Nat Rev Mol Cell Biol. 2003 Dec;4(12):948-59. doi: 10.1038/nrm1256. PMID: 14685173.

Vilas CK, Emery LE, Denchi EL, Miller KM. Caught with One's Zinc Fingers in the Genome Integrity Cookie Jar. Trends Genet. 2018 Apr;34(4):313-325. doi: 10.1016/j.tig.2017.12.011. Epub 2018 Jan 19. PMID: 29370947; PMCID: PMC5878116.

W

Wahlin J, Cohn M. Saccharomyces cerevisiae RAP1 binds to telomeric sequences with spatial flexibility. Nucleic Acids Res. 2000 Jun 15;28(12):2292-301. doi: 10.1093/nar/28.12.2292. PMID: 10871358; PMCID: PMC102728.

Walkey CJ, Luo Z, Madilao LL, van Vuuren HJ. The fermentation stress response protein Aaf1p/Yml081Wp regulates acetate production in Saccharomyces cerevisiae. PLoS One. 2012;7(12):e51551. doi: 10.1371/journal.pone.0051551. Epub 2012 Dec 11. PMID: 23240040; PMCID: PMC3519862.

Wang S, Xu Z, Li M, Lv M, Shen S, Shi Y, Li F. Structural insights into the recognition of telomeric variant repeat TTGGGG by broad-complex, tramtrack and bric-à-brac - zinc finger protein ZBTB10. J Biol Chem. 2023 Mar;299(3):102918. doi: 10.1016/j.jbc.2023.102918. Epub 2023 Jan 16. PMID: 36657642; PMCID: PMC9958480.

Watson JD. Origin of concatemeric T7 DNA. Nat New Biol. 1972 Oct 18;239(94):197-201. doi: 10.1038/newbio239197a0. PMID: 4507727.

Wellinger RJ, Wolf AJ, Zakian VA. Origin activation and formation of single-strand TG1-3 tails occur sequentially in late S phase on a yeast linear plasmid. Mol Cell Biol. 1993 Jul;13(7):4057-65. doi: 10.1128/mcb.13.7.4057-4065.1993. PMID: 8321213; PMCID: PMC359955.

Wellinger RJ, Wolf AJ, Zakian VA. Saccharomyces telomeres acquire single-strand TG1-3 tails late in S phase. Cell. 1993 Jan 15;72(1):51-60. doi: 10.1016/0092-8674(93)90049-v. PMID: 8422682.

Wellinger RJ, Ethier K, Labrecque P, Zakian VA. Evidence for a new step in telomere maintenance. Cell. 1996 May 3;85(3):423-33. doi: 10.1016/s0092-8674(00)81120-4. PMID: 8616897.

Wellinger RJ, Zakian VA. Everything you ever wanted to know about Saccharomyces cerevisiae telomeres: beginning to end. Genetics. 2012 Aug;191(4):1073-105. doi: 10.1534/genetics.111.137851. PMID: 22879408; PMCID: PMC3415994.

Wilson B, Erdjument-Bromage H, Tempst P, Cairns BR. The RSC chromatin remodeling complex bears an essential fungal-specific protein module with broad functional roles. Genetics. 2006 Feb;172(2):795-809. doi: 10.1534/genetics.105.047589. Epub 2005 Oct 3. PMID: 16204215; PMCID: PMC1456245.

Winston F, Dollard C, Ricupero-Hovasse SL. Construction of a set of convenient

Saccharomyces cerevisiae strains that are isogenic to S288C. Yeast. 1995 Jan;11(1):53-5. doi: 10.1002/yea.320110107. PMID: 7762301.

Wotton D, Shore D. A novel Rap1p-interacting factor, Rif2p, cooperates with Rif1p to regulate telomere length in Saccharomyces cerevisiae. Genes Dev. 1997 Mar 15;11(6):748-60. doi: 10.1101/gad.11.6.748. PMID: 9087429.

Wright JH, Zakian VA. Protein-DNA interactions in soluble telosomes from Saccharomyces cerevisiae. Nucleic Acids Res. 1995 May 11;23(9):1454-60. doi: 10.1093/nar/23.9.1454. PMID: 7784196; PMCID: PMC306882.

Wu P, Takai H, de Lange T. Telomeric 3' overhangs derive from resection by Exo1 and Apollo and fill-in by POT1b-associated CST. Cell. 2012 Jul 6;150(1):39-52. doi: 10.1016/j.cell.2012.05.026. Epub 2012 Jun 28. PMID: 22748632; PMCID: PMC3392515.

Wysocki R, Javaheri A, Allard S, Sha F, Côté J, Kron SJ. Role of Dot1-dependent histone H3 methylation in G1 and S phase DNA damage checkpoint functions of Rad9. Mol Cell Biol. 2005 Oct;25(19):8430-43. doi: 10.1128/MCB.25.19.8430-8443.2005. PMID: 16166626; PMCID: PMC1265753.

X

Y

Yang J, Dungrawala H, Hua H, Manukyan A, Abraham L, Lane W, Mead H, Wright J, Schneider BL. Cell size and growth rate are major determinants of replicative lifespan. Cell Cycle. 2011 Jan 1;10(1):144-55. doi: 10.4161/cc.10.1.14455. PMID: 21248481; PMCID: PMC3048081.

Yao S, Feng Y, Zhang Y, Feng J. DNA damage checkpoint and repair: From the budding yeast *Saccharomyces cerevisiae* to the pathogenic fungus *Candida albicans*. Comput Struct Biotechnol J. 2021 Nov 25;19:6343-6354. doi: 10.1016/j.csbj.2021.11.033. PMID: 34938410; PMCID: PMC8645783.

Yesbolatova A, Saito Y, Kitamoto N, Makino-Itou H, Ajima R, Nakano R, Nakaoka H, Fukui K, Gamo K, Tominari Y, Takeuchi H, Saga Y, Hayashi KI, Kanemaki MT. The auxin-inducible degron 2 technology provides sharp degradation control in yeast, mammalian cells, and mice. Nat Commun. 2020 Nov 11;11(1):5701. doi: 10.1038/s41467-020-19532-z. PMID: 33177522; PMCID: PMC7659001.

Yu TY, Kao YW, Lin JJ. Telomeric transcripts stimulate telomere recombination to suppress senescence in cells lacking telomerase. Proc Natl Acad Sci U S A. 2014 Mar 4;111(9):3377-82. doi: 10.1073/pnas.1307415111. Epub 2014 Feb 18. PMID: 24550456; PMCID: PMC3948247.

Z

Zakian VA. Telomeres: the beginnings and ends of eukaryotic chromosomes. Exp Cell Res. 2012 Jul 15;318(12):1456-60. doi: 10.1016/j.yexcr.2012.02.015. Epub 2012 Feb 25. PMID: 22391099; PMCID: PMC3372703.

Zhang W, Xu C, Bian C, Tempel W, Crombet L, MacKenzie F, Min J, Liu Z, Qi C. Crystal structure of the Cys2His2-type zinc finger domain of human DPF2. Biochem Biophys Res

Commun. 2011 Sep 16;413(1):58-61. doi: 10.1016/j.bbrc.2011.08.043. Epub 2011 Aug 24. PMID: 21888896.

Zhou BO, Wang SS, Zhang Y, Fu XH, Dang W, Lenzmeier BA, Zhou JQ. Histone H4 lysine 12 acetylation regulates telomeric heterochromatin plasticity in Saccharomyces cerevisiae. PLoS Genet. 2011 Jan 13;7(1):e1001272. doi: 10.1371/journal.pgen.1001272. PMID: 21249184; PMCID: PMC3020936.

Zhou M, Cui Y, Zuo S, Peng Q, Liu Y, Li X, Yang Y, He Q, Yu X, Zhou J, He Z, He Q. ZBTB40 is a telomere-associated protein and protects telomeres in human ALT cells. J Biol Chem. 2023 Sep;299(9):105053. doi: 10.1016/j.jbc.2023.105053. Epub 2023 Jul 15. PMID: 37454741; PMCID: PMC10480536**.**

Curriculum Vitae

(blank)

(blank)